Extended methods

Biological samples

Peripheral blood mononuclear cells (PBMCs) used in this study were collected from children aged between 10 and 16 years old as part of the longitudinal study Asthma in the Life of Families Today (ALOFT, recruited from November 2010 to July 2018, Wayne State University Institutional Review Board approval #0412110B3F) (Resztak *et al.* (2021)), which was established to explore the effects of family environments on childhood asthma. The 96 samples included in the current study were randomly selected from a pool of 136 samples passing the following criteria: donor's age 10-16 years old, donor's race self-reported as Black, availability of at least 3.5 million cryopreserved PBMCs, and to ensure a 50:50 ratio between female and male participants. For each participant multiple samples were collected longitudinally, but we included in this study only the earliest sample passing the filtering criteria. PBMCs collected into two BD Vacutainer™Glass Mononuclear Cell Preparation Tubes (Becton Dickinson and Co., East Rutherford, NJ) were extracted using a previously-published Ficoll centrifugation protocol (Weckle *et al.* (2015)), cryopreserved in freezing media (70% RPMI, 20% CS-FBS, 10% DMSO; $3-8\times10^6$ cells/ml) and stored in liquid nitrogen until the day of the experiment.

Cell culture and single-cell preparation

Cells were processed in batches of 16. For each batch, PBMCs were removed from liquid nitrogen storage and quickly thawed in 37°C water bath before diluting with 6 ml of warm starvation media (90% RPMI 1640, 10% CS-FBS, 0.1% Gentamycin) and counting using Trypan blue staining on Countess II (Life Technologies Corporation, Bothell, WA). Cells were subsequently centrifuged at 400×g for 10 minutes and resuspended in culture medium at 2×10^6 cells/ml. 500 μl of cell suspension was plated in each of 5 wells of a 96-well round-bottom cell culture plate for each sample. Cells were incubated in starvation media overnight (approx. 16 hours) at 37°C and 5% CO_2. The following morning each of the five wells for each individuals were treated with either: 1 μg/ml LPS (Barreiro *et al.* (2010)) + 1 μM dexamethasone (Moyerbrailean *et al.* (2016)), 1 μg/ml LPS + vehicle control alone, 2.5 μg/ml PHA (Moyerbrailean *et al.* (2016)) + 1 μM dexamethasone, 2.5 μg/ml PHA + vehicle control alone, or vehicle control alone (control). Note that the vehicle control used was 1μl of ethanol in 10 ml of media, so that the effect of the vehicle control was negligible. After six hours, cells were pooled across individuals for a total of five treatment-specific pools. The pools were centrifuged at 300 rcf for 5 min at 4°C, washed with 5 ml ice-cold PBS + 1% BSA and centrifuged again. Each pool was resuspended in 2 ml ice-cold PBS + 1% BSA and filtered through a 40 μm Flow-Mi™strainer (SP Scienceware, Warminster, PA). Cell concentration was determined using Trypan blue staining on Countess II, and adjusted to 0.7×10^6 cells/ml to 1.2×10^6 cells/ml. Each pool was loaded onto a separate channel of 10x Genomics®Chromium machine (10x Genomics, Pleasanton, CA), according to the manufacturer's protocol, with batches 4, 5 and 6 loaded on two separate Chromium Chips for a total of 2 wells per treatment pool. Batches 1-4 and one chip of batch 5 were processed using v2 chemistry, and the other chip of batch 5 and batch 6 were processed using v3 chemistry. Library preparation was done according to the manufacturer's protocol.

Sequencing

Sequencing of the single-cell libraries was performed in the Luca/Pique-Regi lab using the Illumina NextSeq 500 and 75 cycles High Output Kit with 58 cycles for R2, 26 for R1, and 8 for I1.

Genotype data

All individuals in this study were genotyped from low-coverage (∼0.4X) whole-genome sequencing and imputed to 37.5 million variants using the 1000 Genomes database by Gencove (New York, NY). These data were used for all genetic analyses and to calculate PCs of genotypes to be used as covariates in downstream statistical analyses. Genotype PCA was run on all biallelic autosomal SNPs with cohort MAF$<=0.1$ using library SNPRelate (Zheng *et al.* (2012)) in R 4.0 (R Core Team (2020)).

single-cell RNA-seq raw data processing (Alignment and demultiplexing)

The raw FASTQ files were mapped to the GRCh38.p12 human reference genome using the `kb` tool (a wrapper of `kallisto` and `bustools`) with the argument of workflow setting to be `lamanno` (Melsted *et al.* (2021)). Two procedures were performed in the `kb` tool. First, we used `kallisto` to pseudo align reads to the reference genome and quantify abundances of transcripts (Bray *et al.* (2016)). Second, we transformed the `kallisto` outputs into BUS (Barcode, UMI, Set) single cell format using `bustools` (Melsted *et al.* (2019)). A total of 45 pooled libraries were generated in our experiment. Among 45 libraries and 6 batches, 3 experiments (LPS+DEX, PHA and PHA+DEX) in batch 2 and 3 experiments (LPS+DEX, PHA and PHA+DEX) in batch 3, were excluded because of failure of the 10x Genomics instrument resulting in broken emulsions, for a total of 39 libraries remaining for all subsequent analyses. We removed debris-contaminated droplets using the `DIEM R` package (Alvarez *et al.* (2020)). With this procedure, we obtained a count matrix of 301,637 cells with 116,734 genes features (including spliced and unspliced) across 39 library pools. The aligned counts matrix were transformed into a `Seurat` object for the subsequent functional analysis. To demultiplex the 16 individuals pooled together for each batch, we used the `popscle` pipeline (`dsc-pileup` followed by `demuxlet`) with the default parameters (Kang *et al.* (2018)). Two input files are required to provide for dsc-pileup, a BAM file and VCF file. The BAM files were generated by running `cellranger` (v2.1.1) `count` function aligned to the GRCh37 human reference genome (downloaded from 10x Genomics, 3.0.0). The VCF file obtained from DNA genotype data (see above) was filtered to remove any SNP that was not covered by scRNA-seq reads. The resulting VCF contained 935,634 SNPs after removing SNPs with MAF less than 0.05. After assigning the identity to each cell, we removed mismatching barcodes between individual identity and batch. A total of 292,394 cells with 116,734 genes (including spliced and unspliced) were entered into the downstream analysis. For 96 Individuals, we had both control and LPS conditions, while the other three conditions (LPS+DEX, PHA, PHA+DEX) were assayed for 64 individuals because of instrument channel failure in batches 2 and 3 for those experimental conditions. This clean dataset had a median of 7,994 cells (Supplemental Fig. S48), a median of 4,251 UMI counts, and 1,810 genes measured on average in each cell across 39 experiments (Supplemental Fig. S49). In terms of spliced reads, we detected a median of 2,705 UMIs and 892 genes for each cell across all 39 experiments (Supplemental Fig. S50).

Clustering, UMAP and cell type annotation

`Seurat`(V3) was employed for preprocessing, clustering, and visualizing the scRNA-seq data (Stuart *et al.* (2019)). We performed log-normalization on all the data using `NormalizeData` with default parameters and selected 2,000 highly variable genes using `FindVariableFeatures` with variance-stabilizing transformation (`vst`) followed by standardization of these highly variable genes for downstream analysis using `ScaleData`. Linear dimensionality reduction was carried out by `RunPCA` on scaled data with 100 principal components (PCs). We ran `RunHarmony` with chemistry as covariates to correct chemistry effects (V2 and V3), which is scalable to a large number of cells and robust Korsunsky *et al.* (2019). The Harmony-adjusted PCs were then used to construct a Shared Nearest Neighbor (SNN) graph using `FindNeighbors` (dims=1:50) and cell clustering was subsequently implemented by running `FindClusters` with the resolution set to 0.15. Finally, Uniform Manifold Approximation and Projection (UMAP) was applied to visualize the clustering results using the top 50 Harmony-adjusted PCs. Cells from different chemistries, batches, and treatments shared similar clustering patterns (Supplemental Fig. S51, Supplemental Fig. S52, Supplemental Fig. S53).

We identified 13 clusters and then annotated cell clusters based on the following canonical immune cell type marker genes (Supplemental Fig. S2 and S55), B cells (*MS4A1* or *CD79A*), Monocytes (*CD14* or *MS4A7*), natural killer (NK) cells (*GNLY* or *NKG7*) and T cells (*CD3D* or *CD8A*). Clusters 0, 4, 5, and 7-12 were annotated as T cells with 183,289 cells, clusters 3 and 6 were annotated as monocytes (30,393), cluster 1 was defined as NK cells (47,824) and cluster 2 as B cells (30,888). We also explored to break the T cell group into the two major sub-clusters (Cluster 0) which is CD4-like T cell and Cluster 4 (CD8-like cytotoxic T cell); yet we only found

a limited number of differences for Cluster 4 in the genes responding to the treatments (Supplemental Fig. S55). This is likely because we would need to profile a larger number of cells to explore in depth differences in these subtypes of T lymphocytes.

Aggregation of single-cell-level data for differential gene expression and genetic analyses

We generated pseudo-bulk RNA-seq data by summing the spliced counts from `kallisto` for each gene and each sample across all cells belonging to each of the four cell types (B cell, Monocyte, NK cell and T cell), separately. This generated a data matrix of 42,554 genes from autosomes (rows) and 1,536 combinations of cell type+treatment+individual (columns). The number of cells in each combination displayed a similar distribution between treatments for most cell types (Supplemental Fig. S54 and Supplemental Table S2, S24). B cells have the smallest number of cells for each combination while T cells have the most number of cells for each combination (Supplemental Fig. S54), which is consistent with the cell type compositions in PBMCs. Next, we focused on protein coding genes and filtered out genes with less than 20 reads across cells and removed combinations with less than 20 cells. This last filtering step resulted in a data matrix of 15,770 protein coding genes (rows) and 1,419 combinations (columns), which were used for all subsequent differential expression and genetic analyses.

Differential gene expression analysis

We carried out differential gene expression analysis for each of the five batches separately using `R DESeq2` package (Love *et al.* (2014)) and then combined the results across five batches using meta-analysis. For each batch, we estimated gene expression effects of the treatments using four contrasts: (1) LPS, LPS vs CTRL; (2) LPS+DEX, LPS+DEX vs LPS; (3) PHA, PHA vs CTRL; (4) PHA+DEX, PHA+DEX vs PHA. We found that compared to adding a batch covariate in DESeq2, our approach of dividing the analysis by batch produced more robust results in our data , likely because the overdispersion parameter of DESeq2 was estimated for each batch separately. In the meta-analysis procedure, we first extracted the summary statistics, including estimated effects (β_i) and standard error (s_i). Based on the fixed-effects model of meta-analysis, the weighted average effects are calculated by $\hat{\beta} = \frac{\sum 1/s_i^2 \beta_i}{\sum 1/s_i^2}$ and its estimated variance can be expressed by $\hat{\nu} = (\sum 1/s_i^2)^{-1}$. We then constructed the test statistics $z = \frac{\hat{\beta}}{\sqrt{\hat{\nu}}}$ which follows a normal distribution under the null hypothesis. To correct for multiple hypothesis testing, we used the `qvalue` function in `R` 4.0 to estimate false discovery rate (FDR) from a list of p-values from the above z test statistics for each condition, separately. Differentially expressed genes (DEG) were defined as those with FDR less than 0.1 and absolute estimated $\log_2$ fold change larger than 0.5. We carried out Gene Ontology (GO) enrichment analysis [i.e., Biological process (BP), molecular function (MF), and cellular component (CC)], for these DEGs identified across conditions using `R ClusterProfiler` package (V3.16.1) (Yu *et al.* (2012)).

Estimation of gene expression mean and dispersion

Using the single-cell data generated from Fluidigm experiment Sarkar et.al proposed a zero-inflated negative binomial (ZINB) distribution to estimate gene expression variance (Sarkar *et al.* (2019)). Some literature demonstrated that it is not necessary to consider the zero inflation term in the model for droplet-based single-cell RNA data (Svensson (2020)). Based on the computational framework that was established by Sarkar et.al, we adapted a negative binomial (NB) distribution to model the count data for each gene j, using two main parameters for the mean(μ_j) and dispersion(ϕ_j) in our scRNA data. Then, we derived the variance of gene expression by $\hat{\mu_j}^2\hat{\phi}_j$. The details on NB model are described as follows,

$$r_{jk} \sim Poisson(.; R_k\lambda_{jk}) \tag{1}$$

$$\lambda_{jk} \sim Gamma(.; \mu, \phi) \tag{2}$$

Where r_{jk} is the number of molecules for k cell, j gene;R_k is a size factor of each cell, equal to total reads in each cell divided by median reads across cells, to account for difference in cellular sequencing depth; λ_{jk} is a

latent variable, representing gene abundance and further is assumed to be Gamma distribution with mean value μ, variance $\mu^2\phi$. By integrating the latent variable λ_{jk}, we derived density function for each observation as follows,

$$\begin{aligned}\Pr(r_{jk}) &= \int_0^\infty \frac{(R_k\lambda_{jk})^{r_{jk}}\exp^{-(R_k\lambda_{jk})}}{\Gamma(r_{jk}+1)}\frac{(\mu_j^{-1}\phi_j^{-1})^{\phi_j^{-1}}}{\Gamma(\phi_j^{-1})}\lambda_{jk}^{(\phi_j^{-1}-1)}\exp^{-(\mu_j^{-1}\phi_j^{-1})\lambda_{jk}}\,d(\lambda_{jk}) \\ &= \frac{\Gamma(r_{jk}+\phi_j^{-1})}{\Gamma(r_{jk}+1)\Gamma(\phi_j^{-1})}(\frac{R_k}{R_k+\mu_j^{-1}\phi_j^{-1}})^{r_{jk}}(\frac{\mu_j^{-1}\phi_j^{-1}}{R_k+\mu_j^{-1}\phi_j^{-1}})^{\phi_j^{-1}}\end{aligned} \tag{3}$$

Then, we estimated parameters of μ_j and ϕ_j by minimizing the negative log likelihood using the `optim` function in `R` 4.0 using the "L-BFGS-B" algorithm. Two filters were applied prior to estimation of gene expression parameters (mean and dispersion): (1) removing genes with less than 20 reads across cells (with a total of 30,972 autosomal genes remaining for the analysis); (2) removing the combinations (cell type+treatment+individual) with less than 20 cells (with a total of 1,419 combinations across all our data). To guarantee robust parameter estimation, we focused on genes with more than 15 reads that are expressed across at least 15 cells for each cell type/treatment combination.

Similar to what reported in previous studies (Eling *et al.* (2019b,a); Fan *et al.* (2016); Fair *et al.* (2020)), we observed that both gene variance or dispersion linearly depended on mean parameters (Supplemental Fig. S11A,B). To further correct the dependence between dispersion and mean, we defined a residual dispersion, capturing the departure from the global trend. The residual dispersion was calculated by removing the part of dispersion that could be predicted by the overall trend of gene mean across genes in each cell type separately. This adjusted dispersion was uncorrelated with the gene mean value (Supplemental Fig. S11C) across genes.

The well established method (regression BASiCS model) were proposed to perform differential test for gene expression variability, which can correct the mean confounder by fitting a global linear trend of mean and dispersion across genes in a bayesian hierarchical framework (Eling *et al.* (2018)). In analogy to the BASiCS model, we quantified gene expression variability that was not confounded by mean expression by the two discrete stages (1) Use a negative binomial model to obtain the estimation of the parameters mean and dispersion similar to Sakar et al. approach; (2) Fit a linear model between mean and dispersion across genes to remove the part of dispersion that can be predicted by mean expression. We always used the adjusted values unless otherwise stated.

Calculation of pathway specific score

We calculated the score of a specific GO term or pathway using the transcriptional matrices (mean and dispersion) patterns of genes involved in that term/pathway across all the conditions as follows: (1) extracted the subset of differentially expressed genes in at least one condition belonging to a specific GO term or pathway; (2) scaled mean-centered gene matrices values (mean and dispersion) for each gene across individuals for each cell type and batch separately; (3) subtracted gene expression values of individuals in the CTRL condition to calculate relative expression changes; and, (4) calculated the average values as a specific pathway score across genes for each individual.

Differential gene variability analysis

We focused on 15,770 protein-coding genes for differential gene variability analysis. To account for the noise from the batch, we implemented the same strategy for differential gene expression analysis for differential gene variability and differential gene mean analyses via fitting models by batch separately and we meta-analyzed the summary statistics. We first took the $\log_2$ transformation of residual dispersion and mean, then fitted models using linear regression where treatments were considered for each batch, separately. To obtain more robust estimation of the gene expression parameters for statistical inference, we only focused on genes that had at least 3 individuals in the treatment and 3 individuals in the control condition that was being contrasted. The differentially variable genes (DVG) and differential mean genes (DEG) were defined as those with FDR less than 0.1 and absolute value

of $\log_2$ fold change greater than 0.5. We also used `ClusterProfiler` in `R` to carry out GO enrichment analysis for these identified DVGs.

DLDA response pseudotime method

We developed a new pseudotime method based on diagonal linear discriminant analysis (DLDA) to characterize the degree to which single cells respond to immune treatments. A key difference compared to previous methods (Qiu *et al.* (2017); Haghverdi *et al.* (2016)) is that DLDA is supervised and estimates a straight line trajectory between two endpoints which should be particularly suitable for a short time treatment. Basically, the trajectory is a one dimensional line connecting the two centroids of a treatment and control conditions for each cell type. In DLDA only a subset of genes that are highly differentially expressed between the two conditions are used based on the following formula (Pique-Regi *et al.* (2005)):

$$g(x)_A = \sum_{i=1}^{p} \left(\frac{\hat{\mu}_A(x_i) - \hat{\mu}_B(x_i)}{\hat{\sigma}_i} \right) \left(\frac{x_i - \hat{\mu}(x_i)}{\hat{\sigma}_i} \right) \gamma_i \tag{4}$$

Where the subscripts of A and B represent the two conditions considered in each contrast, respectively; $\hat{\mu}_i$ denoting mean gene expression of the i_{th} gene for A, B or across groups and $\hat{\sigma}_i$ meaning standard deviation of the i_{th} gene across conditions. In this application of DLDA we only used the DEGs that were differentially expressed in the corresponding condition (10%FDR by DESeq2) by introducing an indicator variable (γ_i, assigning to 1 if the i_{th} gene is a significant DEG in the contrast of A versus B or 0 otherwise. This is equivalent to denoising by hard thresholding instead of the soft thresholding that a method like nearest shrunken centroids would use. Note that the left term of the summation is a weight that is exactly a standardized effect size, and the right term evaluates for a given gene how far it is from the midpoint between all the cells. By ignoring the off-diagonal terms and only considering genes that are differentially expressed, DLDA achieves a more robust classification performance when the number of samples available for training is relatively limited. While this approach assumes the shortest Euclidean distance alignment between the centroids of the treated and untreated cells, it should be a reasonable assumption for short time-periods (here 6 hours), compared to learning a complex curved one-dimensional manifold in a high dimensional space. This assumption provides a more robust and stable trajectory followed by the cells from the control to the treated state when we iteratively repeat the procedure resampling the data, compared to more complex nonlinear trajectory methods.

Four kinds of DLDA axes were calculated by the following contrasts for each cell type separately, (1) DLDA axis of LPS was estimated in the CTRL and LPS conditions to infer the response pseudotime to LPS; (2) DLDA axis of LPS+DEX was computed in the LPS and LPS+DEX conditions to calibrate the response pseudotime to DEX; (3) DLDA axis of PHA was estimated in the CTRL and PHA conditions to characterize the response pseudotime to PHA stimuli ; and, (4) DLDA axis of PHA+DEX was estimated in the PHA and PHA+DEX conditions to characterize the response pseudotime to DEX. To achieve this, we excluded the data from batches 2 and 3, resulting in 264,545 cells. Next, to correct chemistry effects, we performed standard log-normalization for each subset (split by chemistry) followed by integrating datasets together using Seurat (V3) for each cell type, separately. After the DLDA representing the trajectory pseudotime is calculated for each cell type and treatment, we use a sliding window approach (10% cells in each window, sliding along the defined pseudotime with a step of 0.1% cells), we analyzed gene expression dynamic changes along the response pseudotime within each treatment for each cell type separately and identified different dynamic patterns of gene expression using the *k*-means algorithm

Validation of the accuracy of DLDA in response pseudotime

We performed resampling analysis to demonstrate the robustness and stability of the DLDA compared to two existing methods: Monocle 3 (Qiu *et al.* (2017)) and SCANPY (Wolf *et al.* (2018)). For the simplification of the analysis, we focused on the T -cells treated with PHA+DEX or PHA that were measured using 10x Genomics chemistry V3, including 29,157 cells and 6,571 DEGs. To validate the effectiveness of the novel approach

(DLDA), we randomly re-sampled half the dataset for 50 replications. In each replication, we applied our novel approach DLDA and the two other methods to compute response pseudotime. We do not have the underlying ground truth on how the cells should be exactly ordered according to response pseudotime; yet, we can still assess how expression for each of the responding genes correlates with the estimated pseudotime in each iteration across all cells. Ideally, the cells would be sorted similarly in each iteration, and the correlation of the gene expression with the pseudotime would stay constant. For each iteration, we calculated the Pearson correlation of the pseudotime and each gene expression in cells. Two indexes were employed to assess the performance of the three methods, (1) variance of correlation coefficients for each gene across replications; (2). Jaccard index of the top 20 highly correlated genes between 1,225 pairwise replications.

Data normalization for genetic analyses

For downstream genetic analyses, we first removed all lowly-expressed genes, defined as having less than 0.1 CPM in more than 20% of the samples in each condition, separately. We quantile-normalized the count data using the voom function in the `limma` v3.44.3 package (Ritchie *et al.* (2015)) in `R` 4.0 and regressed out the following confounding factors: experimental batch, sex, age, and top three principal components of genotypes in each cell type-treatment combination, separately.

For gene expression variability, for each gene-treatment-cell type combination, we discarded data from batches represented by less than 3 individuals. We considered genes with gene expression variability measures available for at least 20% of remaining individuals in each treatment-cell type combination. We quantile-normalized the data using the `voom` function in the `limma` v3.44.3 package (Ritchie *et al.* (2015)) in `R` 4.0. We regressed out the following confounding factors on the subset of genes with no missing data across all individuals in each condition: experimental batch, sex, age, and top three principal components of genotypes processing each cell type-condition combination and performed PCA on variability residuals to use as covariates in variability-eQTL mapping. Mean gene expression estimates were processed using the same pipeline as gene expression variability data.

cis-eQTL mapping

We used `FastQTL` v2.076 (Ongen *et al.* (2016)) to perform eQTL mapping on gene expression residuals calculated for each cell type and condition as outlined above. For each gene, we tested all genetic variants within 50 kb of the transcription start site (TSS) and with cohort minor allele frequency (MAF)> 0.1. We optimized the number of gene expression PCs in the model to maximize the number of eGenes across all conditions combined. The model that yielded the largest number of eGenes included 4 gene expression PCs. eQTL discovery for mean and variability data was performed similarly, except we modelled quantile-normalized data and regressed out the effects of experimental batch, sex, age, and top three principal components of genotypes and PCs of residuals in the `FastQTL` model. The model that yielded the largest number of significant genes at 10% FDR included 5 PCs of residuals for variability and 7 PCs of residuals for mean data.

Multivariate adaptive shrinkage

To improve power of eQTL discovery by taking advantage of parallel measures of genetic effects across many cell types and conditions, we employed the multivariate adaptive shrinkage (mash) method using the `mashr` package v.0.2.40 in `R` v4.0 (Urbut *et al.* (2019)). As input, we provided the genetic effect size estimates from `FastQTL` analysis in each cell type-treatment combination, and their corresponding standard errors calculated as absolute effect size estimates divided by its z-score. We kept the gene-variant pairs with estimates across all cell types and conditions and eliminated the two genes causing a singular matrix. We fitted mash across all 20 cell type-condition combinations on a random subset of 200,000 gene-SNP pairs providing both canonical and data-driven covariance matrices (the latter estimated using mashr in-built `cov_ed` function on strong eQTLs from full data set, defined as those with ashr local false sign rate (LFSR)< 0.05).The LFSR refers to the probability that we incorrectly inferred the sign of genetic effects size (β_j), $LFSR_j = \min\left\{\Pr\left(\beta_j \geq 0|D\right), \Pr\left(\beta_j \leq 0|D\right)\right\}$

(Stephens (2017)). We considered gene-variant pairs with posterior LFSR< 0.1 to be eQTLs. To analyze sharing of genetic effects across all conditions, we considered the direction of genetic effect across all conditions. Genetic effects are shared across conditions if they have the same sign and are significant in at least one of the conditions considered. To analyze treatment- or cell type–specificity, we focused on pairwise comparisons of genetic effect sizes. An eQTL is specific to a condition if it is significant at LFSR< 0.1 in either condition and either the direction of effect differs or the difference in the magnitude of the genetic effects is at least two-fold. A gene is considered shared/specific if at least one eQTL for that gene is shared/specific across the given set of conditions. To discover response eQTLs (reQTLs) we considered the pair-wise union of significant eQTLs in each of the 16 treatment-control combinations. We defined reQTLs as genetic variants whose effect size on gene expression differed by at least two-fold between treatment and control conditions. Mash analyses on mean and variability estimates were conducted following this pipeline.

DLDA-eQTL mapping

For mapping dynamic eQTLs that have genetic effects on gene expression interacting with pseudotime, we first equally divided cells in one immune treatment into three tertiles of the corresponding DLDA pseudotime. The three tertiles denoted 1, 2 and 3, represent early, middle and latter response pseudotime, respectively. Then, we mapped eQTLs interacting with these representative tertiles as dynamic eQTLs across cell types in the corresponding immune treatments as follows:(1) eQTLs interacting with LPS pseudotime were identified in cells treated with LPS; (2) eQTLs interacting with LPS+DEX pseudotime were identified in cells treated with LPS+DEX; (3) eQTLs interacting with PHA pseudotime were identified in cells treated with PHA; and (4) eQTLs interacting with PHA+DEX pseudotime were identified in cells treated with PHA+DEX. To do this, we summed gene expression data in each of the three DLDA bins for individuals with at least two bins containing at least 5 cells for each treatment. We considered genes with $>$0.1 CPM for at least 20% of remaining individuals in each treatment-cell type combination. We quantile-normalized the data followed by regressing out the following confounding factors: experimental batch, sex, age, and top three principal components of genotypes processing each cell type-condition combination separately. To identify genetic variants interacting with each DLDA, we fitted a linear model using the `lm` function in `R` 4.0 that included both the genotype dosage and the DLDA bin (numerically encoded as 1-3), as well as their interaction: $\texttt{Expression} \sim \texttt{dosage} + \texttt{DLDA\_bin} + \texttt{dosage} \times \texttt{DLDA\_bin}$ in each condition separately. Using the same cis-regions to the above analysis, we perform the interaction analysis for all genetic variants within 50 kb of the transcription start site (TSS) in the genes. We then applied Storey's q-value method on the p-values for the interaction term using a stratified FDR approach on significant and non-significant eGenes (from the `FastQTL` analysis, Supplemental Fig. S45).

Extended results

Comparison between genetic effects on gene expression mean and variability

To compare eQTLs and vQTLs, we considered the genetic effects on mean and variability estimated from the same model (Supplemental Fig. S34B, Supplemental Table S20, Table S8, Table S21, and Table S22). We identified three distinct patterns (Figure 6F, Supplemental Fig. S40): genetic variants affecting gene expression levels only (7,155-11,314 gene-SNP pairs), genetic variants affecting gene expression variability only (1,709-2,128 gene-SNP pairs), and genetic variants affecting both gene expression levels and variability (669-1,207 gene-SNP pairs). Genetic effects in this last category were negatively correlated with opposite signs for eQTLs and vQTLs (Pearson correlation -0.25 - -0.8, p-value< 0.05).

For example, rs2071464 is an eQTL for the *PSMB9* gene in B cells stimulated with LPS+DEX, but we found no genetic effect of this variant on gene expression variability (Figure 6G, Supplemental Fig. S41). The *PSMB9* located in the MHC class II region encodes a member of the proteasome B-type family, which is a 20S core beta subunit of the proteasome. Several studies indicated the proteasome plays a critical role in cardiovascular diseases (Sandri and Robbins (2014); Wang and Hill (2015)), inflammatory response and autoimmune diseases (Karin and Delhase (2000)). The subunit of proteasome encoded by *PSMB9* was found to be involved in the process of infectious diseases (Silva *et al.* (2013)), autoimmune diseases (Khuder *et al.* (2015)) and oncology (Wang *et al.* (2014)). Previous TWAS study revealed that expression of *PSMB9* has also been implicated in a number of autoimmune disorders including asthma (Zhang *et al.* (2020)). We found the C allele at the genomic position rs1197452483 to increase the gene expression variability of *RPS18* gene in monocytes treated with PHA+DEX, without any effect on mean gene expression levels (Figure 6H, Supplemental Fig. S42). This gene encodes a ribosomal protein that is a component of the 40S subunit, and its expression has been implicated in rheumatoid arthritis, multiple sclerosis, and psoriasis (Zhang *et al.* (2020)). *In vitro* silencing of this gene leads to decreased rate of viral infection (Tai *et al.* (2009); Sivan *et al.* (2013)). Genetic polymorphism at rs400063 confers effects on both gene expression mean and variability of the *RNASET2* gene in the T cells treated with PHA+DEX, but in opposite directions (Figure 6I, Supplemental Fig. S43). RNASET2 plays a crucial role in innate immune response by recognizing and degrading RNAs from microbial pathogens that are sensed by *TLR8* (Greulich *et al.* (2019)). Expression of *RNASET2* has been implicated in Crohn's disease, inflammatory bowel disease, and rheumatoid arthritis (Zhang *et al.* (2020)) via TWAS. eQTLs were likely to be also vQTLs (OR=10.45, p-value$< 2.2 \times 10^{-16}$); however, for the majority of vQTLs, we did not detect significant genetic effects on gene expression levels. vGenes were significantly enriched for genes with differential mean expression for six of the 16 conditions considered (LPS, LPS+DEX and PHA in B cells and T cells, Fisher's exact test p-value< 0.05, Supplemental Table S9). vGenes were also enriched for genes with differential variability for seven contrasts (LPS and PHA in B cells and T cells; LPS and PHA+DEX in NK cells; and PHA+DEX in Monocytes; Fisher's exact test p-value < 0.05).

References

Alvarez, M., Rahmani, E., Jew, B., Garske, K. M., Miao, Z., Benhammou, J. N., Ye, C. J., Pisegna, J. R., Pietiläinen, K. H., Halperin, E., and Pajukanta, P. (2020). Enhancing droplet-based single-nucleus RNA-seq resolution using the semi-supervised machine learning classifier DIEM. *Sci Rep*, **10**(1), 11019.

Barreiro, L. B., Marioni, J. C., Blekhman, R., Stephens, M., and Gilad, Y. (2010). Functional comparison of innate immune signaling pathways in primates. *PLoS Genet*, **6**(12), e1001249.

Bray, N. L., Pimentel, H., Melsted, P., and Pachter, L. (2016). Near-optimal probabilistic RNA-seq quantification. *Nat Biotechnol*, **34**(5), 525–527.

Eling, N., Richard, A. C., Richardson, S., Marioni, J. C., and Vallejos, C. A. (2018). Correcting the Mean-Variance Dependency for Differential Variability Testing Using Single-Cell RNA Sequencing Data. *Cell Syst*, **7**(3), 284–294.

Eling, N., Morgan, M. D., and Marioni, J. C. (2019a). Challenges in measuring and understanding biological noise. *Nat Rev Genet*, **20**(9), 536–548.

Eling, N., Richard, A. C., Richardson, S., Marioni, J. C., and Vallejos, C. A. (2019b). Correcting the Mean-Variance Dependency for Differential Variability Testing Using Single-Cell RNA Sequencing Data. *Cell Syst*, **9**(4), 401–413.

Fair, B. J., Blake, L. E., Sarkar, A., Pavlovic, B. J., Cuevas, C., and Gilad, Y. (2020). Gene expression variability in human and chimpanzee populations share common determinants. *Elife*, **9**.

Fan, J., Salathia, N., Liu, R., Kaeser, G. E., Yung, Y. C., Herman, J. L., Kaper, F., Fan, J. B., Zhang, K., Chun, J., and Kharchenko, P. V. (2016). Characterizing transcriptional heterogeneity through pathway and gene set overdispersion analysis. *Nat Methods*, **13**(3), 241–244.

Greulich, W., Wagner, M., Gaidt, M. M., Stafford, C., Cheng, Y., Linder, A., Carell, T., and Hornung, V. (2019). TLR8 Is a Sensor of RNase T2 Degradation Products. *Cell*, **179**(6), 1264–1275.

Haghverdi, L., Büttner, M., Wolf, F. A., Buettner, F., and Theis, F. J. (2016). Diffusion pseudotime robustly reconstructs lineage branching. *Nat Methods*, **13**(10), 845–848.

Kang, H. M., Subramaniam, M., Targ, S., Nguyen, M., Maliskova, L., McCarthy, E., Wan, E., Wong, S., Byrnes, L., Lanata, C. M., Gate, R. E., Mostafavi, S., Marson, A., Zaitlen, N., Criswell, L. A., and Ye, C. J. (2018). Multiplexed droplet single-cell RNA-sequencing using natural genetic variation. *Nat Biotechnol*, **36**(1), 89–94.

Karin, M. and Delhase, M. (2000). The I kappa B kinase (IKK) and NF-kappa B: key elements of proinflammatory signalling. *Semin Immunol*, **12**(1), 85–98.

Khuder, S. A., Al-Hashimi, I., Mutgi, A. B., and Altorok, N. (2015). Identification of potential genomic biomarkers for Sjögren's syndrome using data pooling of gene expression microarrays. *Rheumatol Int*, **35**(5), 829–836.

Korsunsky, I., Millard, N., Fan, J., Slowikowski, K., Zhang, F., Wei, K., Baglaenko, Y., Brenner, M., Loh, P. R., and Raychaudhuri, S. (2019). Fast, sensitive and accurate integration of single-cell data with Harmony. *Nat Methods*, **16**(12), 1289–1296.

Love, M. I., Huber, W., and Anders, S. (2014). Moderated estimation of fold change and dispersion for RNA-seq data with DESeq2. *Genome Biol*, **15**(12), 550.

Maranville, J. C., Luca, F., Richards, A. L., Wen, X., Witonsky, D. B., Baxter, S., Stephens, M., and Di Rienzo, A. (2011). Interactions between glucocorticoid treatment and cis-regulatory polymorphisms contribute to cellular response phenotypes. *PLoS Genet*, **7**(7), e1002162.

Melsted, P., Ntranos, V., and Pachter, L. (2019). The barcode, UMI, set format and BUStools. *Bioinformatics*, **35**(21), 4472–4473.

Melsted, P., Booeshaghi, A. S., Liu, L., Gao, F., Lu, L., Min, K. H. J., da Veiga Beltrame, E., Hjörleifsson, K. E., Gehring, J., and Pachter, L. (2021). Modular, efficient and constant-memory single-cell RNA-seq preprocessing. *Nat Biotechnol*, **39**(7), 813–818.

Moyerbrailean, G. A., Richards, A. L., Kurtz, D., Kalita, C. A., Davis, G. O., Harvey, C. T., Alazizi, A., Watza, D., Sorokin, Y., Hauff, N., Zhou, X., Wen, X., Pique-Regi, R., and Luca, F. (2016). High-throughput allele-specific expression across 250 environmental conditions. *Genome Res*, **26**(12), 1627–1638.

Ongen, H., Buil, A., Brown, A. A., Dermitzakis, E. T., and Delaneau, O. (2016). Fast and efficient QTL mapper for thousands of molecular phenotypes. *Bioinformatics*, **32**(10), 1479–1485.

Pique-Regi, R., Ortega, A., and Asgharzadeh, S. (2005). Sequential diagonal linear discriminant analysis (seqdlda) for microarray classification and gene identification. *2005 IEEE Computational Systems Bioinformatics Conference-Workshops*, pages 112–113.

Qiu, X., Mao, Q., Tang, Y., Wang, L., Chawla, R., Pliner, H. A., and Trapnell, C. (2017). Reversed graph embedding resolves complex single-cell trajectories. *Nat Methods*, **14**(10), 979–982.

R Core Team (2020). *R: A Language and Environment for Statistical Computing*. R Foundation for Statistical Computing, Vienna, Austria.

Resztak, J. A., Farrell, A. K., Mair-Meijers, H., Alazizi, A., Wen, X., Wildman, D. E., Zilioli, S., Slatcher, R. B., Pique-Regi, R., and Luca, F. (2021). Psychosocial experiences modulate asthma-associated genes through gene-environment interactions. *Elife*, **10**.

Ritchie, M. E., Phipson, B., Wu, D., Hu, Y., Law, C. W., Shi, W., and Smyth, G. K. (2015). limma powers differential expression analyses for RNA-sequencing and microarray studies. *Nucleic Acids Res*, **43**(7), e47.

Sandri, M. and Robbins, J. (2014). Proteotoxicity: an underappreciated pathology in cardiac disease. *J Mol Cell Cardiol*, **71**, 3–10.

Sarkar, A. K., Tung, P. Y., Blischak, J. D., Burnett, J. E., Li, Y. I., Stephens, M., and Gilad, Y. (2019). Discovery and characterization of variance QTLs in human induced pluripotent stem cells. *PLoS Genet*, **15**(4), e1008045.

Silva, M. M., Gil, L. H., Marques, E. T., and Calzavara-Silva, C. E. (2013). Potential biomarkers for the clinical prognosis of severe dengue. *Mem Inst Oswaldo Cruz*, **108**(6), 755–762.

Sivan, G., Martin, S. E., Myers, T. G., Buehler, E., Szymczyk, K. H., Ormanoglu, P., and Moss, B. (2013). Human genome-wide RNAi screen reveals a role for nuclear pore proteins in poxvirus morphogenesis. *Proc Natl Acad Sci U S A*, **110**(9), 3519–3524.

Stephens, M. (2017). False discovery rates: a new deal. *Biostatistics*, **18**(2), 275–294.

Stuart, T., Butler, A., Hoffman, P., Hafemeister, C., Papalexi, E., Mauck, W. M., Hao, Y., Stoeckius, M., Smibert, P., and Satija, R. (2019). Comprehensive Integration of Single-Cell Data. *Cell*, **177**(7), 1888–1902.

Svensson, V. (2020). Droplet scRNA-seq is not zero-inflated. *Nat Biotechnol*, **38**(2), 147–150.

Tai, A. W., Benita, Y., Peng, L. F., Kim, S. S., Sakamoto, N., Xavier, R. J., and Chung, R. T. (2009). A functional genomic screen identifies cellular cofactors of hepatitis C virus replication. *Cell Host Microbe*, **5**(3), 298–307.

Urbut, S. M., Wang, G., Carbonetto, P., and Stephens, M. (2019). Flexible statistical methods for estimating and testing effects in genomic studies with multiple conditions. *Nat Genet*, **51**(1), 187–195.

Wang, C., Cicek, M. S., Charbonneau, B., Kalli, K. R., Armasu, S. M., Larson, M. C., Konecny, G. E., Winterhoff, B., Fan, J. B., Bibikova, M., Chien, J., Shridhar, V., Block, M. S., Hartmann, L. C., Visscher, D. W., Cunningham, J. M., Knutson, K. L., Fridley, B. L., and Goode, E. L. (2014). Tumor hypomethylation at 6p21.3 associates with longer time to recurrence of high-grade serous epithelial ovarian cancer. *Cancer Res*, **74**(11), 3084–3091.

Wang, Z. V. and Hill, J. A. (2015). Protein quality control and metabolism: bidirectional control in the heart. *Cell Metab*, **21**(2), 215–226.

Weckle, A., Aiello, A. E., Uddin, M., Galea, S., Coulborn, R. M., Soliven, R., Meier, H., and Wildman, D. E. (2015). Rapid Fractionation and Isolation of Whole Blood Components in Samples Obtained from a Community-based Setting. *J Vis Exp*, (105).

Wolf, F. A., Angerer, P., and Theis, F. J. (2018). SCANPY: large-scale single-cell gene expression data analysis. *Genome Biol*, **19**(1), 15.

Yu, G., Wang, L. G., Han, Y., and He, Q. Y. (2012). clusterProfiler: an R package for comparing biological themes among gene clusters. *OMICS*, **16**(5), 284–287.

Zhang, Y., Quick, C., Yu, K., Barbeira, A., Luca, F., Pique-Regi, R., Kyung Im, H., and Wen, X. (2020). PTWAS: investigating tissue-relevant causal molecular mechanisms of complex traits using probabilistic TWAS analysis. *Genome Biol*, **21**(1), 232.

Zheng, X., Levine, D., Shen, J., Gogarten, S. M., Laurie, C., and Weir, B. S. (2012). A high-performance computing toolset for relatedness and principal component analysis of SNP data. *Bioinformatics*, **28**(24), 3326–3328.

Supplementary Figures

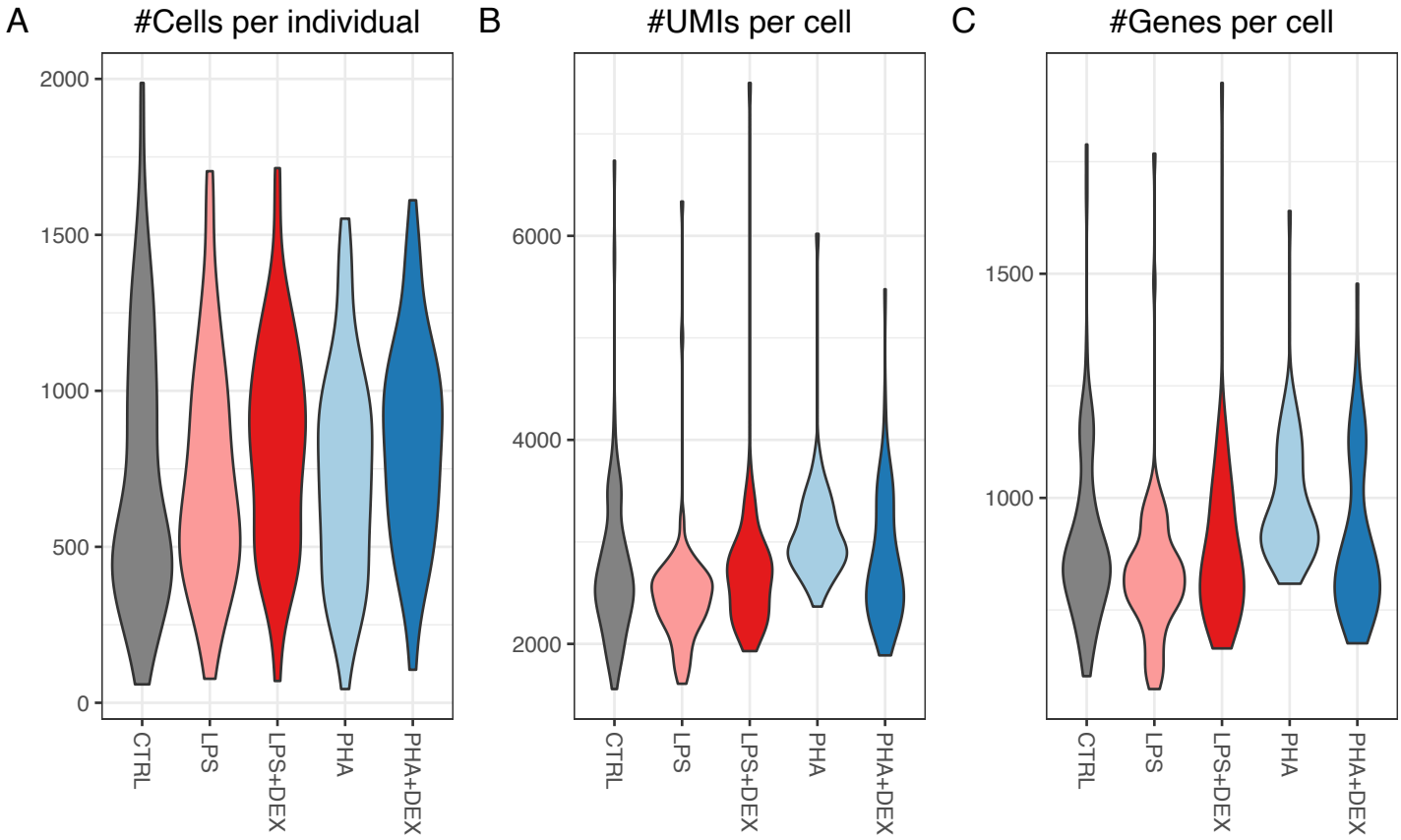

Figure S1: **Violin plots of summary statistics per individual across five conditions (A)** number of measured cells per individual for each treatment. **(B)** average UMIs per cell from one individual for each treatment. **(C)** average number of detected genes per cell from one individual for each treatment.

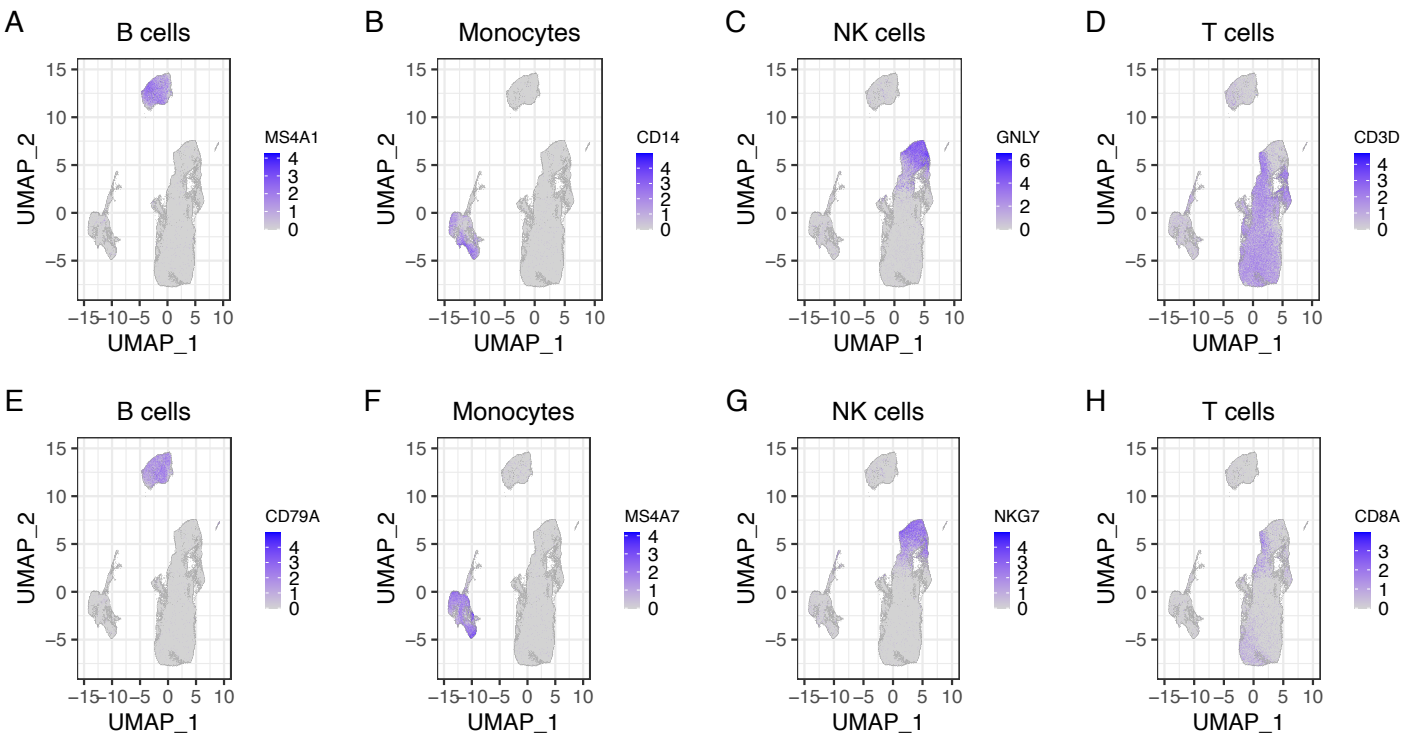

Figure S2: **Canonical immune cell type–specific markers expressed on UMAP: (A and E)** represent B cell-specific gene expressions (*MS4A1* and *CD79A*) on UMAP; **(B and F)** represent Monocyte-specific gene expressions (*MS4A7* and *CD14*) on UMAP; **(C and G)** represent NK cell-specific gene expressions (*GNLY* and *NKG7*) on UMAP; **(D and H)** represent T cell specific gene expressions (*CD3D* and *CD8A*) on UMAP.

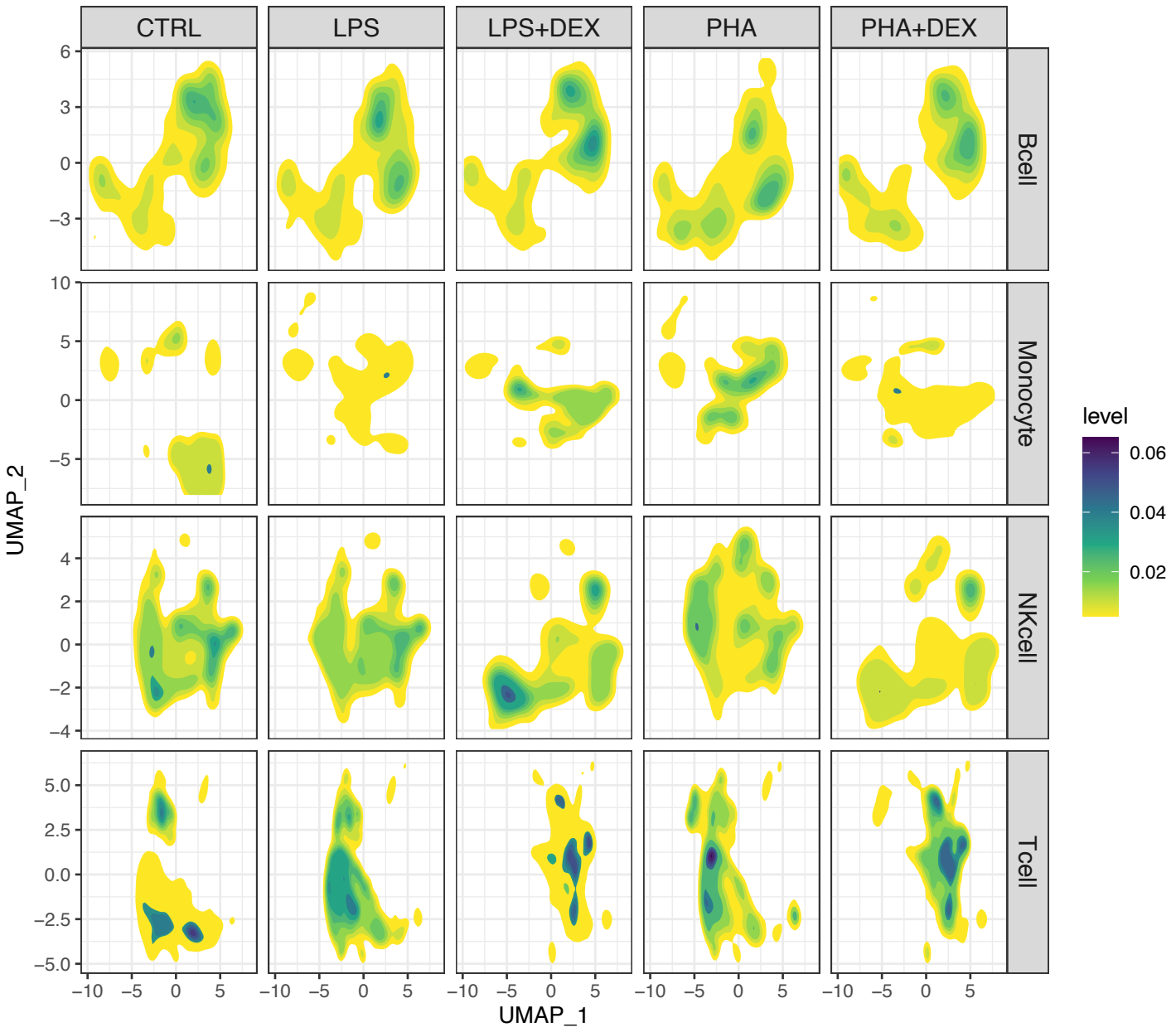

Figure S3: **Density distribution of cells on UMAP for cell types and treatment separately**. Blue color indicates high density of cells while yellow color indicates lower density.

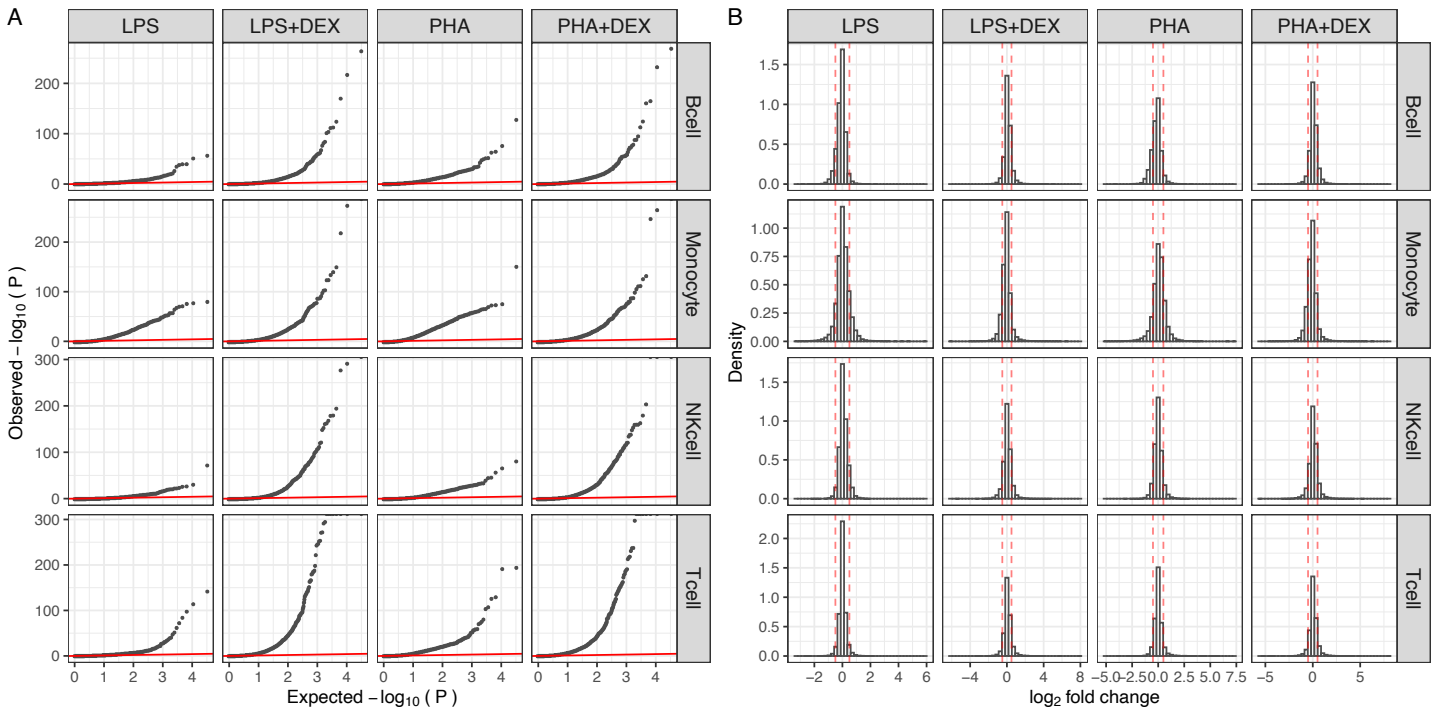

Figure S4: **Overview of results of differential expression analysis: (A)** Q-Q plots for 4 contrasts (LPS, LPS+DEX, PHA and PHA+DEX) across cell types, **(B)** Histograms of $\log_2$ fold changes of gene expression, red dashed lines denoting the $|\log_2 FoldChange|$ being 0.5, the cutoff value that is used for defining differentially expressed genes (DEGs).

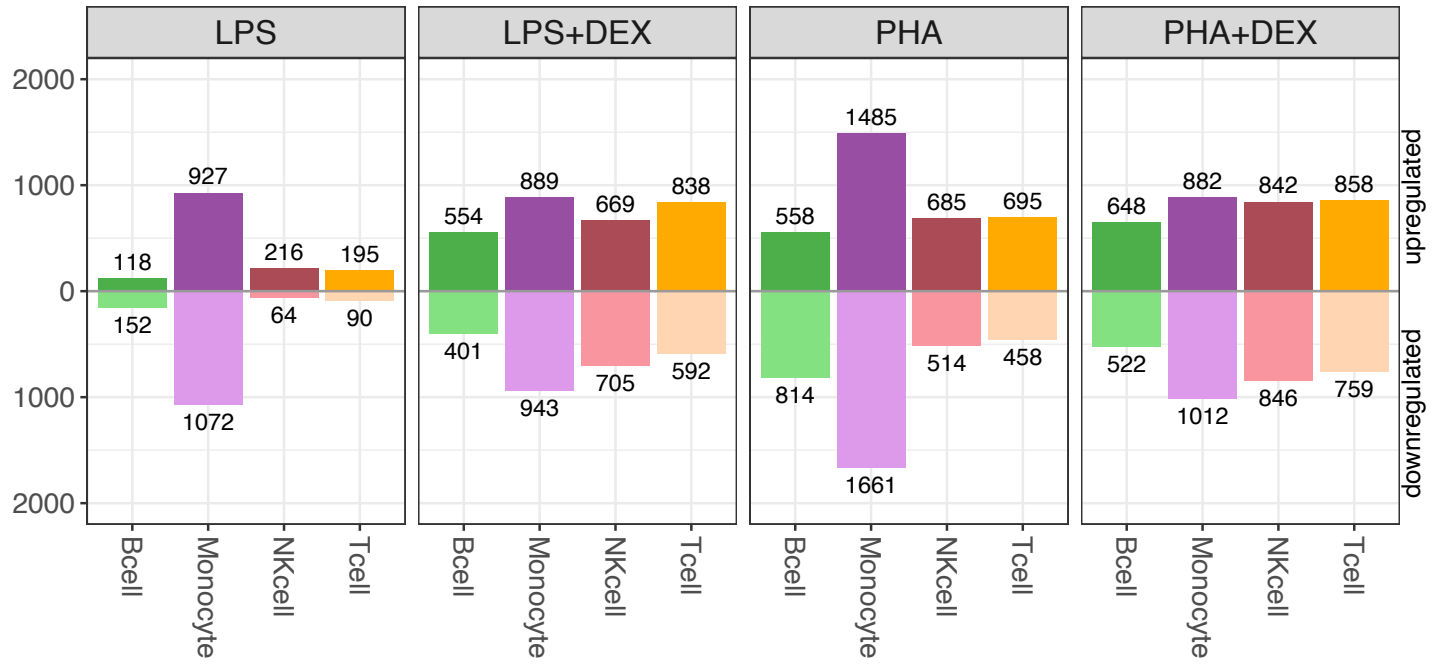

Figure S5: **Number of DEGs across contrasts and cell types;** B cells (green), Monocytes (purple), NK cells (maroon) and T cells (orange), below axis representing down-regulated genes and above axis representing up-regulated genes (FDR<10% and $|LFC| > 0.5$).

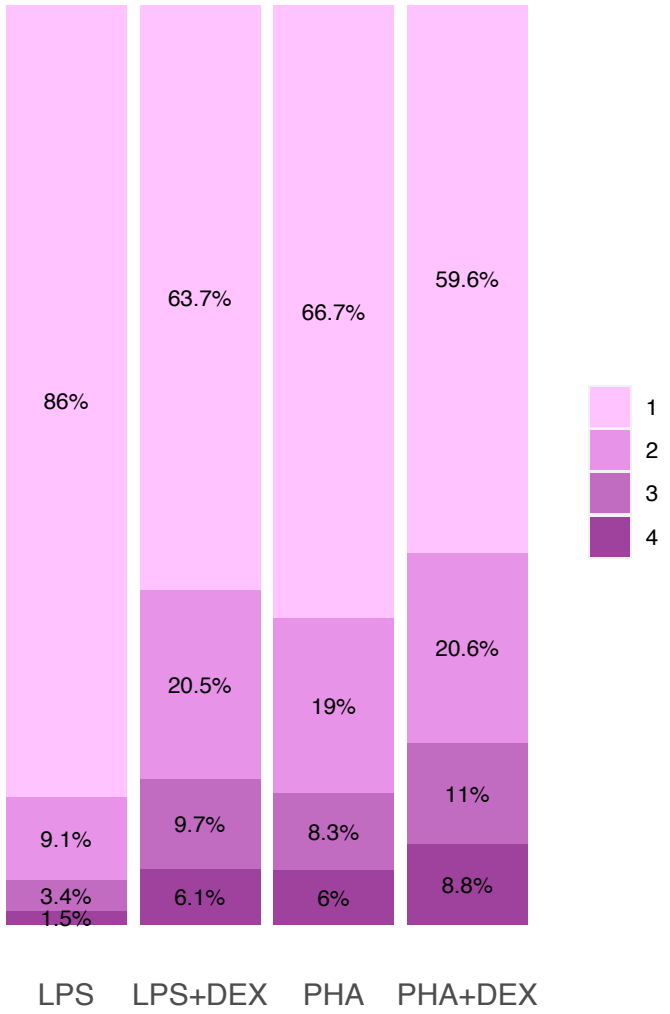

Figure S6: **Cell type sharing of DEGs in four contrast conditions, 1=DEGs detected in only a single cell type and 4=DEGs detected across all the four cell types.**

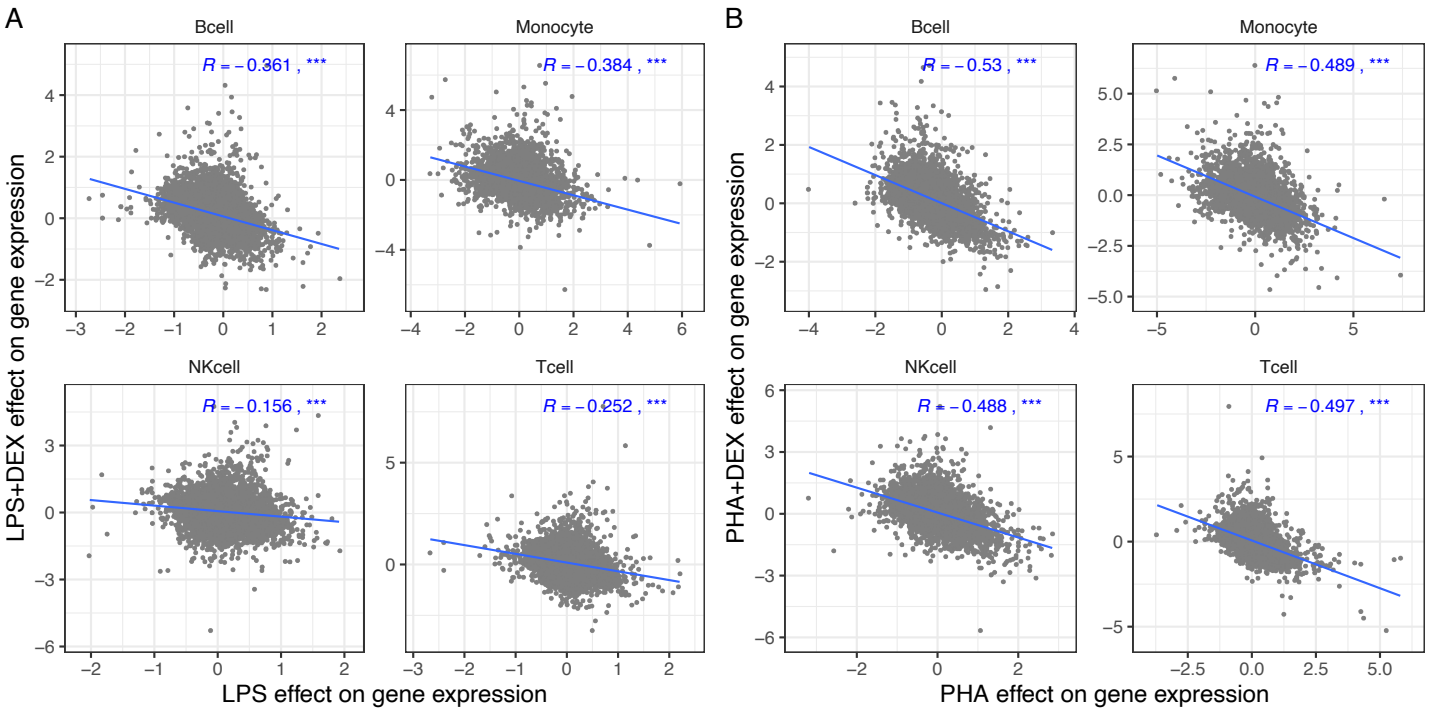

Figure S7: **Dexamethasone (DEX) reverses effects of activation by immune stimuli on gene expression:**. **(A)** Scatterplots of LPS effect on gene expression (x axis) against DEX effect on gene expression (y axis). **(B)** Scatterplots of PHA effect on gene expression (x axis) against DEX effect on gene expression (y axis). Blue lines represent the linear trend between the effects of immune stimuli and DEX treatments on gene expression. *R* represents the correlation coefficients of the effects of two types of immune treatments on gene expression, *denoting $p < 0.05$, ** denoting $p < 0.01$ and *** denoting $p < 0.001$.

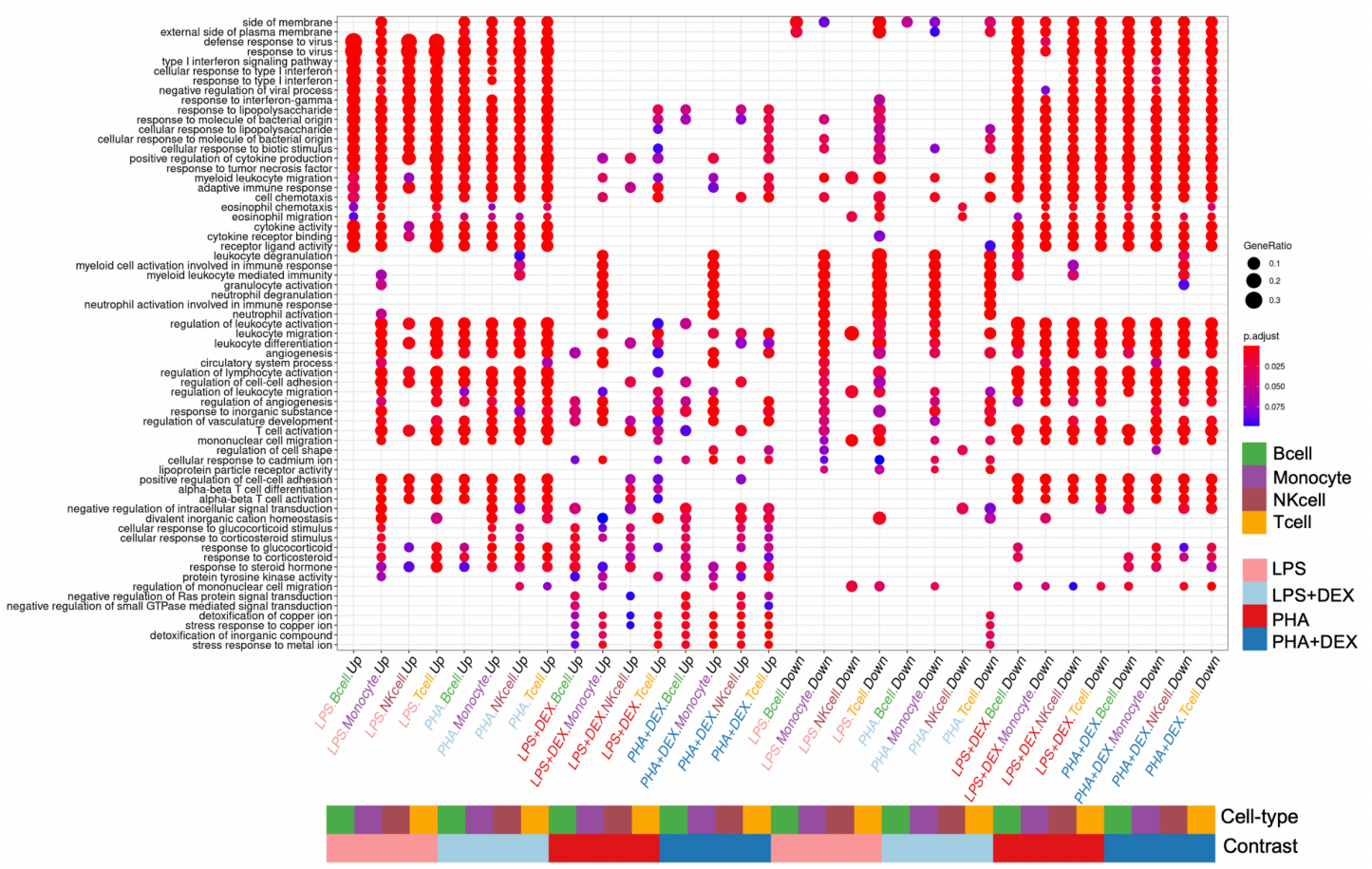

Figure S8: **Visualization of Gene Ontology (GO) enrichment analysis:** The dotplots show the union of the top 5 GO terms for each condition (down-regulated and up-regulated separately) across 16 conditions (4 contrasts $\times$ 4 cell types).

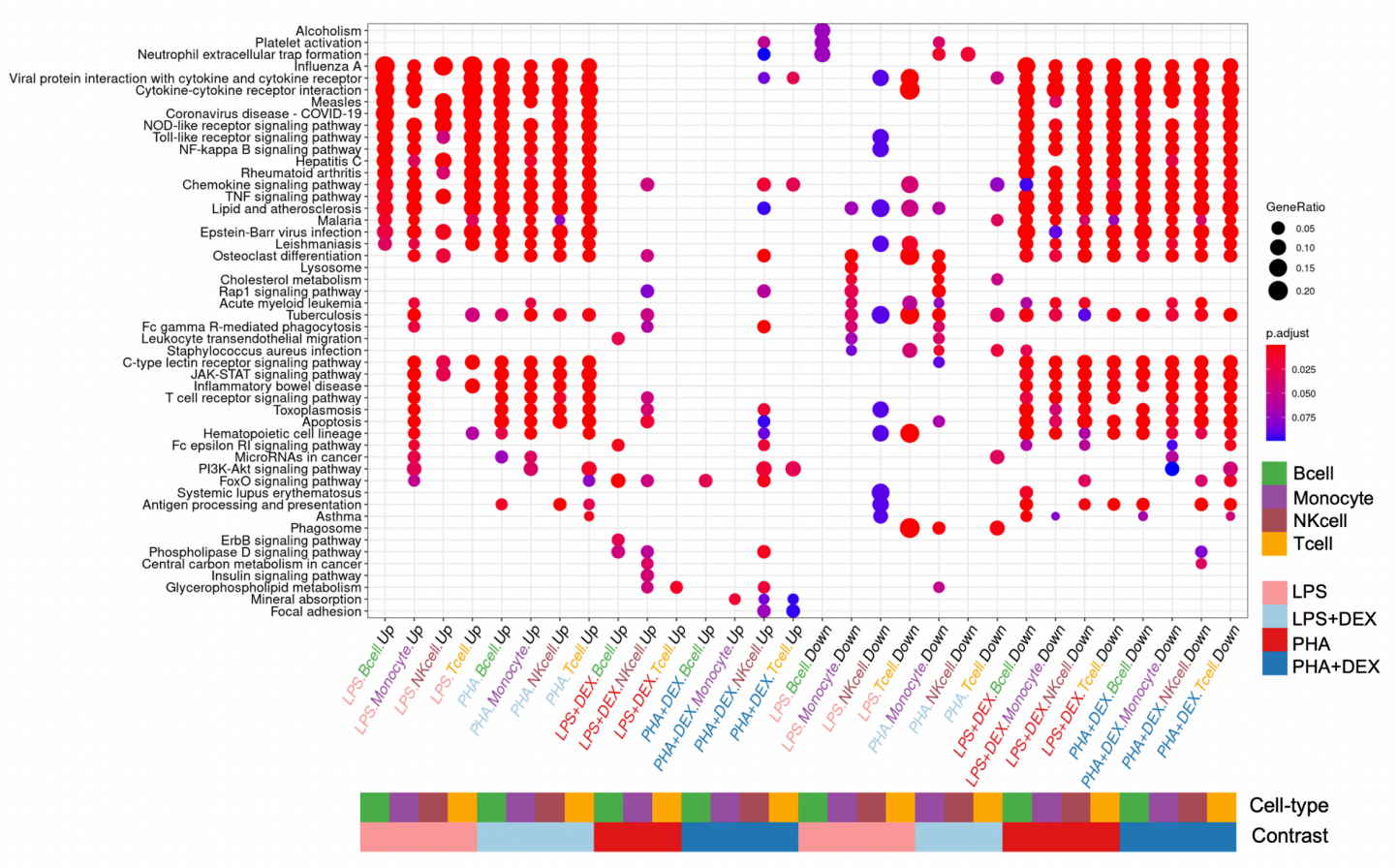

Figure S9: **Visualization of Kyoto Encyclopedia of Genes and Genomes (KEGG) enrichment analysis:** The dotplots show the union of the top 5 KEGG terms for each condition(down-regulated and up-regulated separately) across 16 conditions (4 contrasts $\times$ 4 cell types).

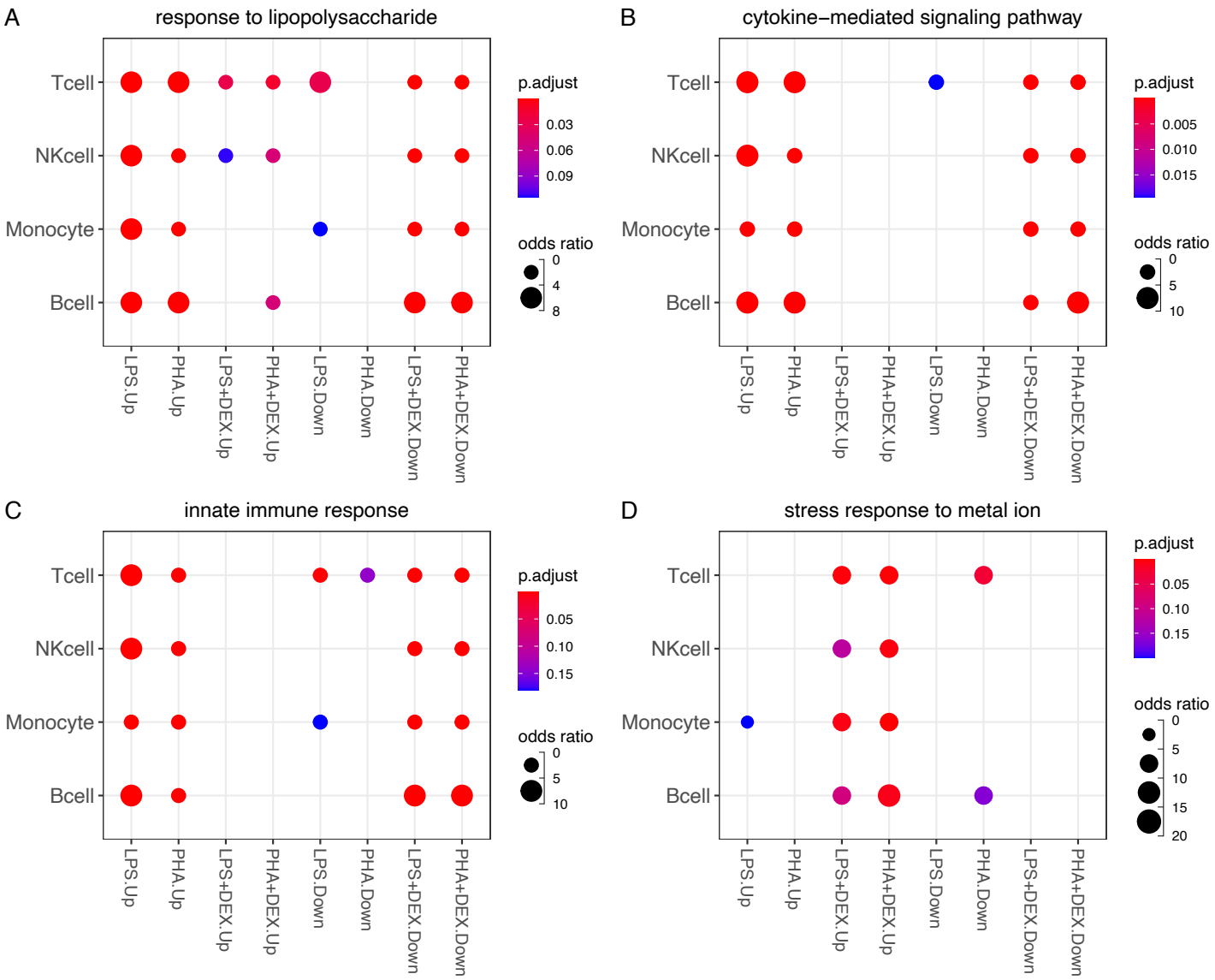

Figure S10: **Examples of the enriched pathways for DEGs: (A-D)**represents the enrichment results of the four example pathways across cell types and conditions,, response to lipopolysaccharide, cytokine-mediated signaling pathway, innate immune response and cellular response to glucocorticoid stimulus, respectively.

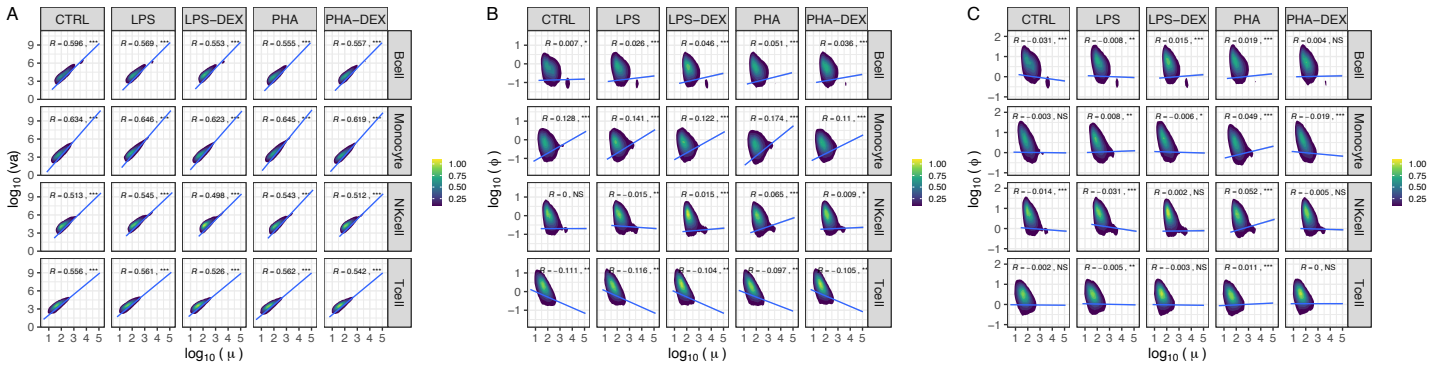

Figure S11: **Both variance and dispersion of gene expression strongly depend on mean gene expression while mean-corrected dispersion is relatively independent on mean expression value: (A)** Scatter plots of $\log_{10}$ mean gene expression (x axis) against $\log_{10}$ variance of gene expression. **(B)** Scatter plots of $\log_{10}$ mean gene expression (x axis) against $\log_{10}$ dispersion of gene expression. **(C)** Scatter plots of $\log_{10}$ mean gene expression (x axis) against $\log_{10}$ mean-corrected dispersion of gene expression, eventually used for measuring gene expression variability.

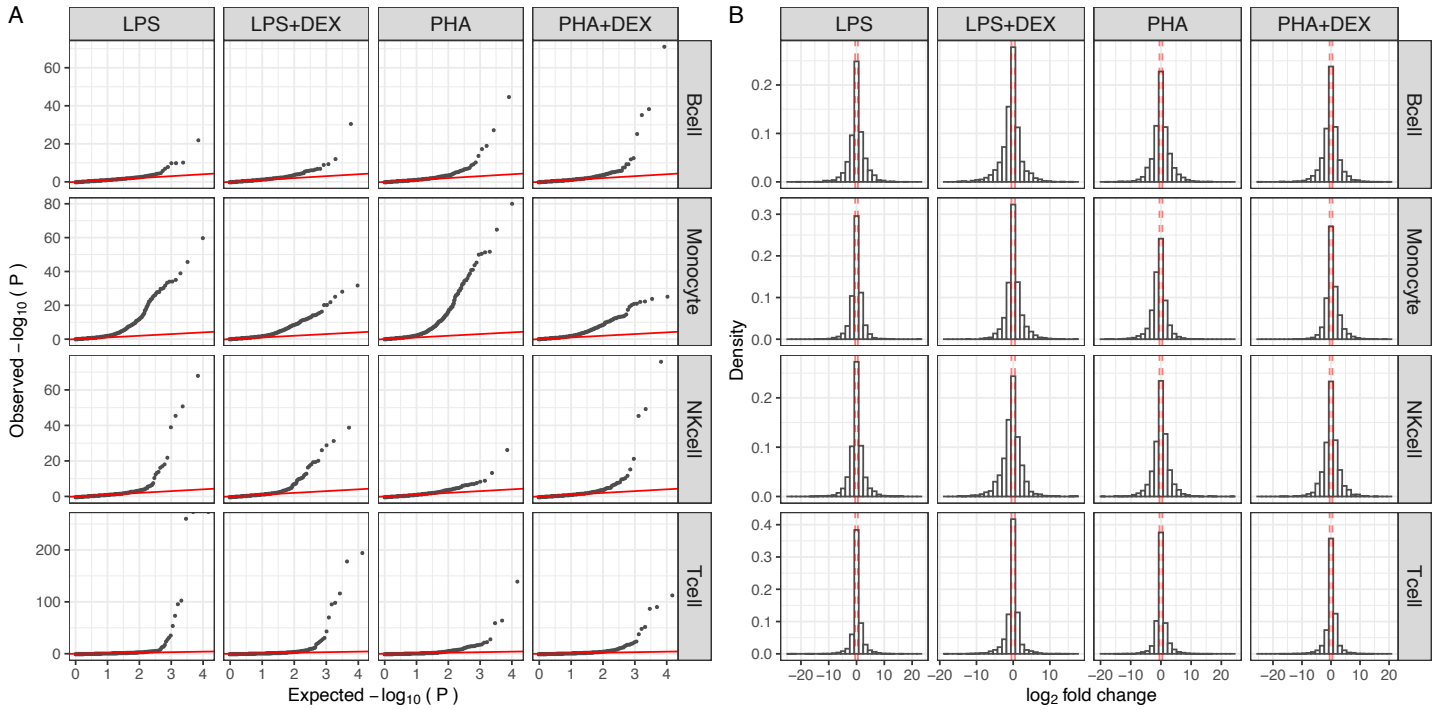

Figure S12: **Overview of results of differential gene variability analysis: (A)** Q-Q plots for 4 contrasts (LPS, LPS+DEX, PHA and PHA+DEX) across 4 cell types. **(B)** Histograms of $\log_2$ fold changes of gene variability, red dashed lines denoting the $|\log_2 FoldChange|$ being 0.5, the cutoff value that is used for defining differentially variable genes (DVGs)

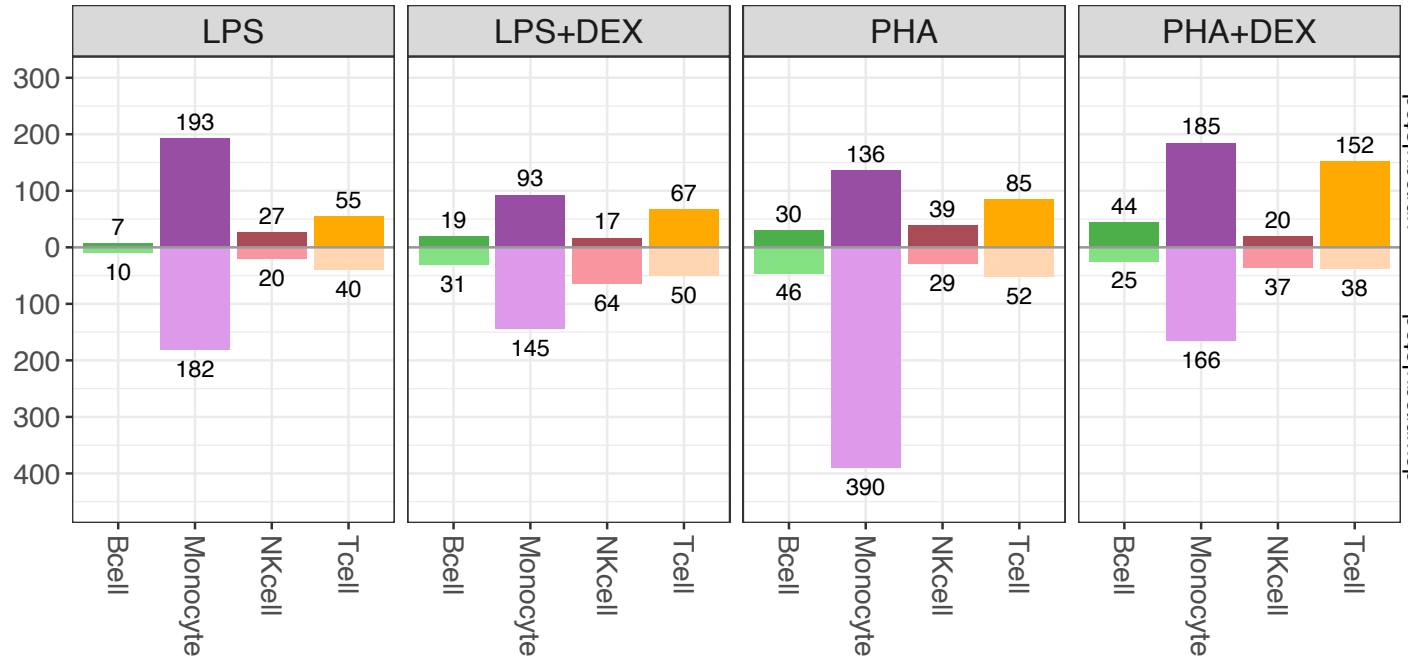

Figure S13: **Number of DVGs across contrasts and cell types:** B cells (green), Monocytes (purple), NK cells (maroon) and T cells (orange), below axis representing genes with decreased variability and above axis representing genes with increased variability (FDR$<$10% and $|LFC| > 0.5$)

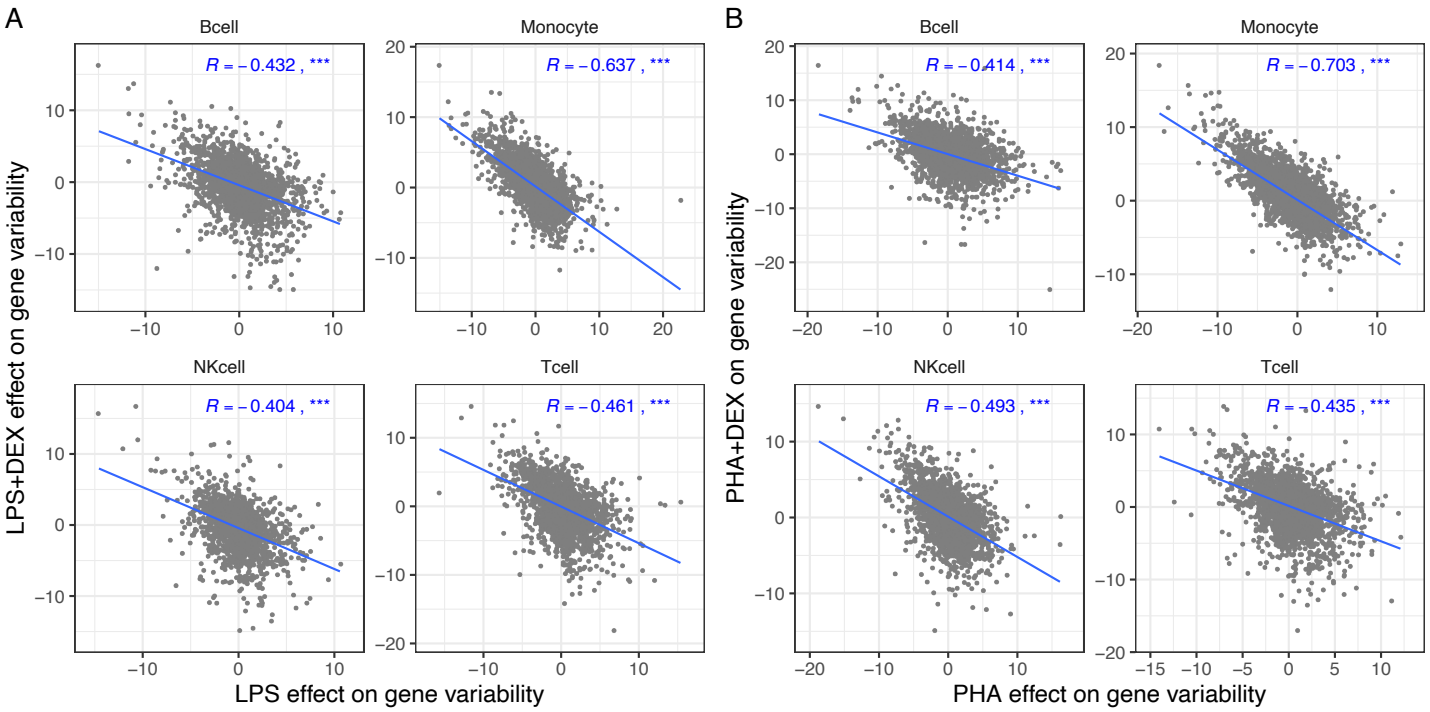

Figure S14: **Dexamethasone (DEX) reverses effect of activation by immune stimuli on gene variability A** Scatterplots of LPS effect on gene variability (x axis) against DEX effect on gene variability (y axis). **B** Scatterplots of PHA effect on gene variability (x axis) against DEX effect on gene variability (y axis). Blue lines represent the linear trend between the effects of immune stimuli and DEX treatments on gene expression. *R* represents the correlation coefficients of the effects of two types of immune treatments on gene expression, *denoting $p \leq 0.05$, ** denoting $p \leq 0.01$ and *** denoting $p \leq 0.001$.

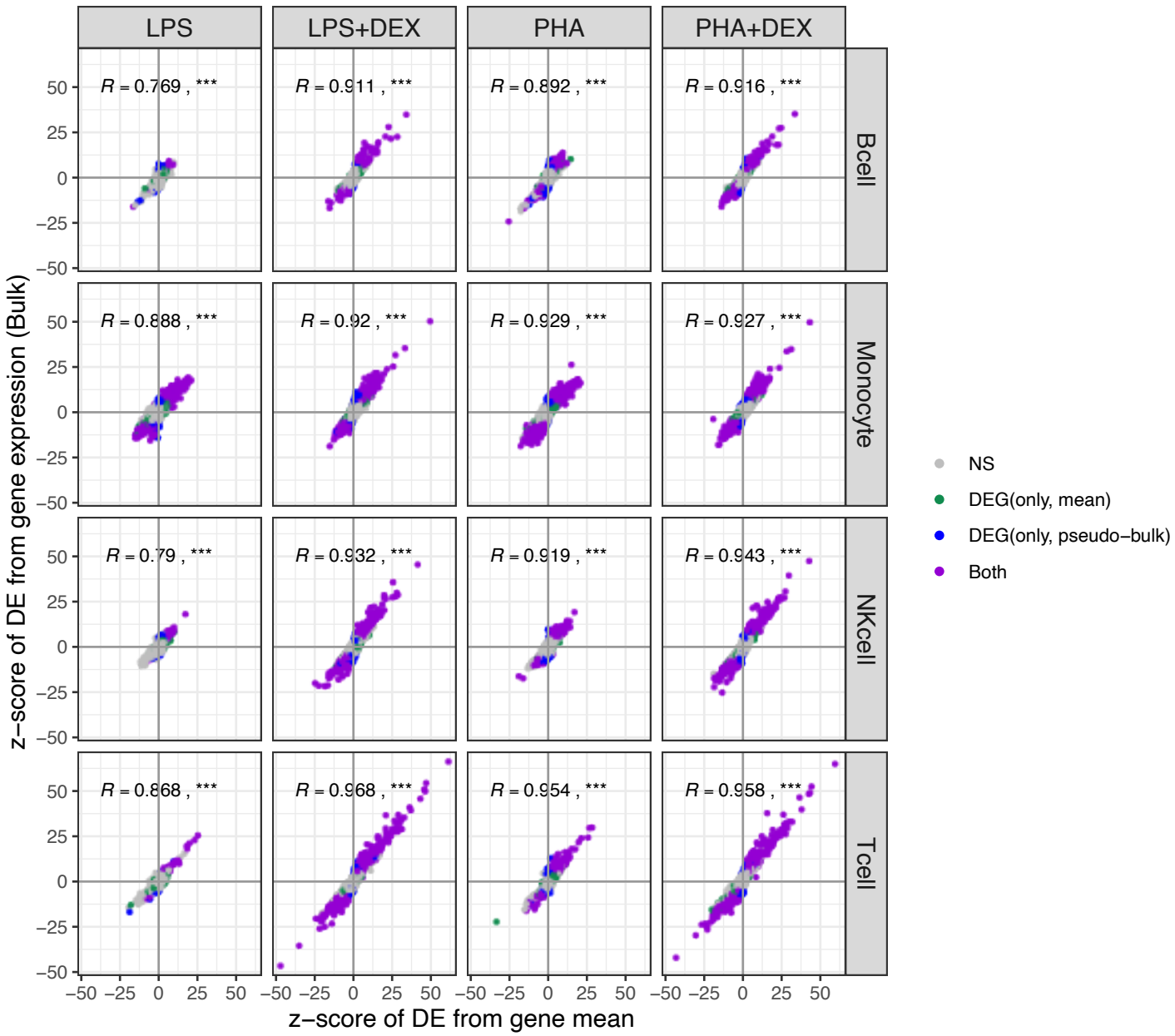

Figure S15: **The scatter plots of the z score of treatment effects on gene mean (x axis) from Negative bionomial distribution against the z score of treatment effects on gene expression (y axis) from bulk data:** Color represents significant treatment effects on gene mean only (green), bulk-derived DEGs only (blue), both (purple) and neither (gray). The *R* represents the correlation coefficients of the treatment effects on gene mean expression and gene bulk expression , $p \geq 0.05$ (NS), $p < 0.05$ (*), $p < 0.01$ (**) and $p < 0.001$(***).

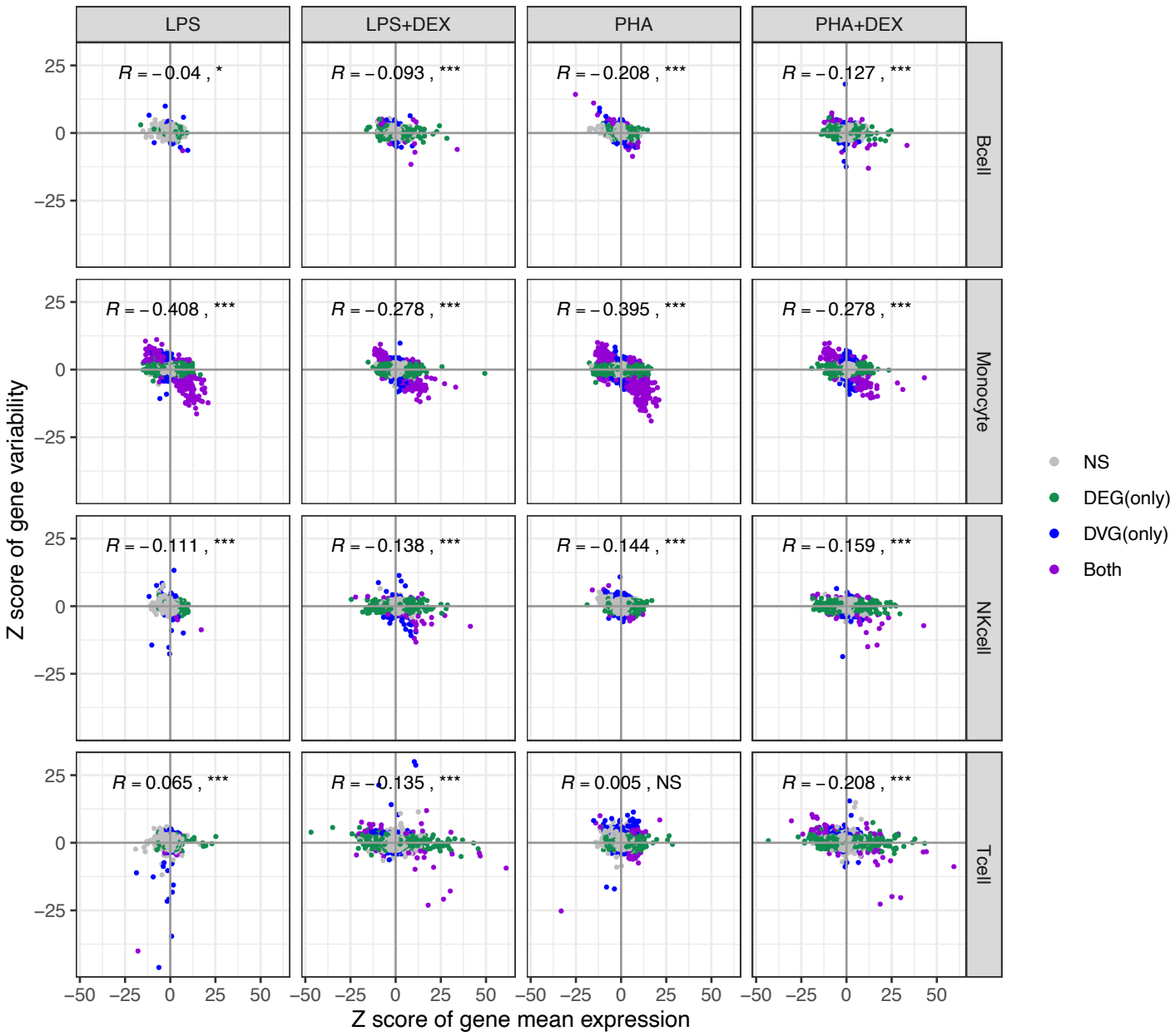

Figure S16: **The scatter plots of the z score of treatment effects on gene mean (x axis) against the z score of treatment effects on gene variability (y axis):** Color represents significant treatment effects on gene mean only (green), gene variability only (blue), both (purple) and neither (gray). The R represents the correlation coefficients of the treatment effects on gene mean and gene variability, $p \geq 0.05$ (NS), $p < 0.05$ (*), $p < 0.01$ (**) and $p < 0.001$(***).

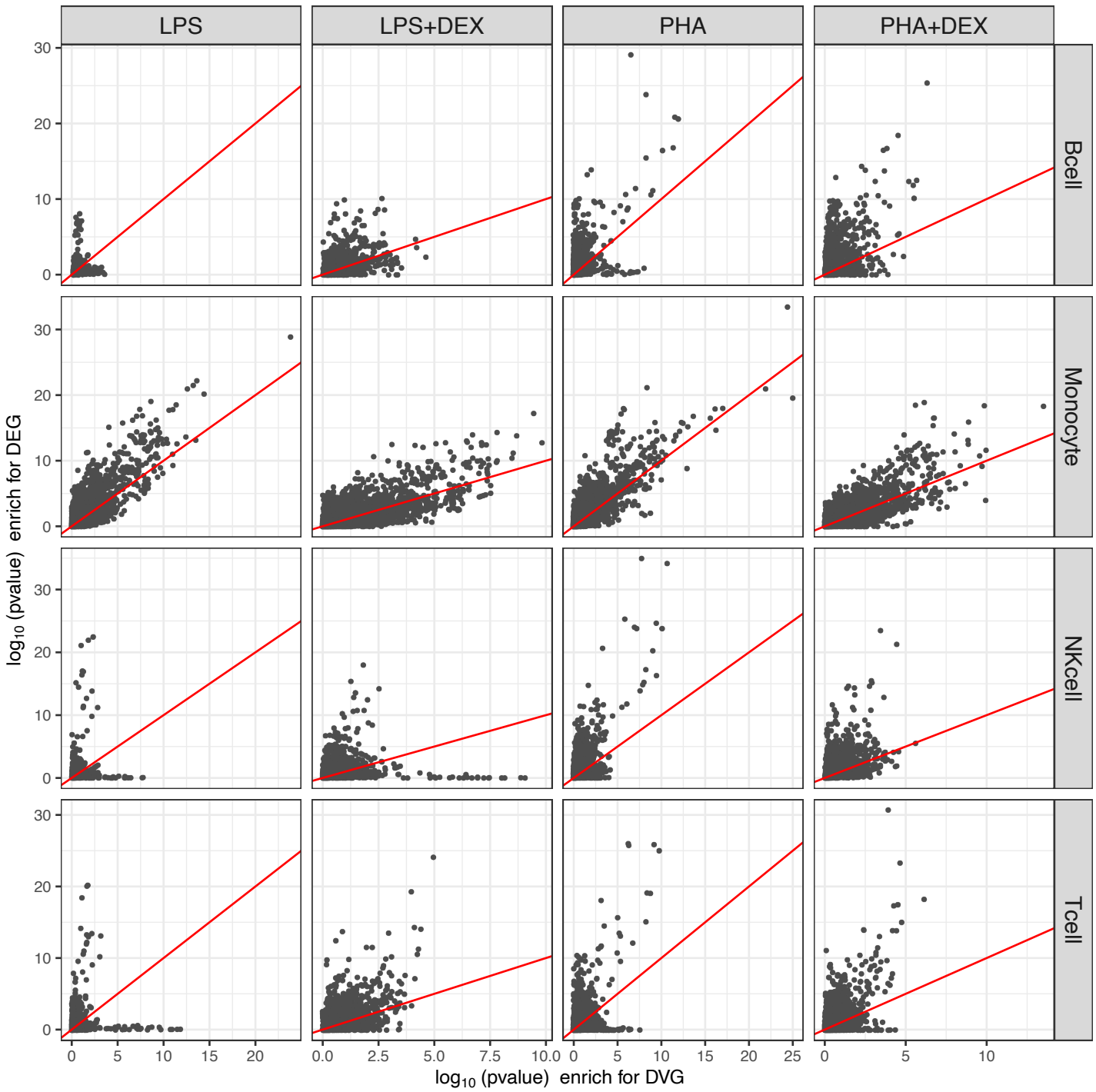

Figure S17: **Comparison of the results of GO enrichment between DEG and DVG**, x axis representing $-\log_{10}(p)$ of the GO terms that are enriched by DVG and Y axis representing $-\log_{10}(p)$ of the GO terms that are enriched by DEG.

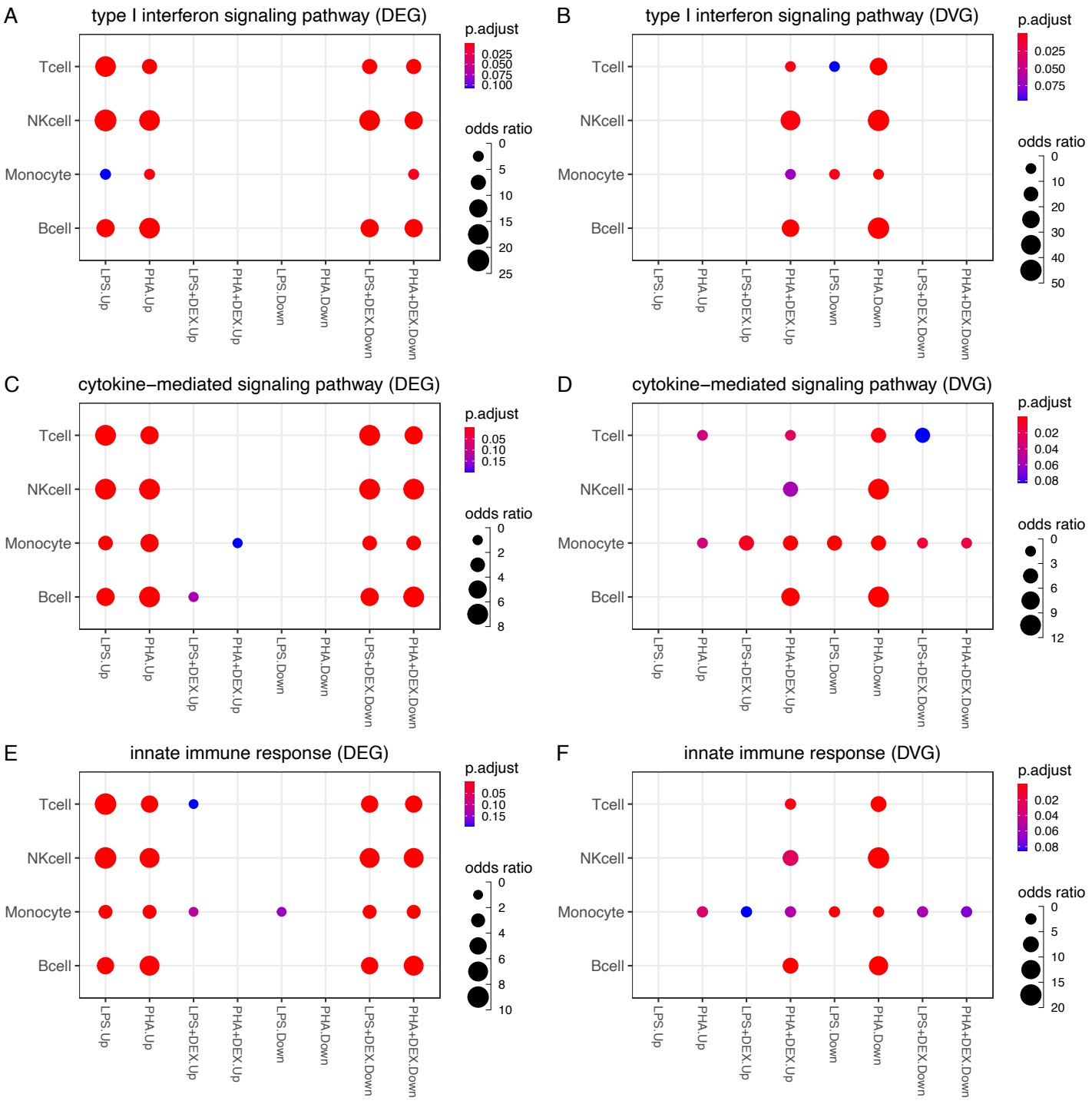

Figure S18: **Examples of shared enrichment pathways for DEG and DVG: (A and B)** represent enrichment results in the type I interferon signaling pathway for DEG and DVG, respectively, **(C and D)** represent enrichment results in the cytokine-mediated signaling pathway for DEG and DVG, respectively, and **(E and F)** represent enrichment results in innate immune response for DEG and DVG, respectively.

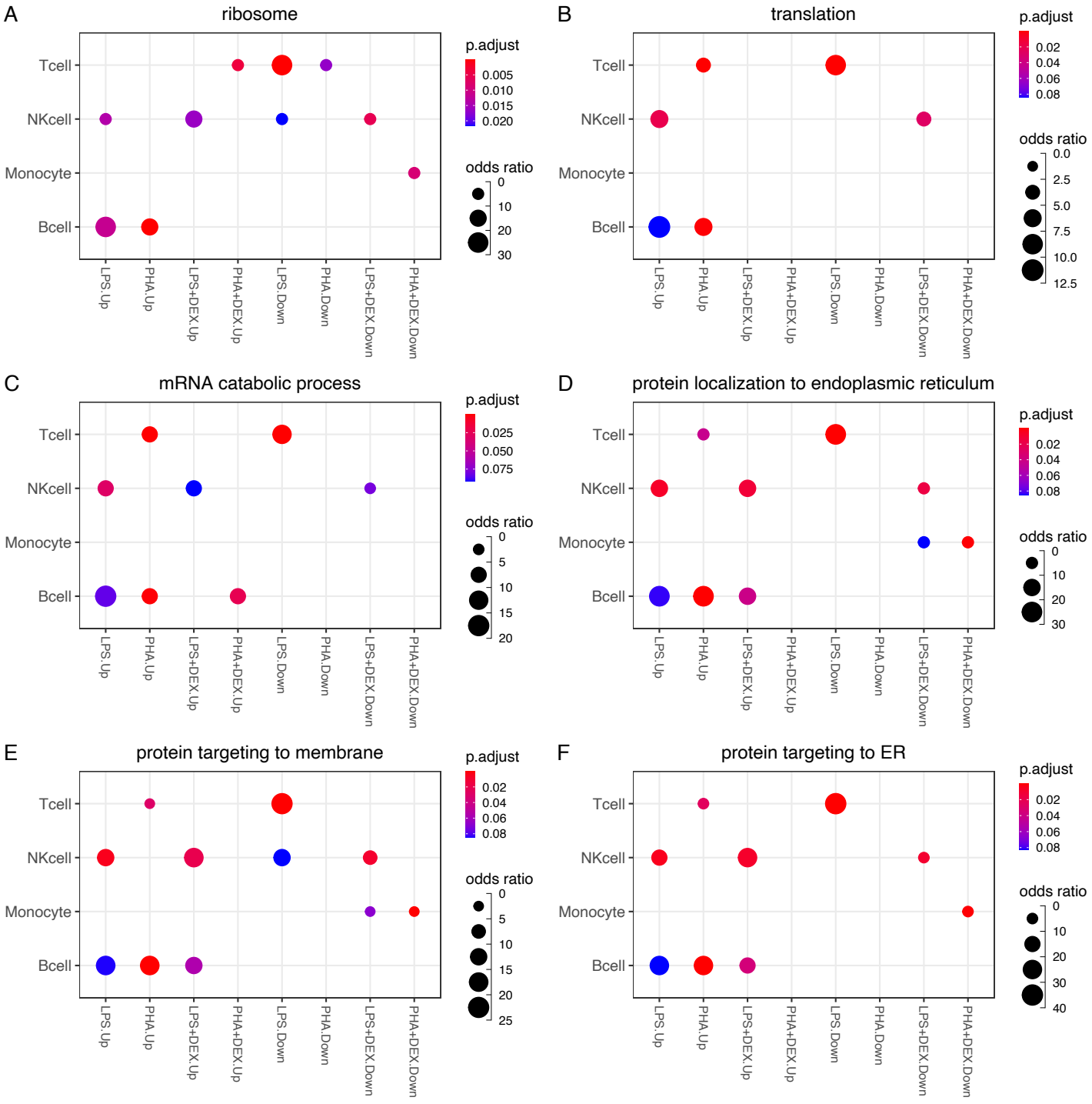

Figure S19: **Examples of the pathways that are only enriched in DVGs: (A-F)** represent enrichment results in ribosome, translation, mRNA catabolic process, protein localization to endoplasmic reticulum, protein targeting to membrane and protein targeting to ER, respectively.

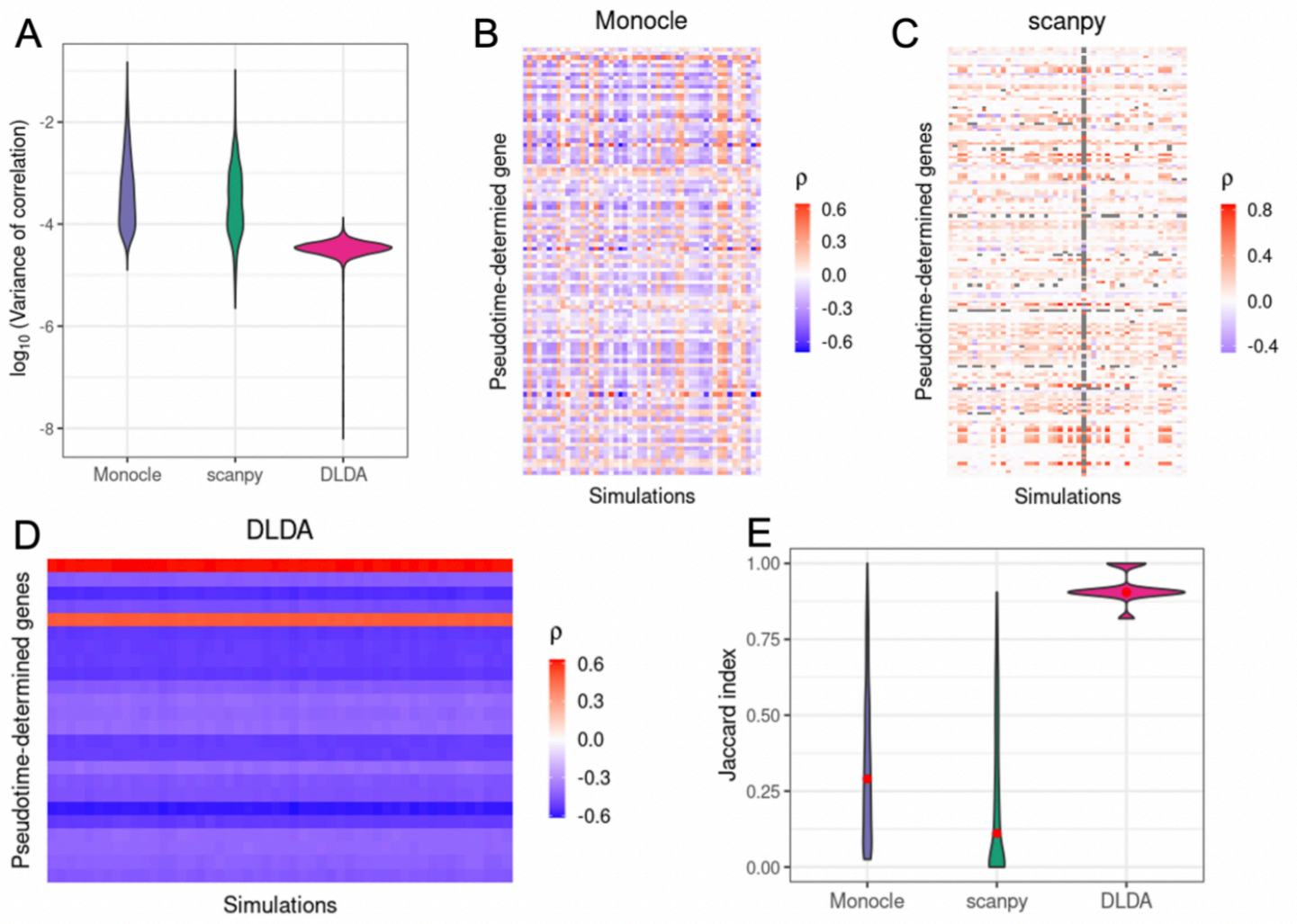

Figure S20: footnotesize **Validation of effectiveness and robustness of the treatment pseudotime trajectory using resampling (A)** Violin plot of the variance of correlation coefficients for each gene across 50 resamplings from Monocle, SCANPY and DLDA. **(B-D)** Heatmaps of the correlation coefficients of top 20 ranking pseudotime driving genes across resampling. Each row represents the same gene and each column a resampling iteration with the color representing the magnitude of the correlation between gene expression and the derived pseudo-time variable; ideally we would like to see that correlation be approximately constant. The resamplings are from **(B)** Monocle, **(C)** SCANPYand **(D)**DLDA, respectively. **(E)** Violin plot of jaccard index of the stability of the top 20 pseudotime correlated genes for each pair of resamplings across 1,225 pairwise comparisons from Monocle, SCANPY and DLDA.

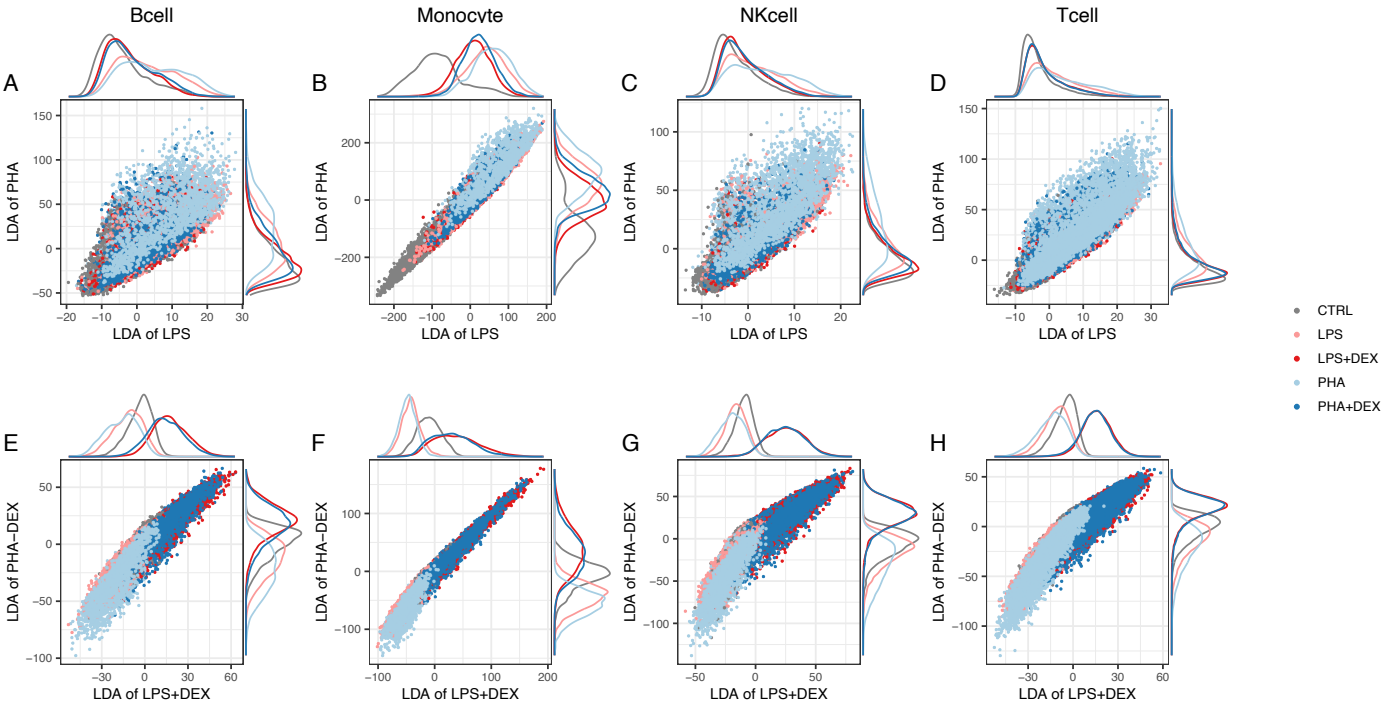

Figure S21: **Low dimensional manifold plots from DLDA across cell types: (A-D)** represent the scatter plots of the DLDA from LPS (x axis) against the DLDA from PHA (y axis) and **(E-H)** represent the scatter plots of the DLDA from LPS+DEX (x axis) against PHA+DEX (y axis).

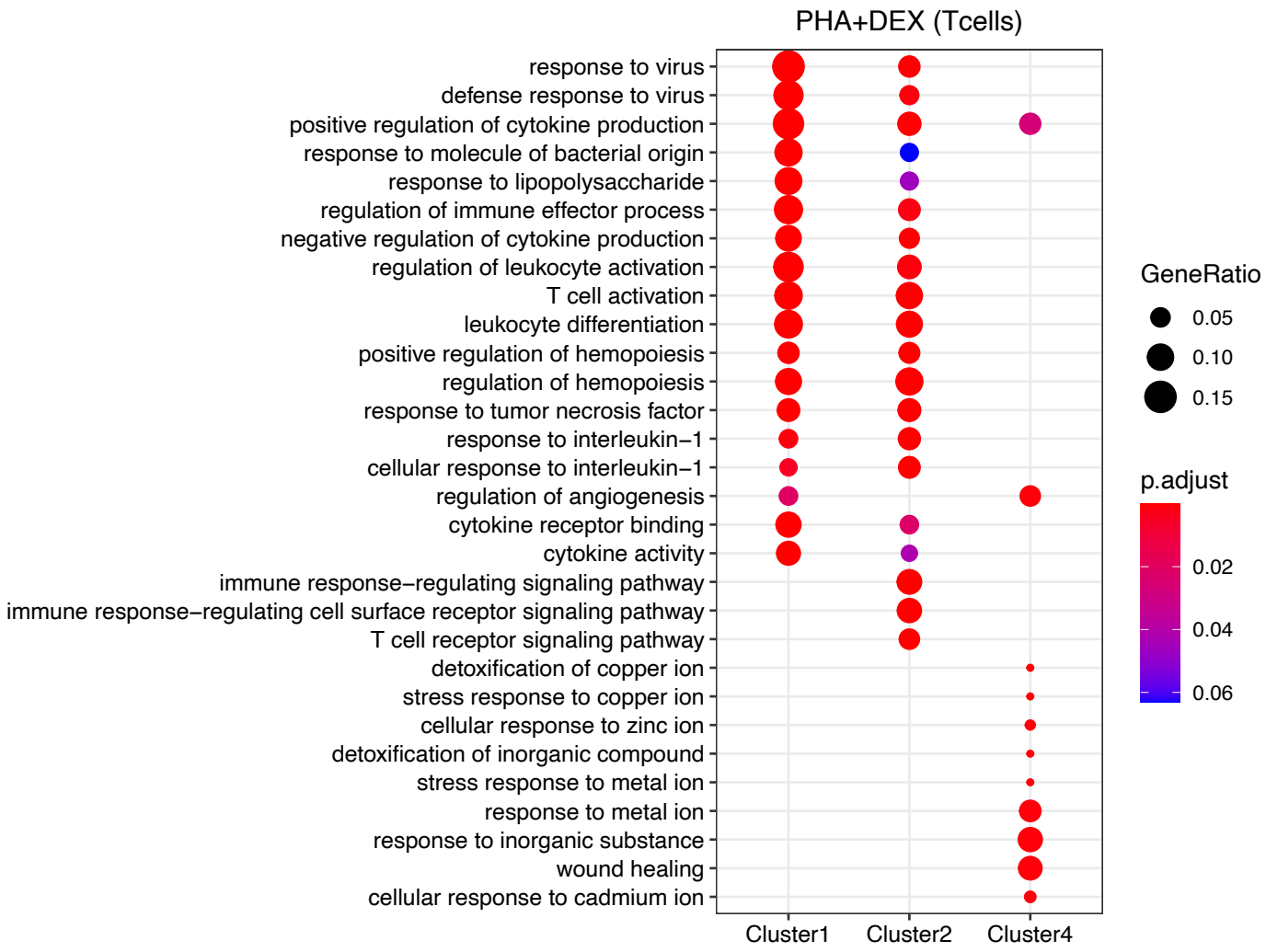

Figure S22: **Gene Ontology enrichment results for four dynamic patterns DEGs respectively**

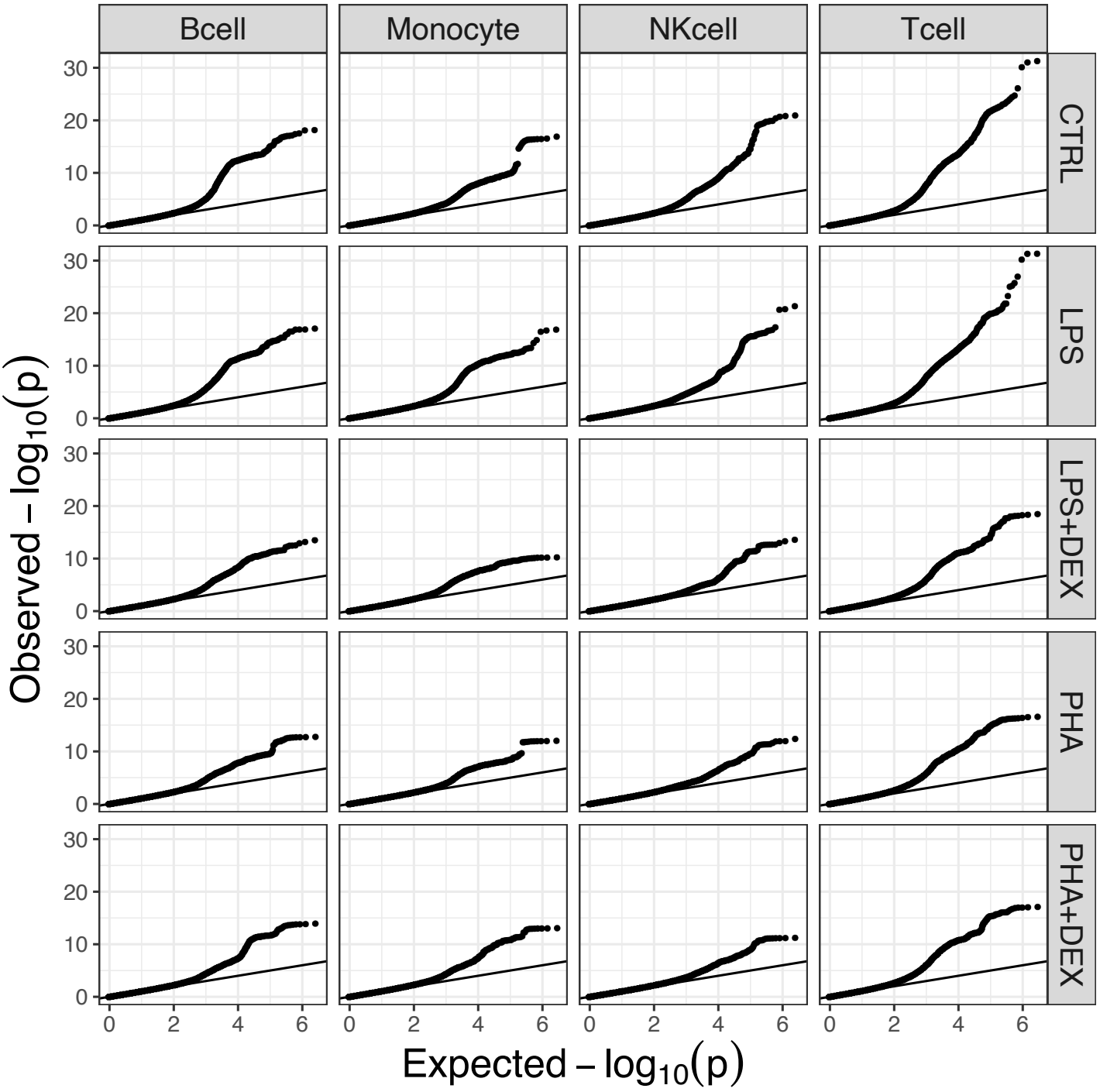

Figure S23: **QQplots of p-values from eQTL mapping with FastQTL on pseudobulk gene expression data across the 20 conditions.**

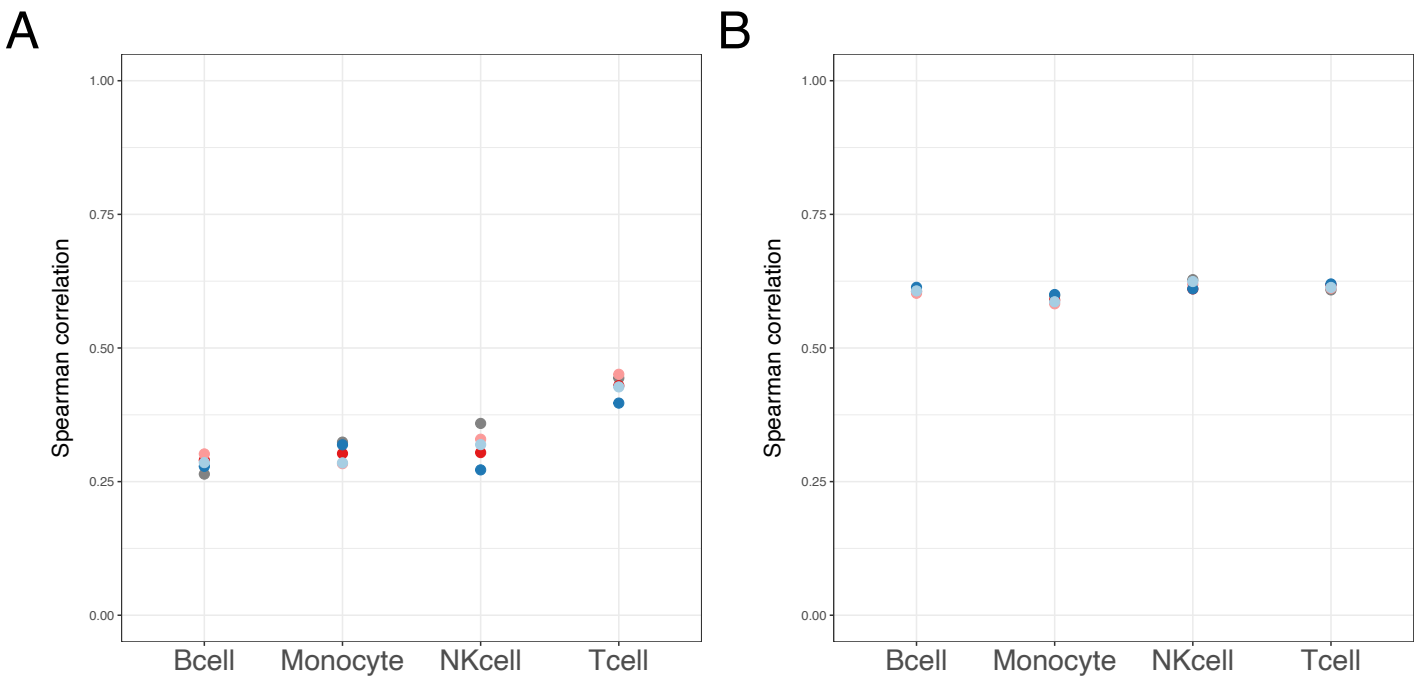

Figure S24: **Correlations between genetic effect sizes assessed in single-cell data and in bulk RNA-seq Resztak *et al.* (2021)A** Spearman's correlations for significant genetic effect sizes assessed by condition-by-condition analysis (FDR< 0.1) **B** Spearman's correlations for significant genetic effect sizes assessed by multivariate adaptive shrinkage analysis (LFSR< 0.1). Color denotes treatment: grey – control, light blue – PHA, dark blue – PHA+DEX, pink – LPS, red – LPS+DEX. All values are significant (p-value< 0.05).

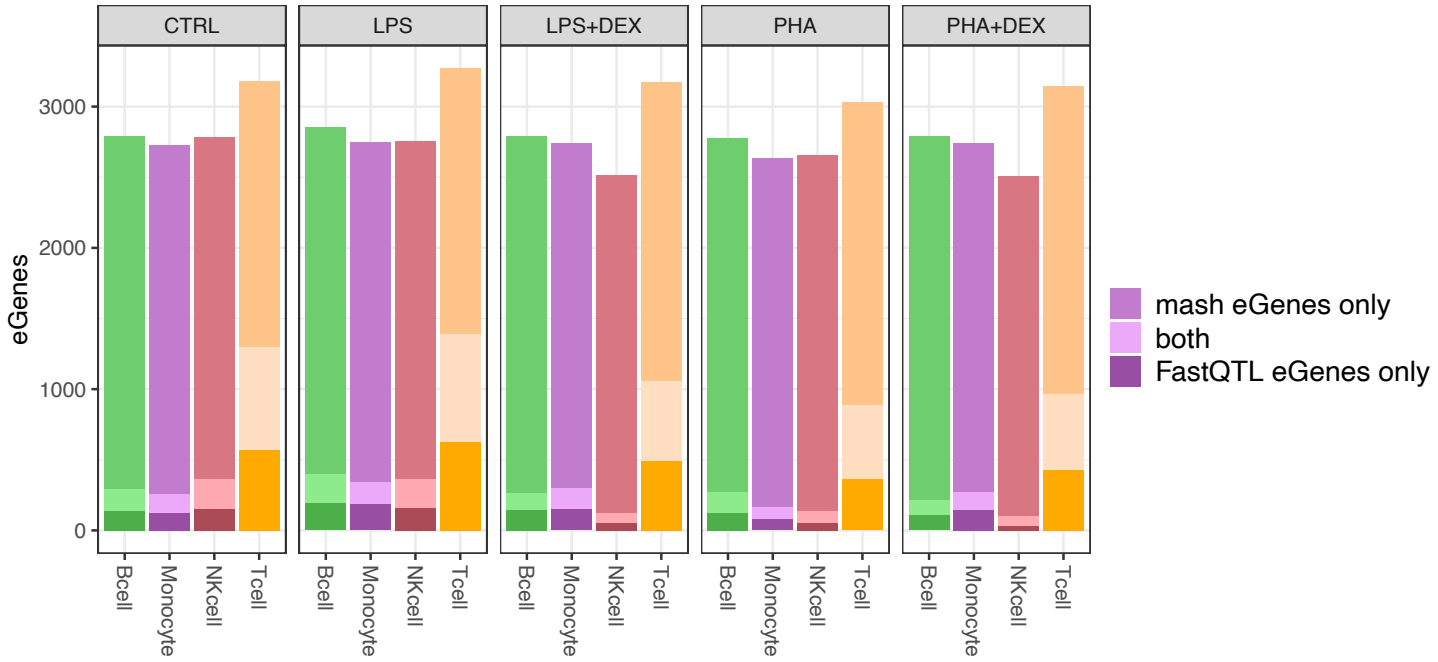

Figure S25: **eQTL mapping results.** Barplot represents the number of genes with eQTLs (eGenes) significant in only condition-by-condition analysis (FDR$<$ 0.1, dark shading), significant in multivariate adaptive shrinkage analysis only (LFSR$<$ 0.1, medium shading), and significant in both analyses (light shading).

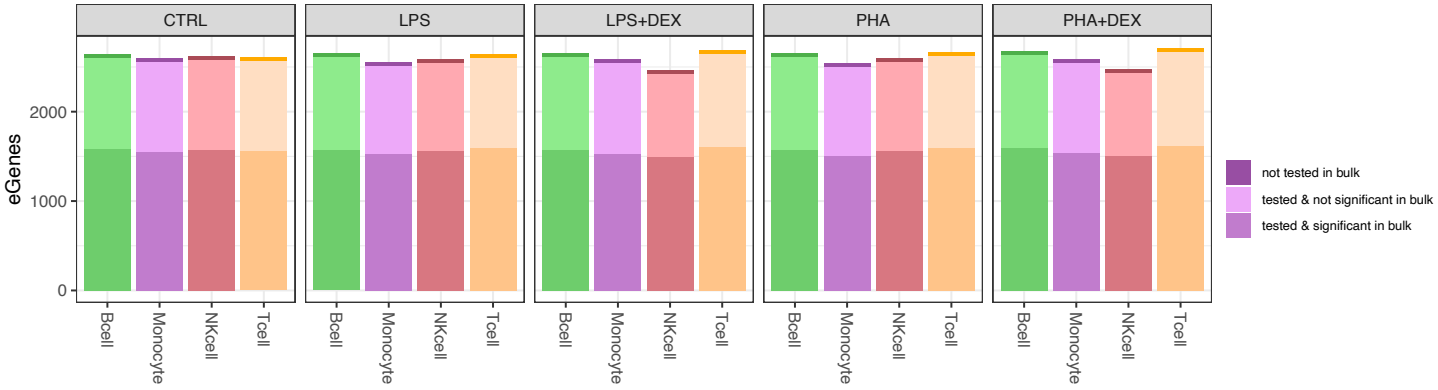

Figure S26: **Barplot represents the number of genes with significant eQTLs as assessed by multivariate adaptive shrinkage analysis (eGenes, LFSR$<$ 0.1).** Shading denotes significance in bulk dataset: significant in bulk RNA-seq data (Resztak *et al.* (2021), dark shading), not tested in bulk RNA-seq data (light shading), and not significant in bulk RNA-seq data (medium shading).

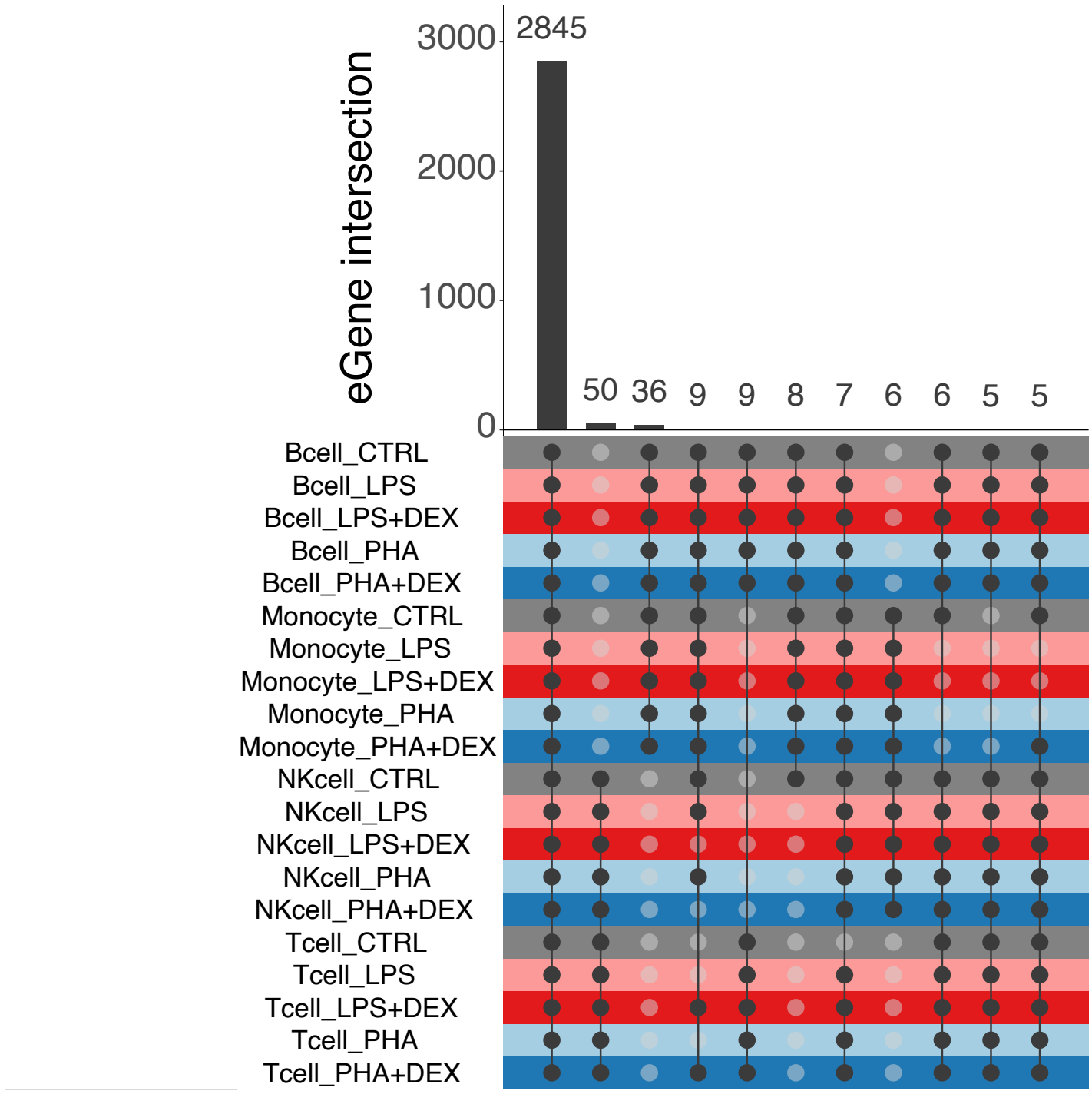

Figure S27: **eGene sharing by sign across all conditions.** Upset plot represents the number of eGenes with eQTLs shared by sign (i.e., with genetic effects in the same direction) for each unique set of conditions with intersection size of at least 5.

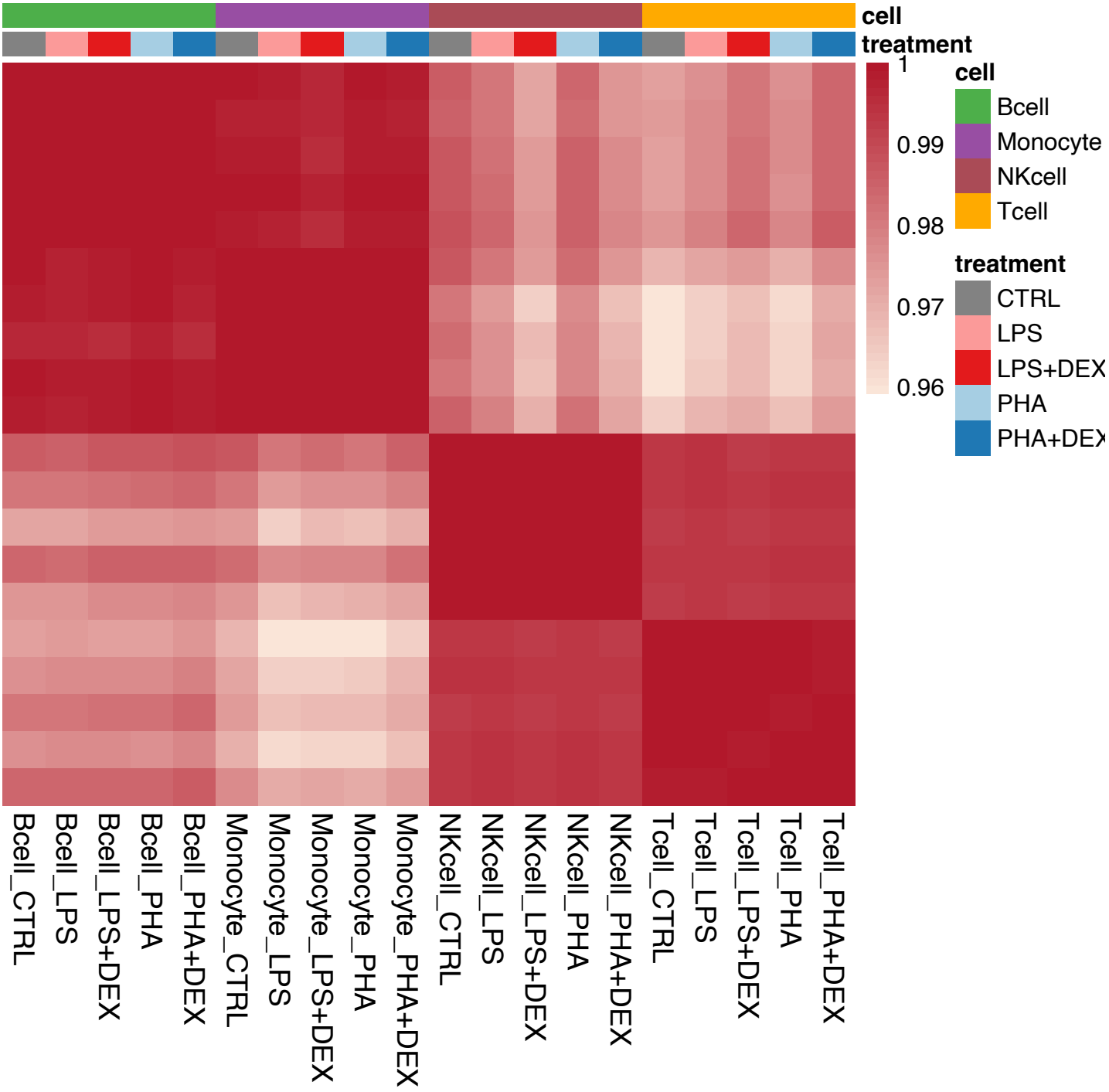

Figure S28: **eGene differences in the direction of effect across all pairs of conditions.** Heatmap represents proportion of eGenes significant in either of the two conditions which have at least one eQTL significant in either of the two conditions with opposite sign of genetic effect size estimated by multivariate adaptive shrinkage.

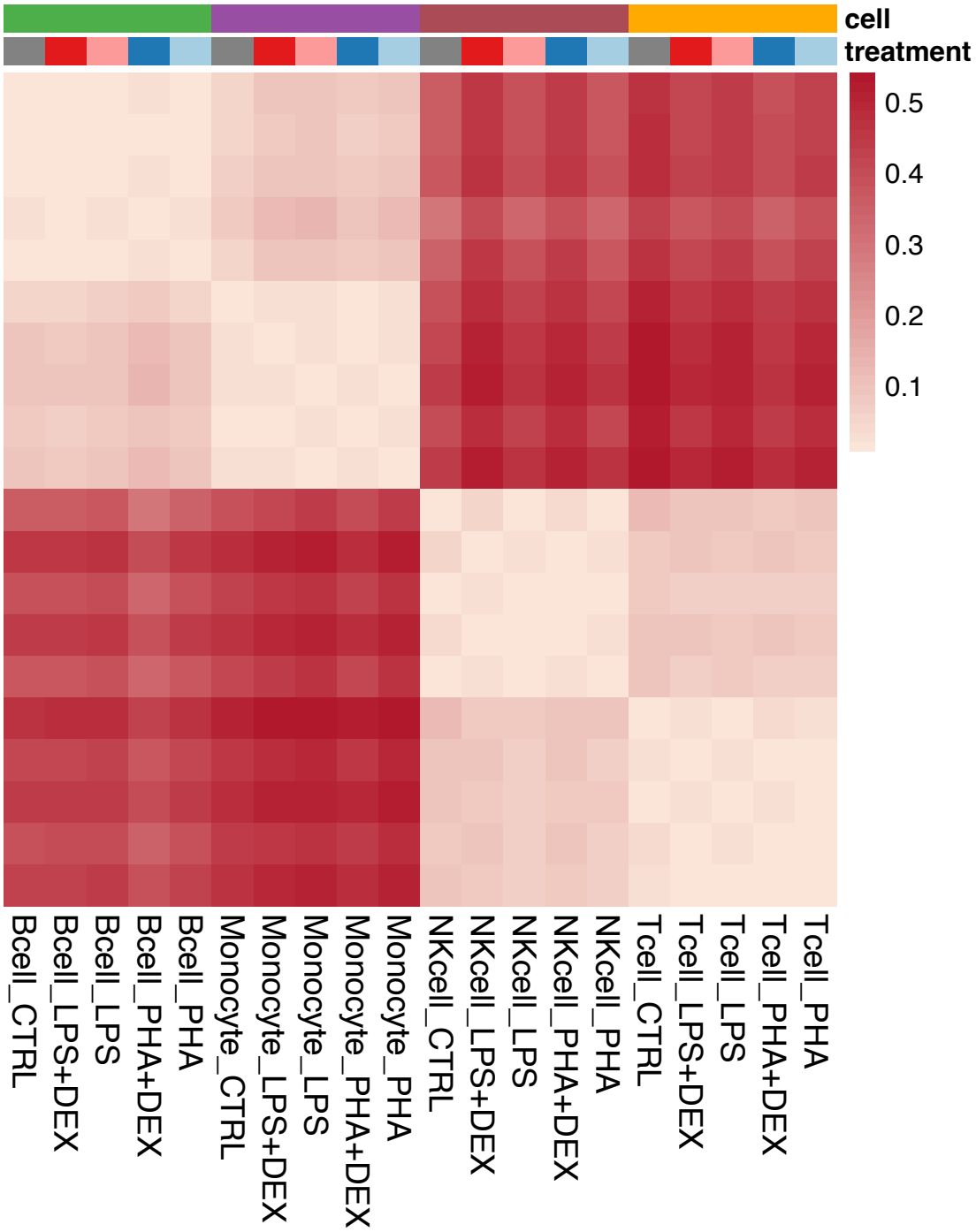

Figure S29: **eGene differences across all pairs of conditions.** Heatmap represents proportion of eGenes significant in either of the two conditions which have at least one eQTL significant in either of the two conditions with at least two-fold difference of genetic effect size estimated by multivariate adaptive shrinkage.

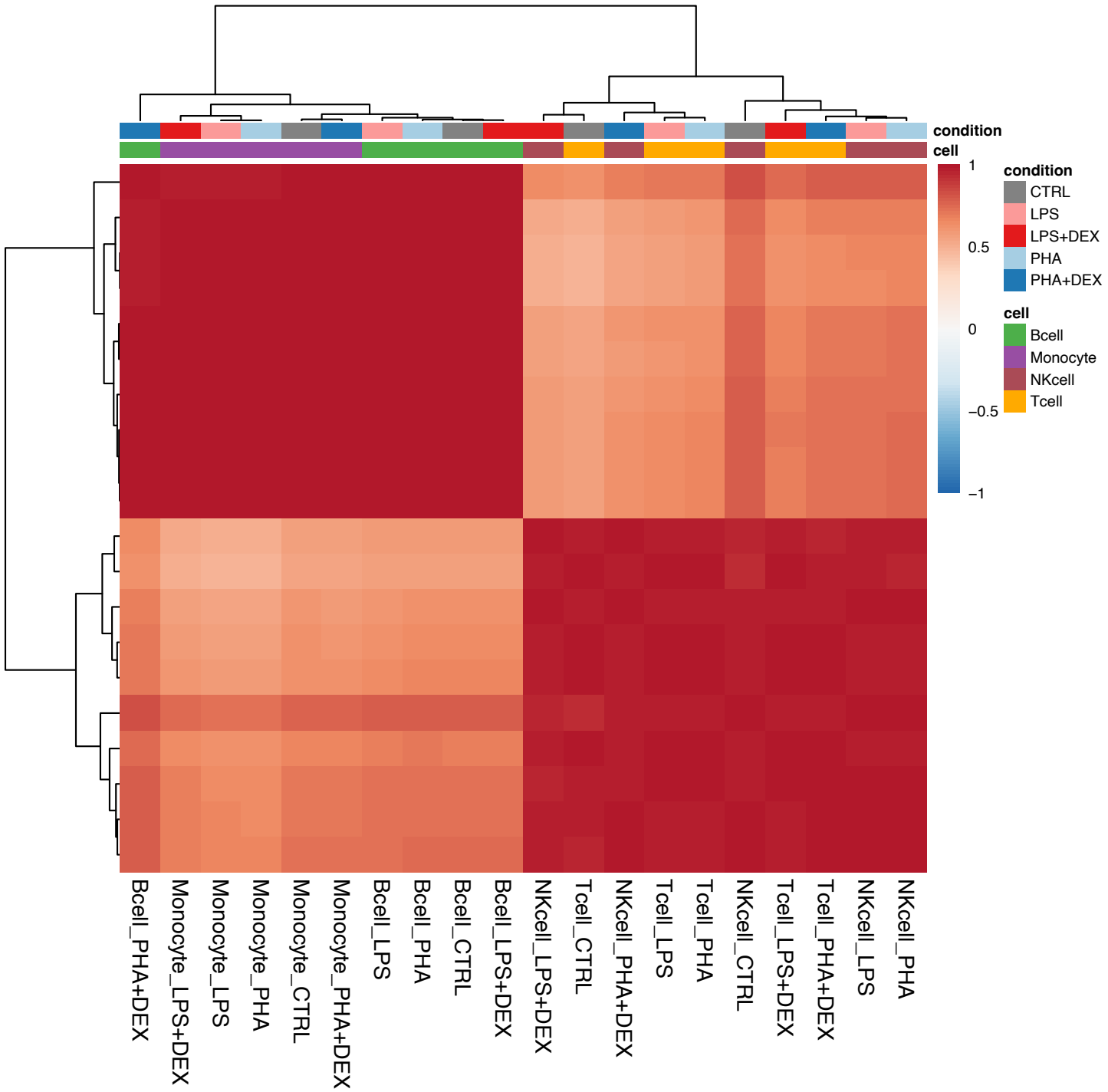

Figure S30: **Correlations between genetic effect sizes estimated with multivariate adaptive shrinkage.** Heatmap represents pairwise Pearson correlations based on union of significant eQTLs in either of the two conditions (LFSR<0.1). All values are significant (p-value<0.05).

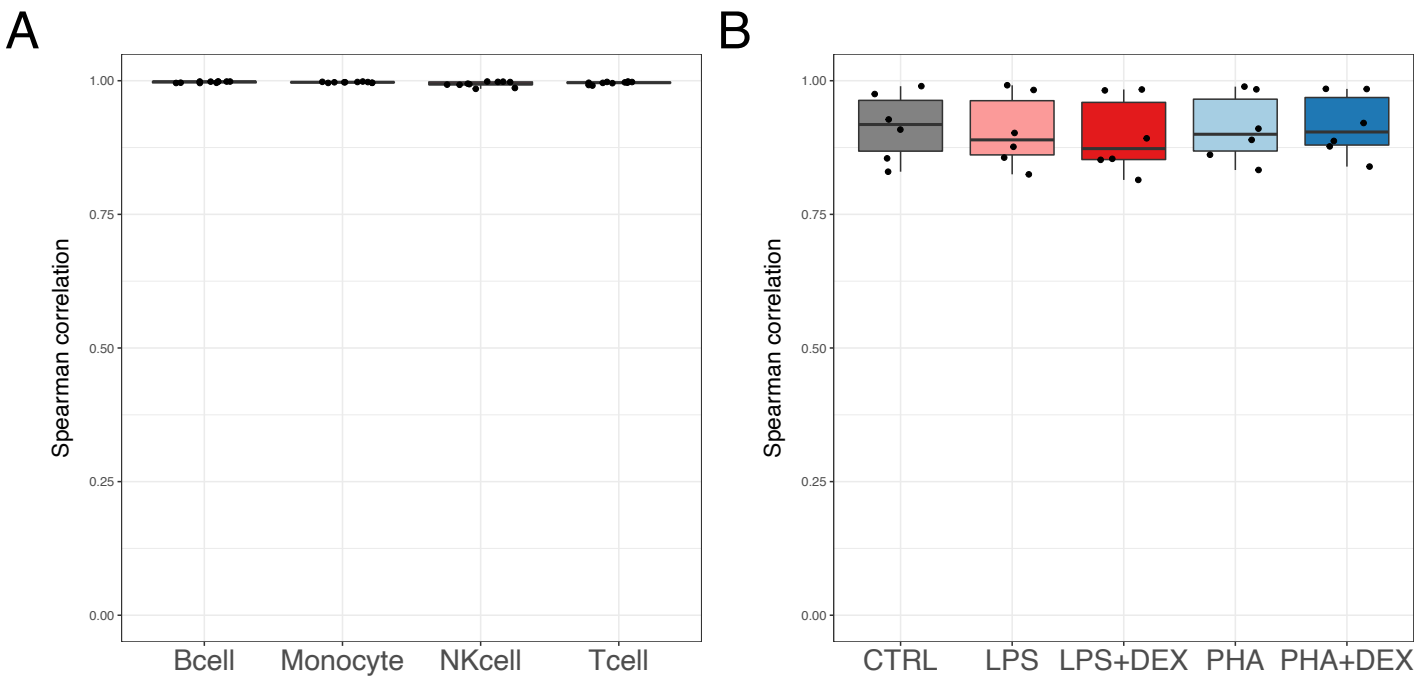

Figure S31: **Spearman's correlations between significant genetic effect sizes estimated with multivariate adaptive shrinkage (LFSR**< 0.1**). A** pair-wise correlations between all treatment conditions within each cell type **B** pair-wise correlations between all cell types within each treatment. All values are significant (p-value< 0.05).

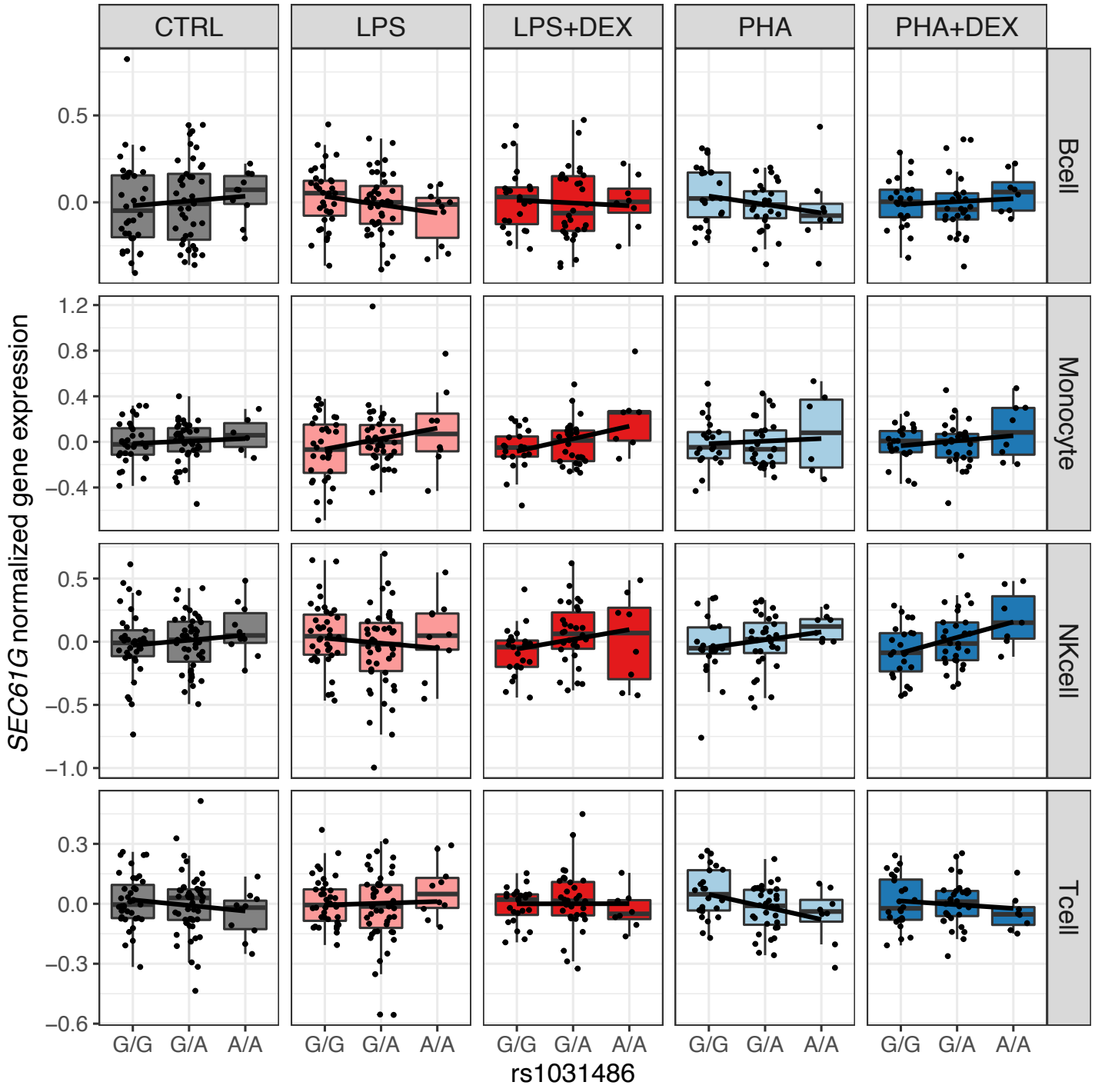

Figure S32: **Genetic effect of rs1031486 on gene expression of *SEC61G*.** Boxplots represent normalized expressions of the *SEC61G* gene (y axis) across the three genotype classes of rs1031486 (x axis) across all conditions.

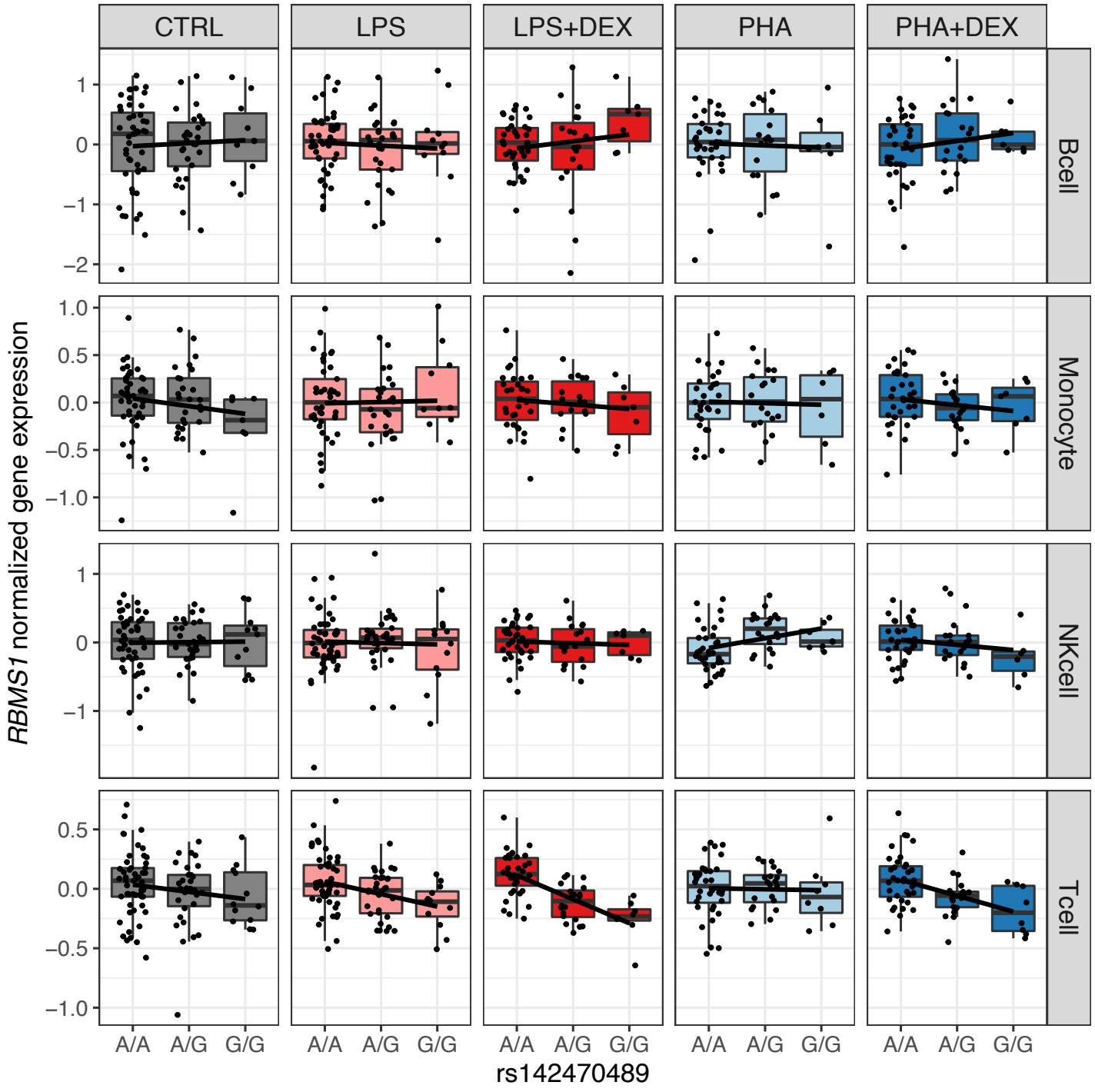

Figure S33: **Genetic effect of rs142470489 on gene expression of *RBMS1*.** Boxplots represent normalized expressions of the *RBMS1* gene (y axis) across the three genotype classes of rs142470489 (x axis) across all conditions.

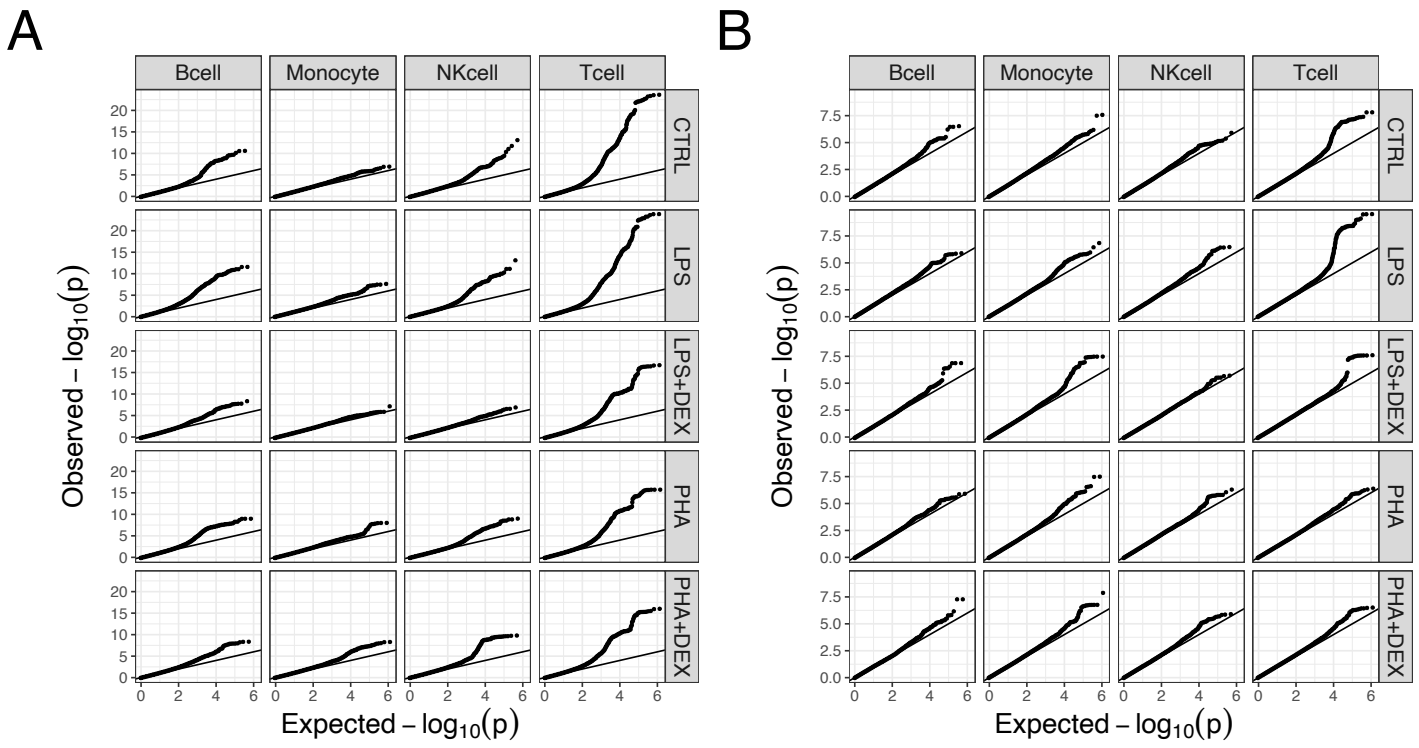

Figure S34: **QQplots for genetic analyses of mean and variability. A** p-values from mean-eQTL mapping with FastQTL **B** p-values from variability QTL mapping with FastQTL.

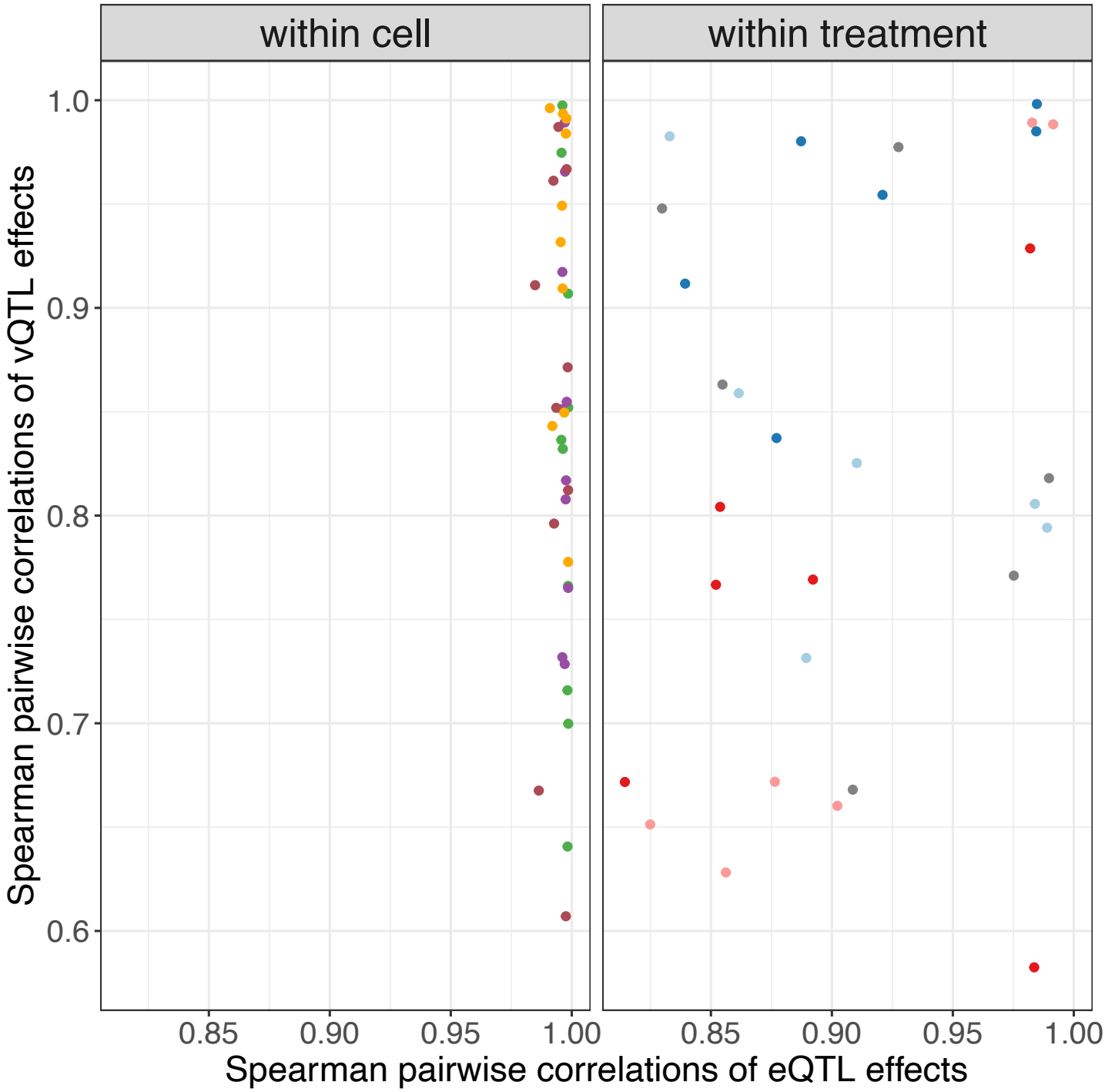

Figure S35: **Cell type- and treatment-specificity of genetic effects on gene expression and gene expression variability.** Scatterplots represent pairwise Spearman's correlations between significant genetic effects (LFSR$<$ 0.1) on gene expression (x axis), and gene expression variability (y axis) across all treatment conditions within each cell type (left panel) and across all cell types within each treatment condition (right panel).

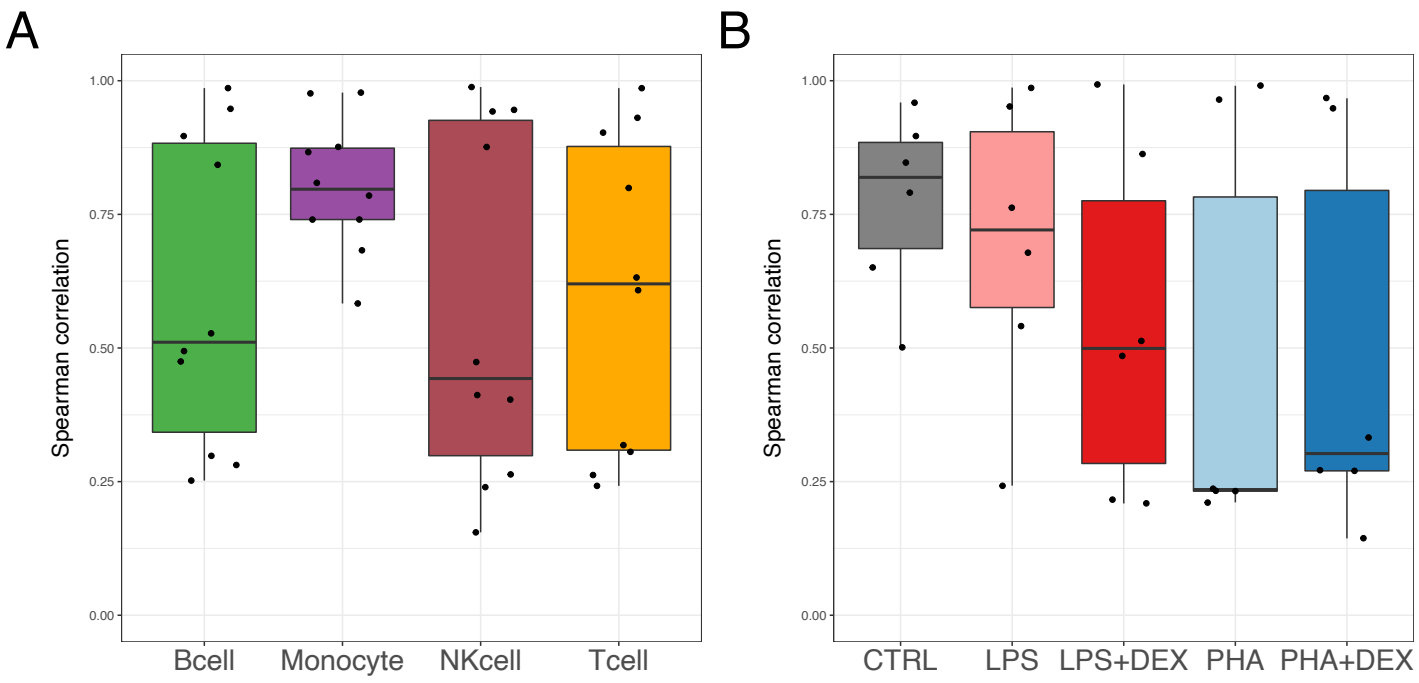

Figure S36: **Spearman's correlations between significant genetic effects on gene expression variability estimated with multivariate adaptive shrinkage (LFSR$<$ 0.1). A** – pair-wise correlations between all treatment conditions within each cell type **B** – pair-wise correlations between all cell types within each treatment condition

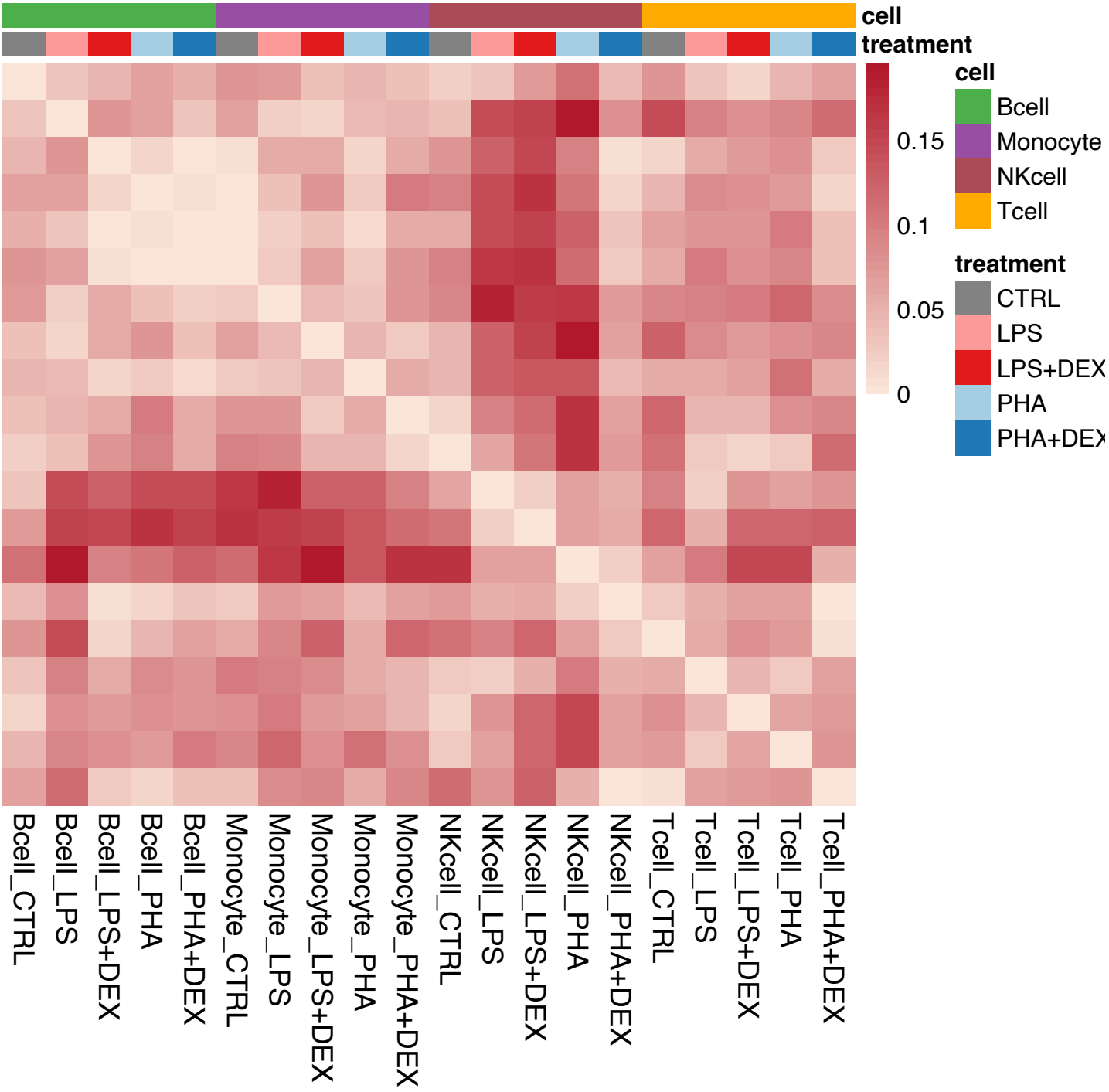

Figure S37: **vGene differences in the direction of effect across all pairs of conditions.** Heatmap represents proportion of vGenes significant in either of the two conditions which have at least one vQTL significant in either of the two conditions with opposite sign of genetic effect size estimated by multivariate adaptive shrinkage.

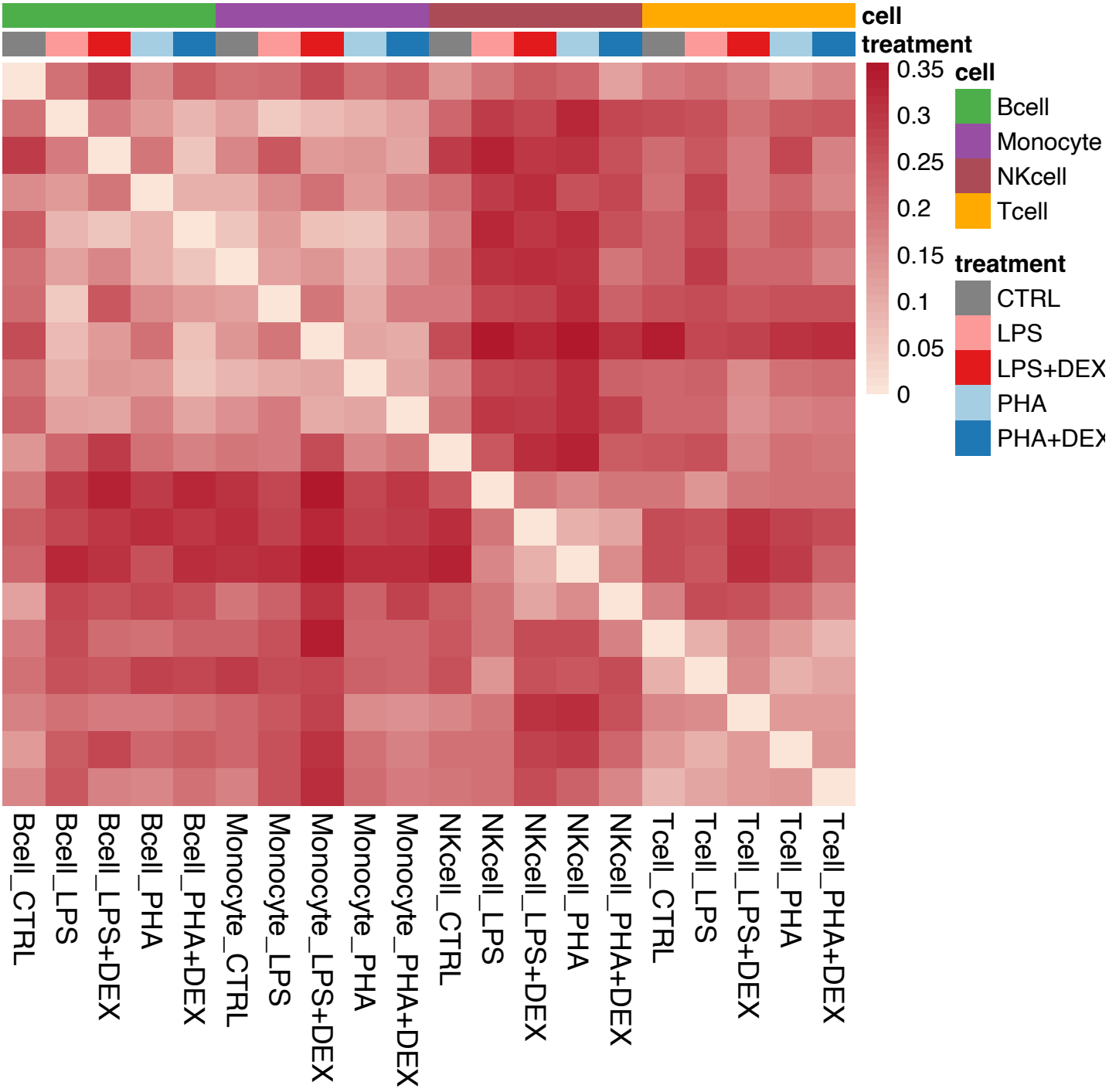

Figure S38: **vGene differences across all pairs of conditions.** Heatmap represents the proportion of vGenes not shared by magnitude (i.e., with at least 2-fold difference between genetic effects in each condition) over the union of all significant vGenes in each pair-wise comparison.

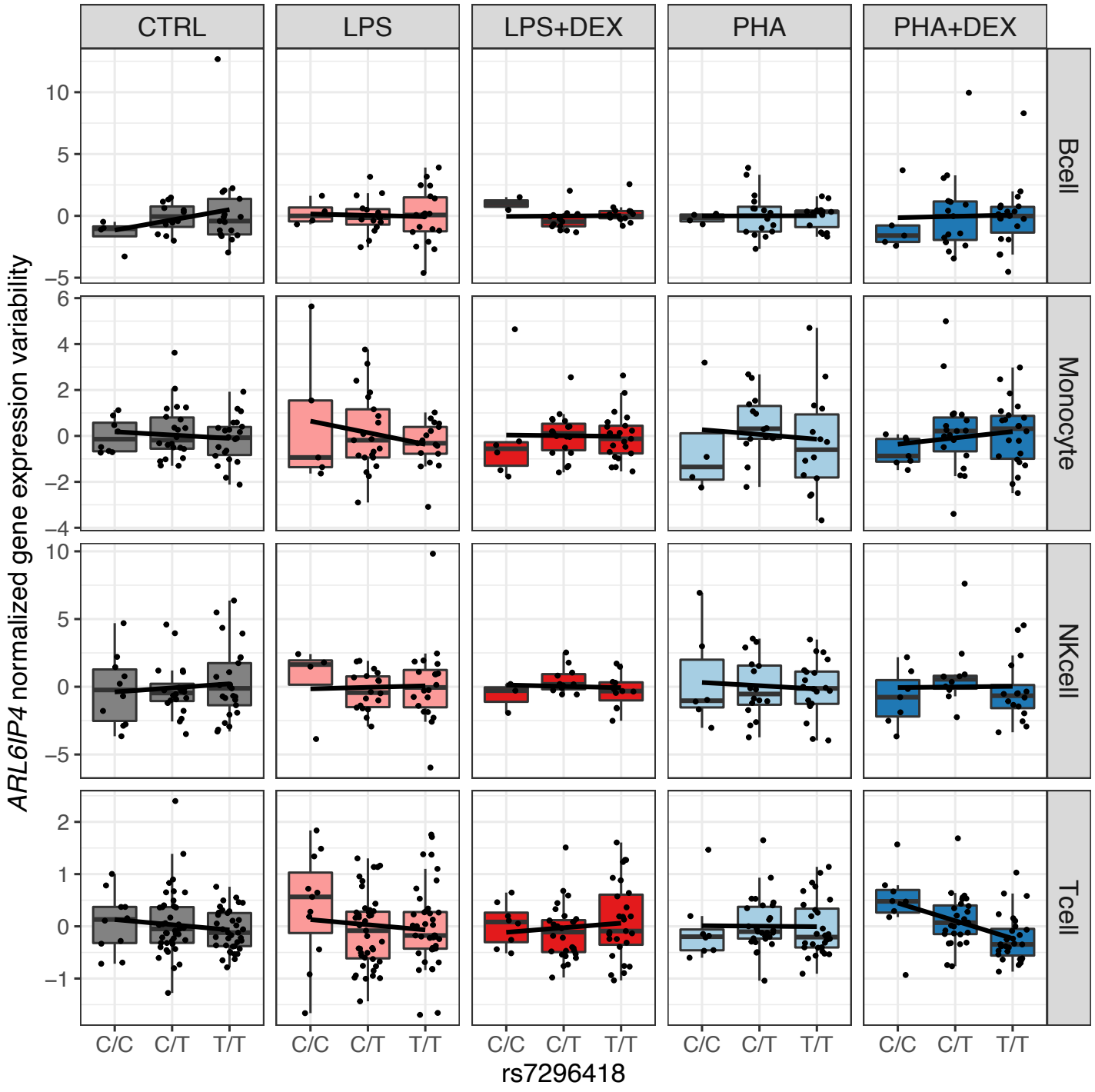

Figure S39: **Genetic effect of rs7296418 on gene expression of *ARL6IP4*. A** Boxplots represent normalized mean expression of the *ARL6IP4* gene (y axis) across the three genotype classes of rs7296418 (x axis) across all conditions **B** Boxplots represent normalized gene expression variability of the *ARL6IP4* gene (y axis) across the three genotype classes of rs7296418 (x axis) across all conditions.

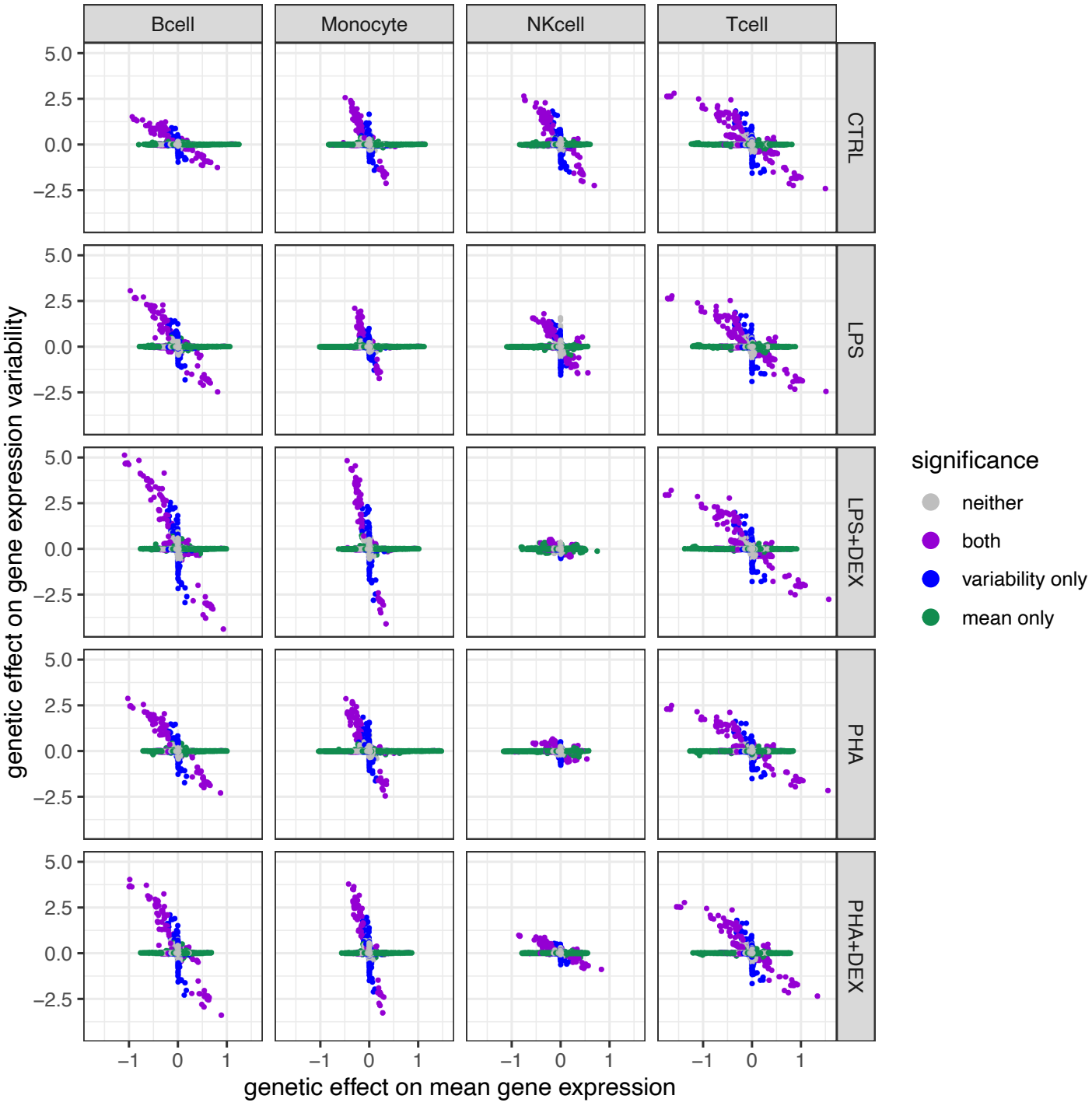

Figure S40: **Genetic effects on gene expression variability.** Scatterplots represent genetic effects on mean gene expression (x axis) versus genetic effects on gene expression variability (y axis) across all 20 conditions. Color represents genetic variants with significant effects on mean gene expression only (green), gene expression variability only (blue), both (purple), and neither (grey).

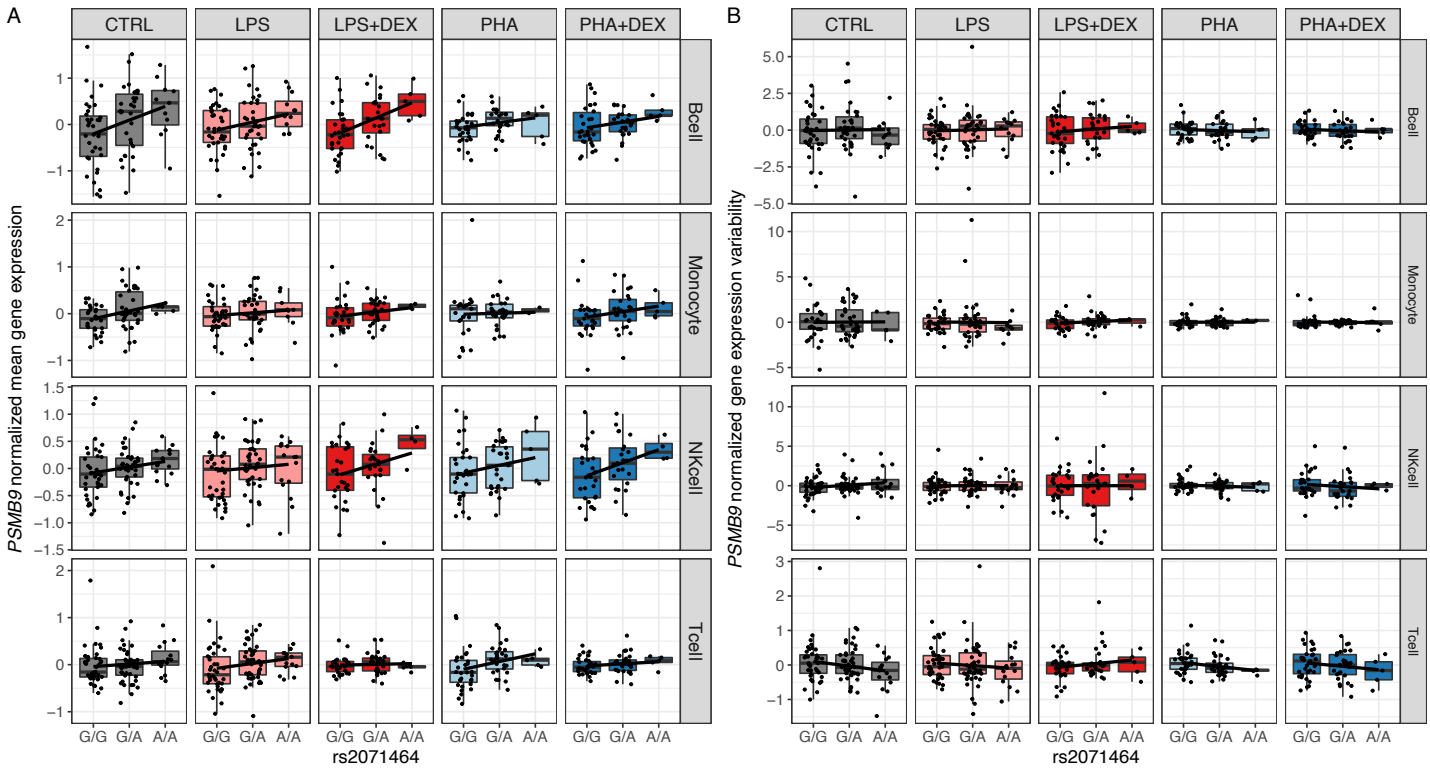

Figure S41: **Genetic effect of rs2071464 on gene expression of *PSMB9*. A** Boxplots represent normalized mean expression of the *PSMB9* gene (y axis) across the three genotype classes of rs2071464 (x axis) across all conditions **B** Boxplots represent normalized gene expression variability of the *PSMB9* gene (y axis) across the three genotype classes of rs2071464 (x axis) across all conditions.

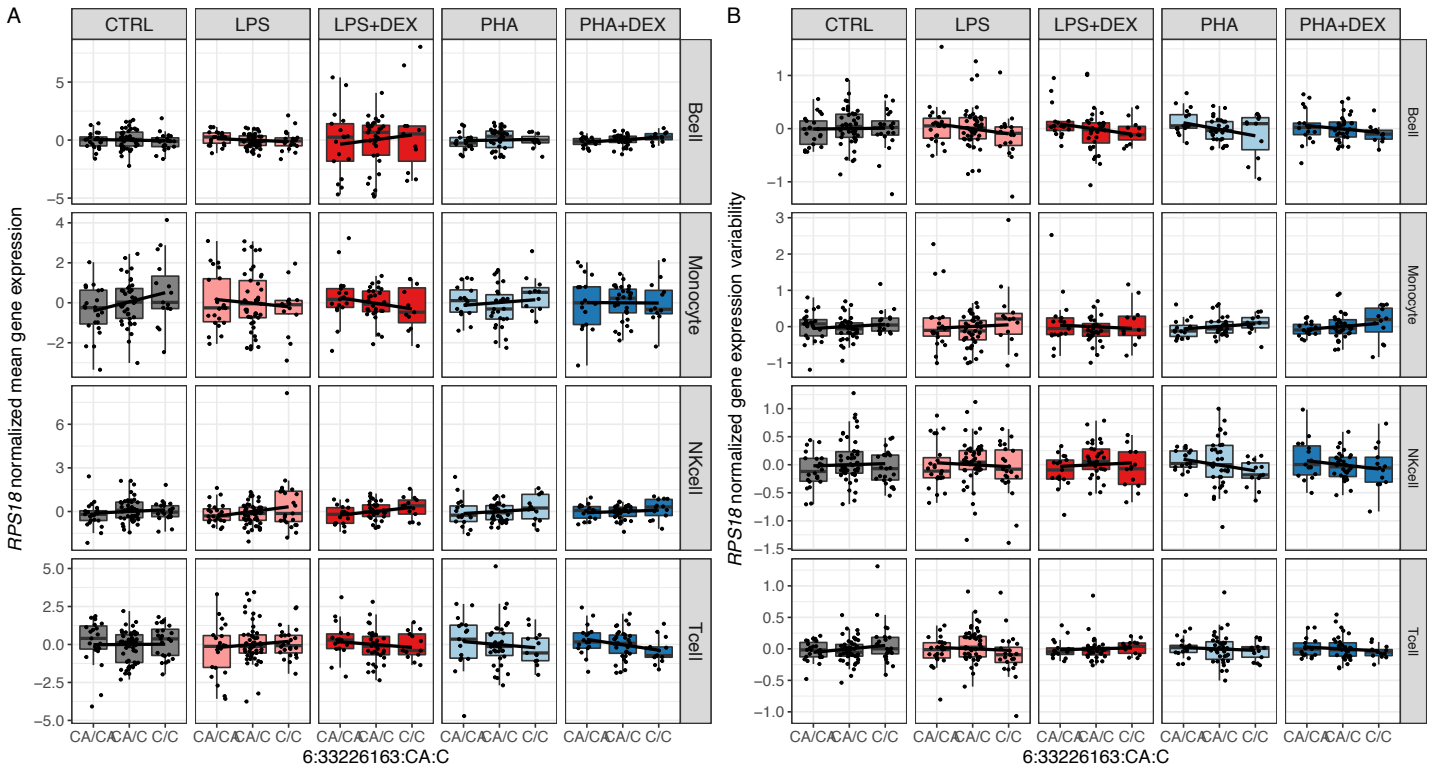

Figure S42: **Genetic effect of the SNP at 6:33226163 on gene expression of *RPS18*.** **A** Boxplots represent normalized mean expression of the RPS18 gene (y axis) across the three genotype classes of the SNP at 6:33226163 (x axis) across all conditions **B** Boxplots represent normalized gene expression variability of the RPS18 gene (y axis) across the three genotype classes of the SNP at 6:33226163 (x axis) across all conditions.

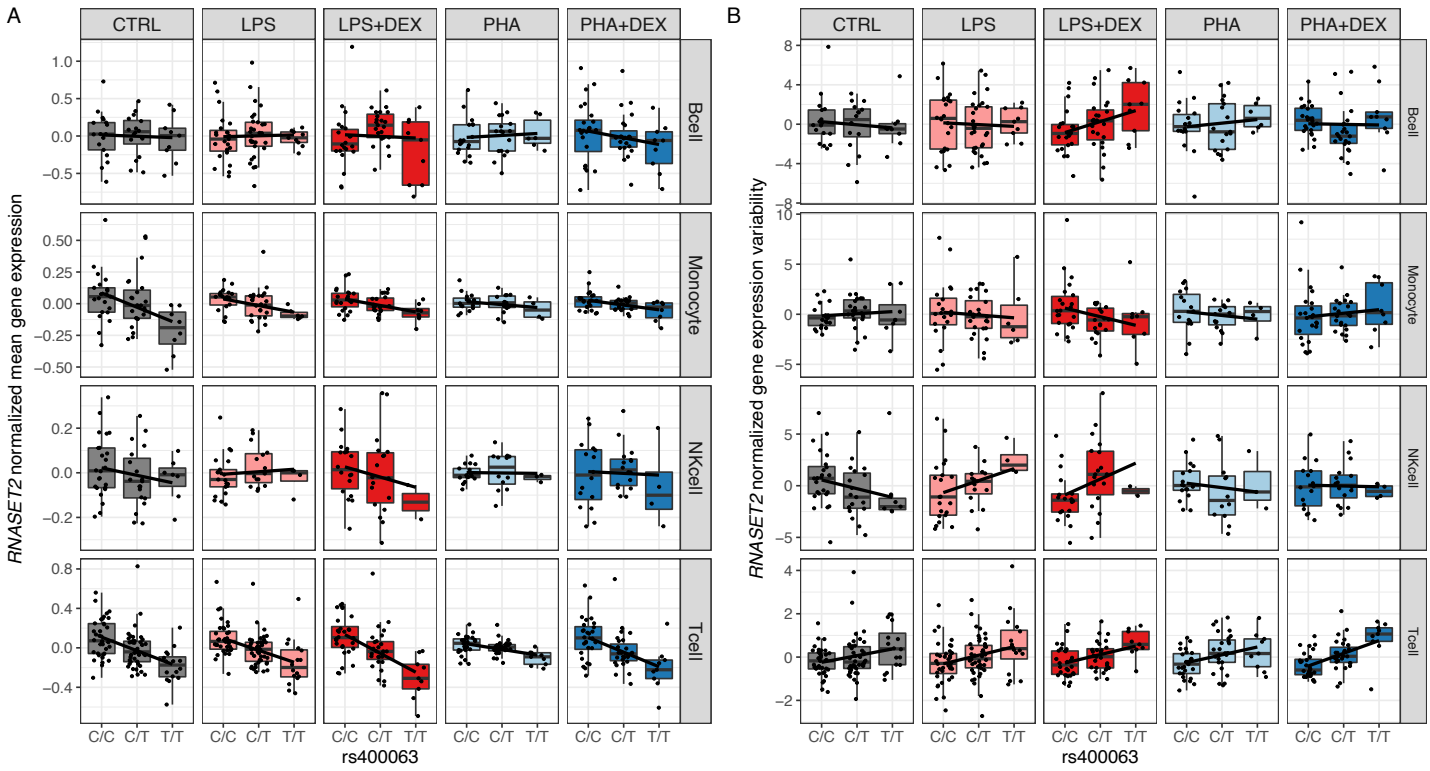

Figure S43: **Genetic effect of rs12507413 on gene expression of *RNASET2*. A** Boxplots represent normalized mean expression of the *RNASET2* gene (y axis) across the three genotype classes of rs400063 (x axis) across all conditions **B** Boxplots represent normalized gene expression variability of the *RNASET2* gene (y axis) across the three genotype classes of rs400063 (x axis) across all conditions.

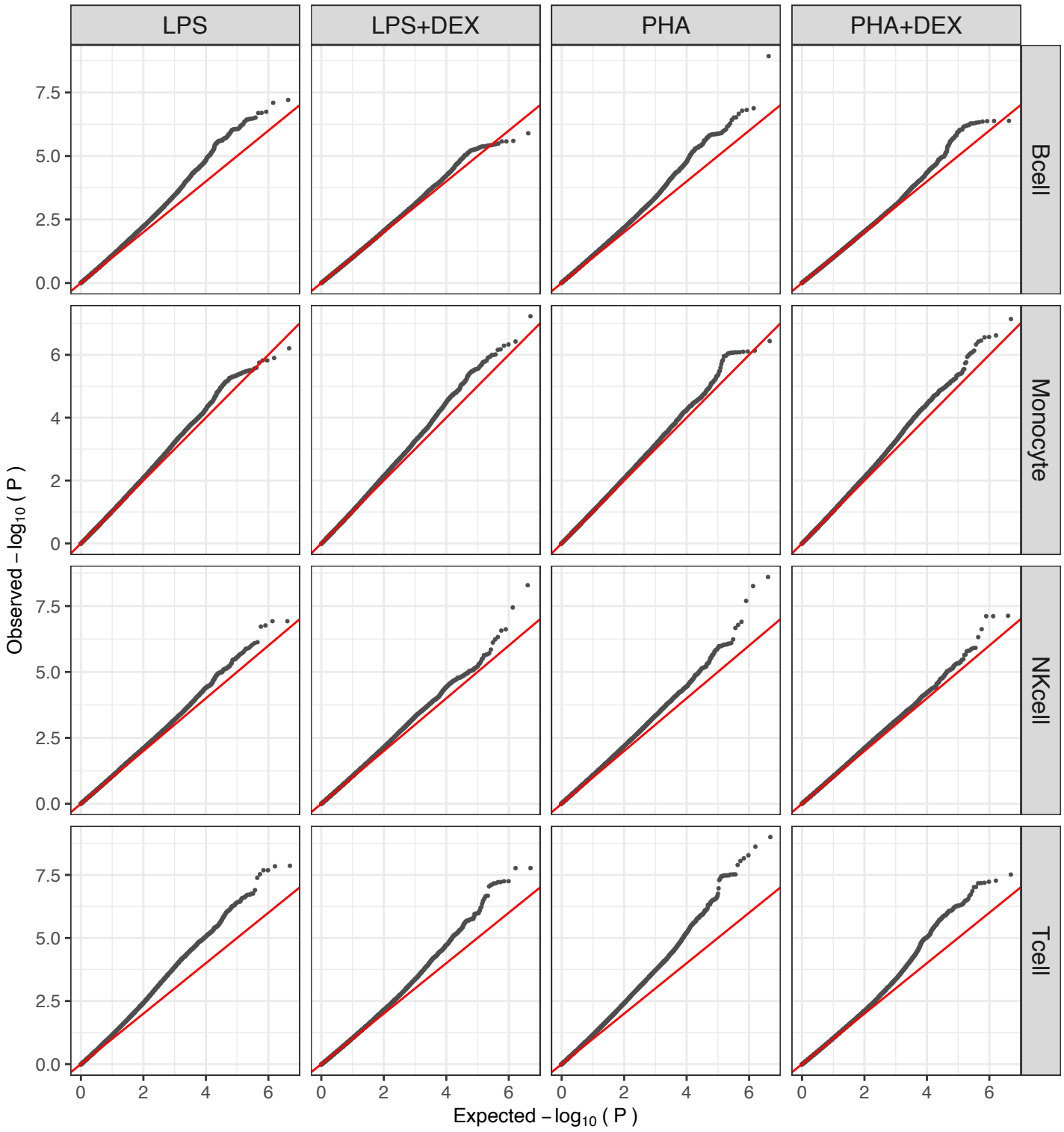

Figure S44: **QQplots of p-values from DLDA-interacting eQTL mapping across the 16 conditions.**

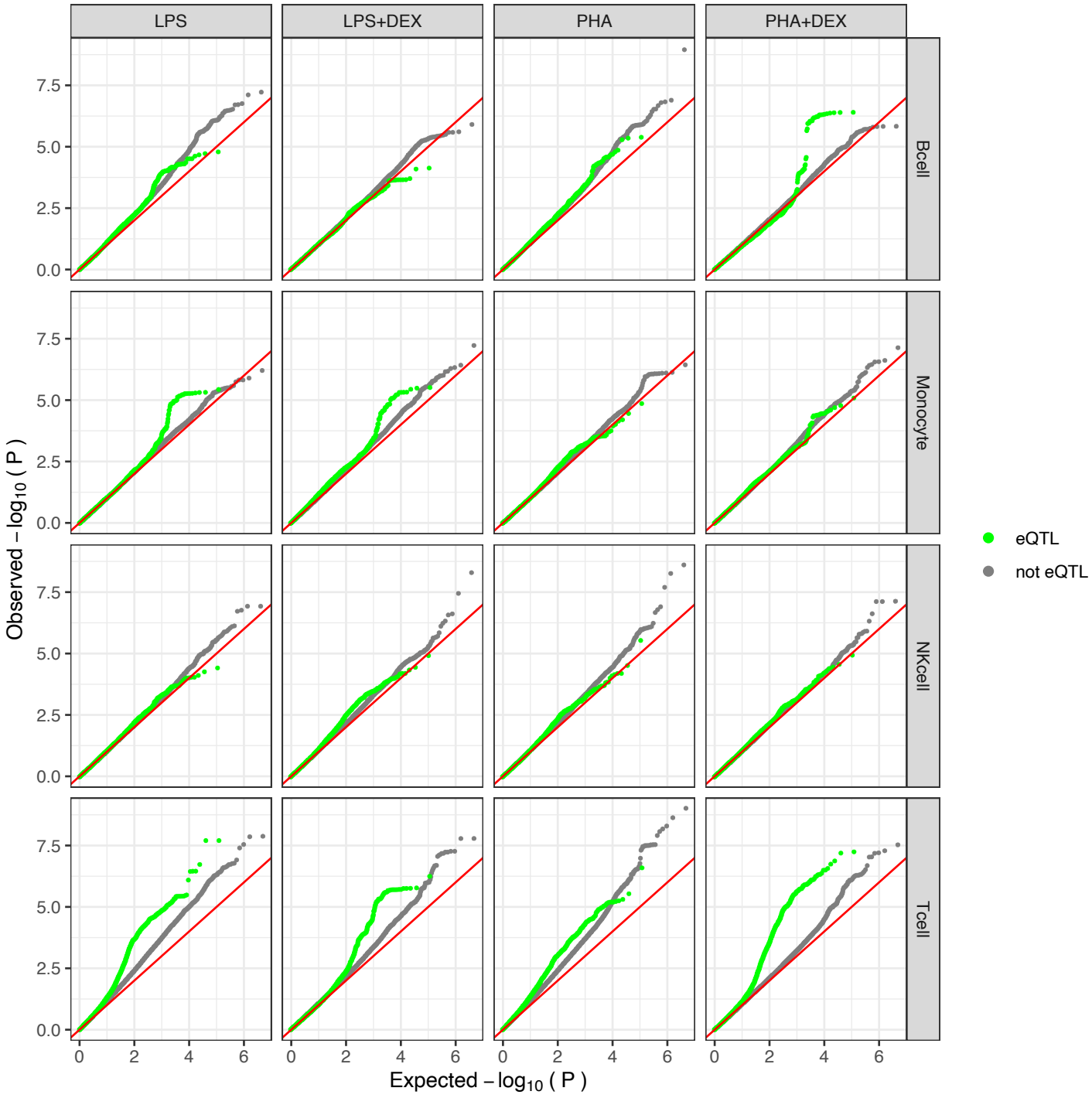

Figure S45: **Q-Qplots of p-values from DLDA-interacting eQTL mapping across the 16 conditions stratified by eQTL or not**, green colors representing the tested genetic variants are eQTLs that were detected in any condition.

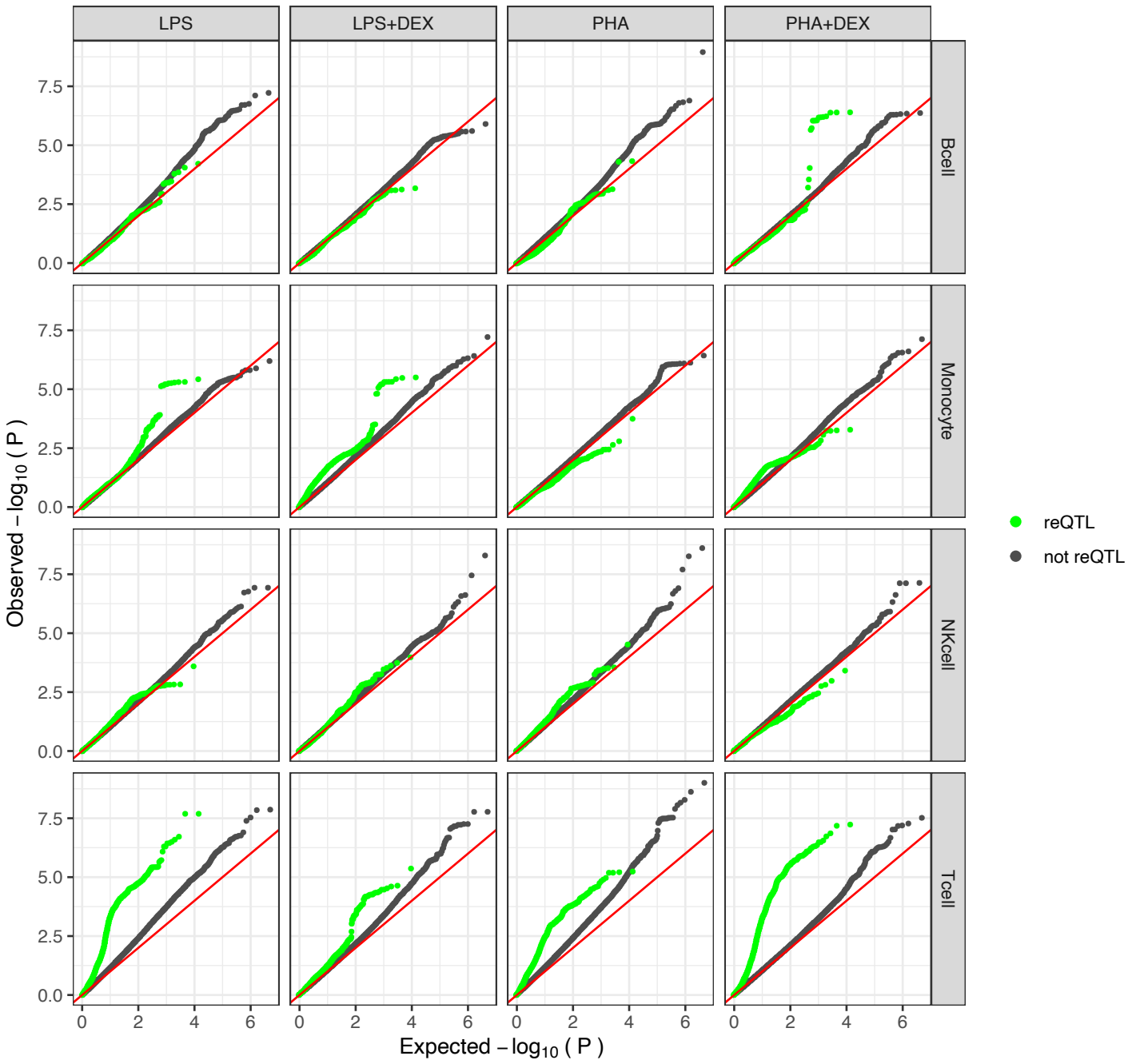

Figure S46: **Q-Qplots of p-values from DLDA-interacting eQTL mapping across the 16 conditions stratified by reQTL or not**, green colors representing the tested genetic variants are reQTLs that were detected in any condition.

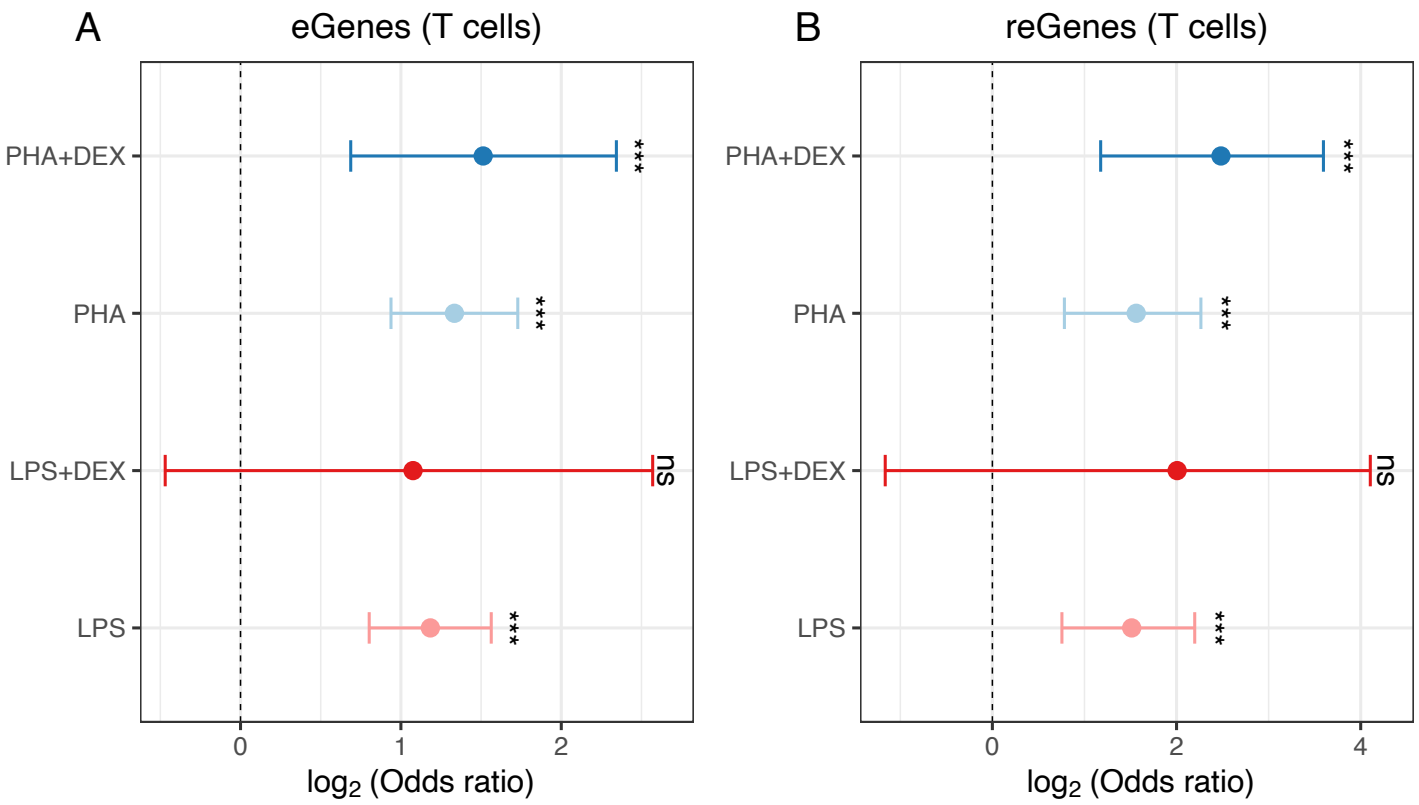

Figure S47: **Forest plots of log odds ratio across 4 conditions in the T cells**, to show if dynamic eGenes are significantly enriched in eGenes or reGenes across 4 conditions in the T cells. **(A)** test if dynamic eGenes are enriched in the eGenes discovered in the same condition, **(B)** test if dynamic eGenes are enriched in the reGenes discovered in the same condition

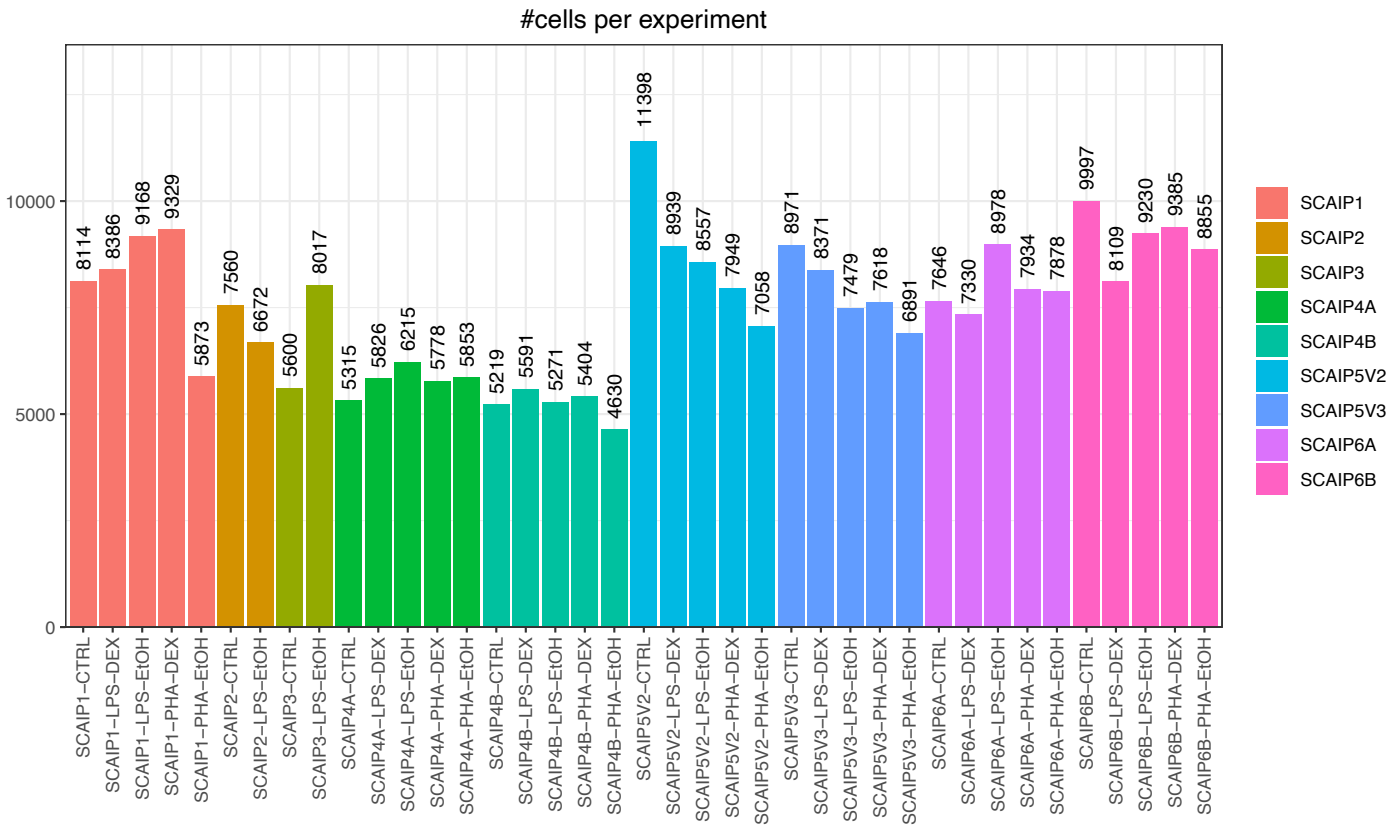

Figure S48: **Number of measured cells across 39 experiments**

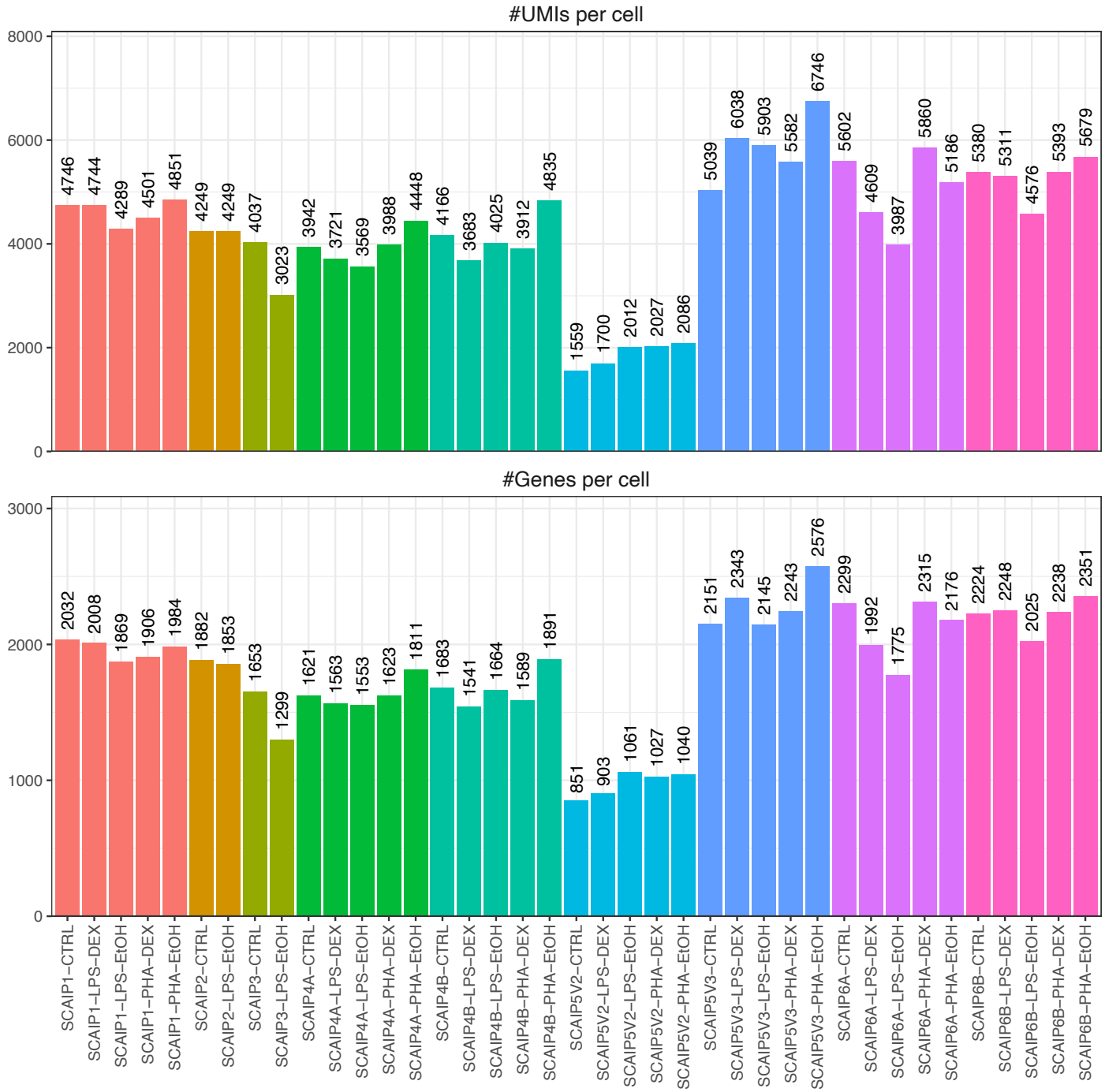

Figure S49: **Unique molecular identifiers(UMIs) and gene features per cell across 39 experiments, including spliced and unspliced reads**

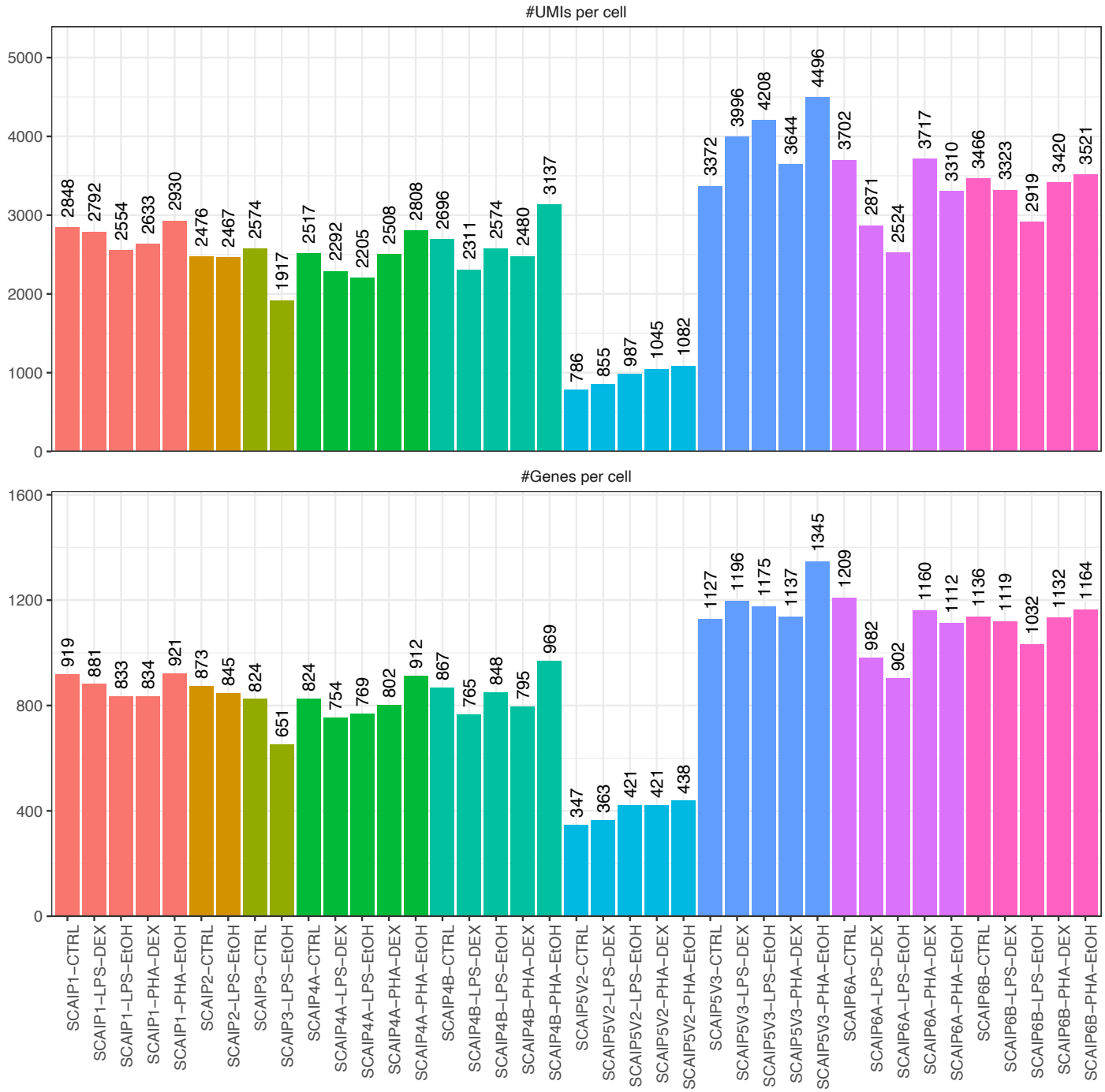

Figure S50: **Unique molecular identifiers(UMIs) and gene features per cell across 39 experiments for spliced reads**

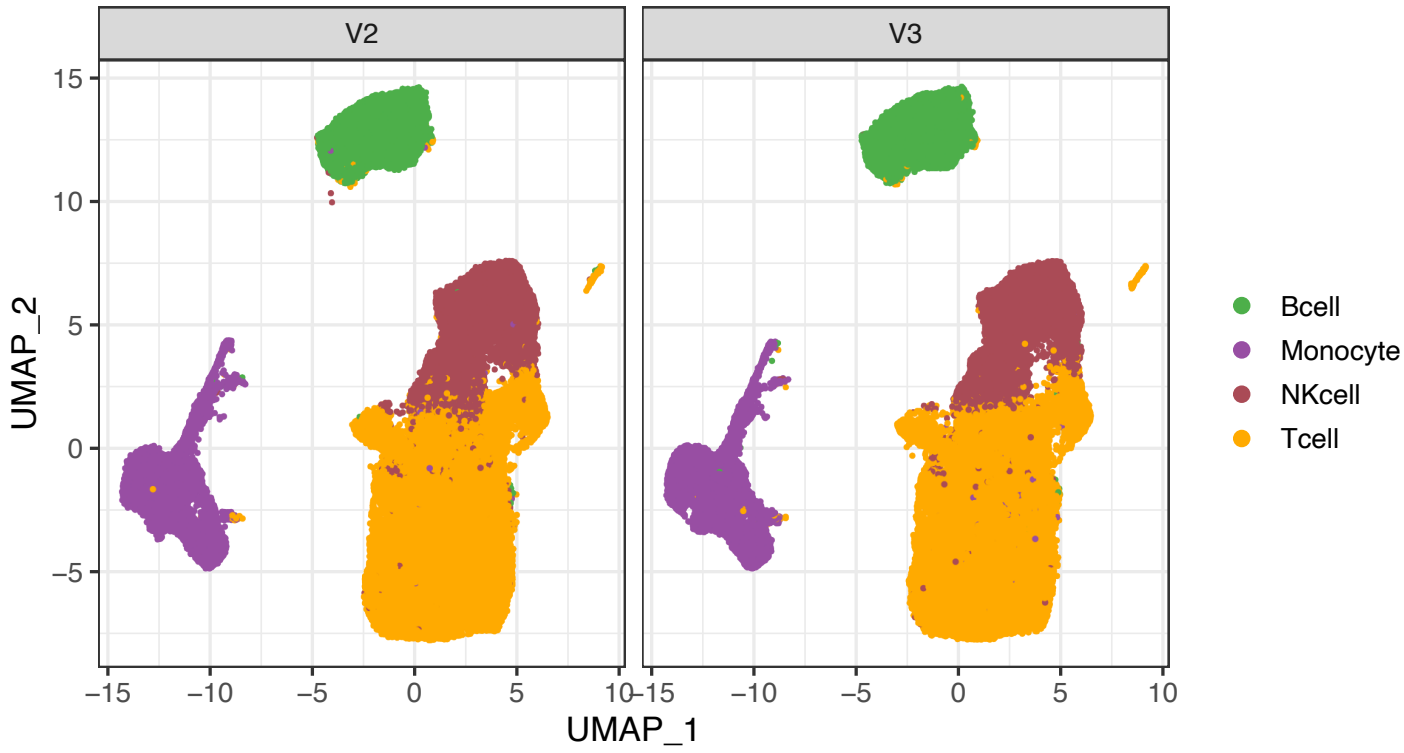

Figure S51: **UMAP of cells split by chemistry**

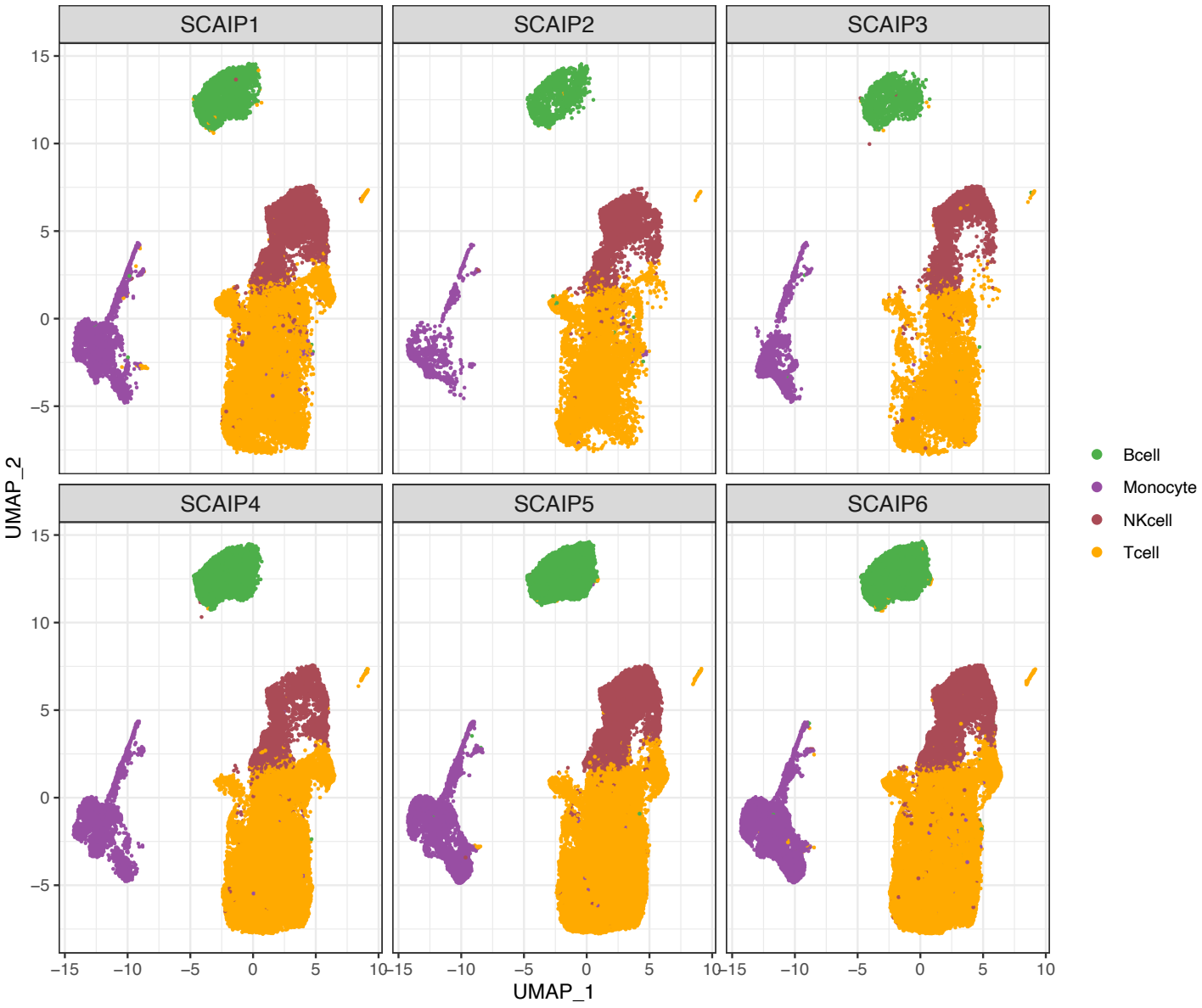

Figure S52: **UMAP of cells split by BATCH**

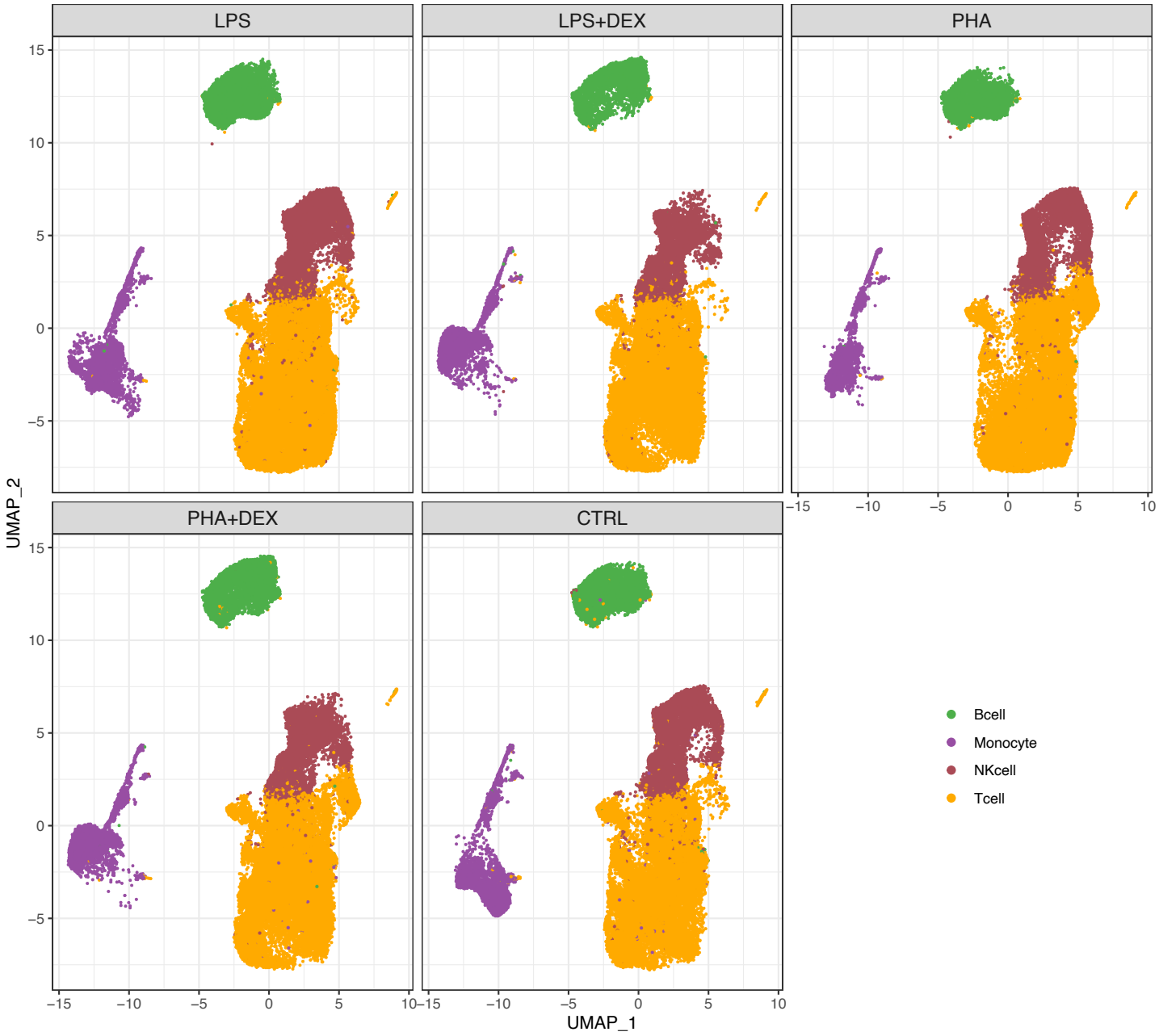

Figure S53: **UMAP of cells split by treatment**

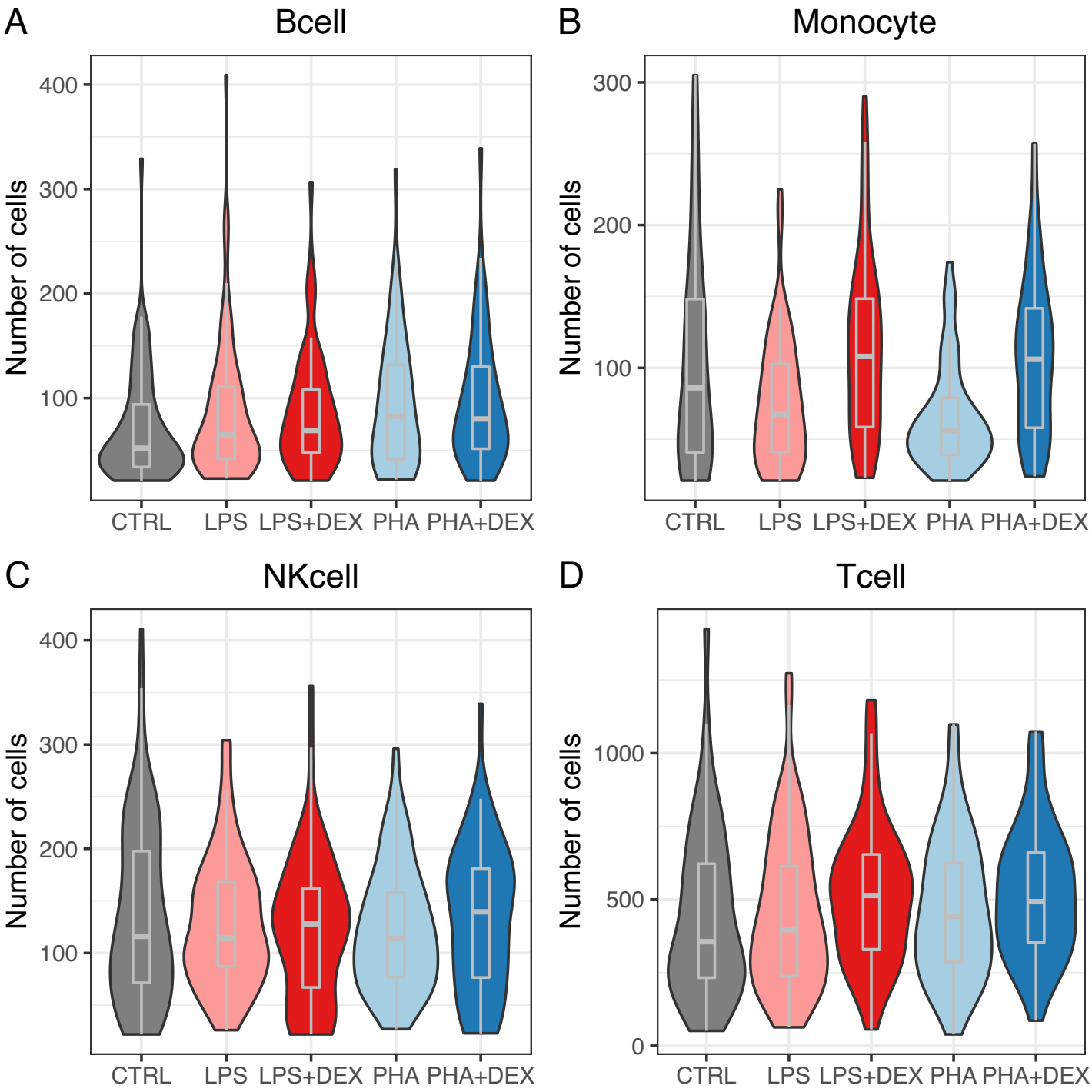

Figure S54: **Violin plots of number of cells in each combination (cell type+treatment+individual)** **A-D** represents the distribution of the number of cells in each combination across individuals in different treatments for B cells, monocytes, NK cells and T cells.

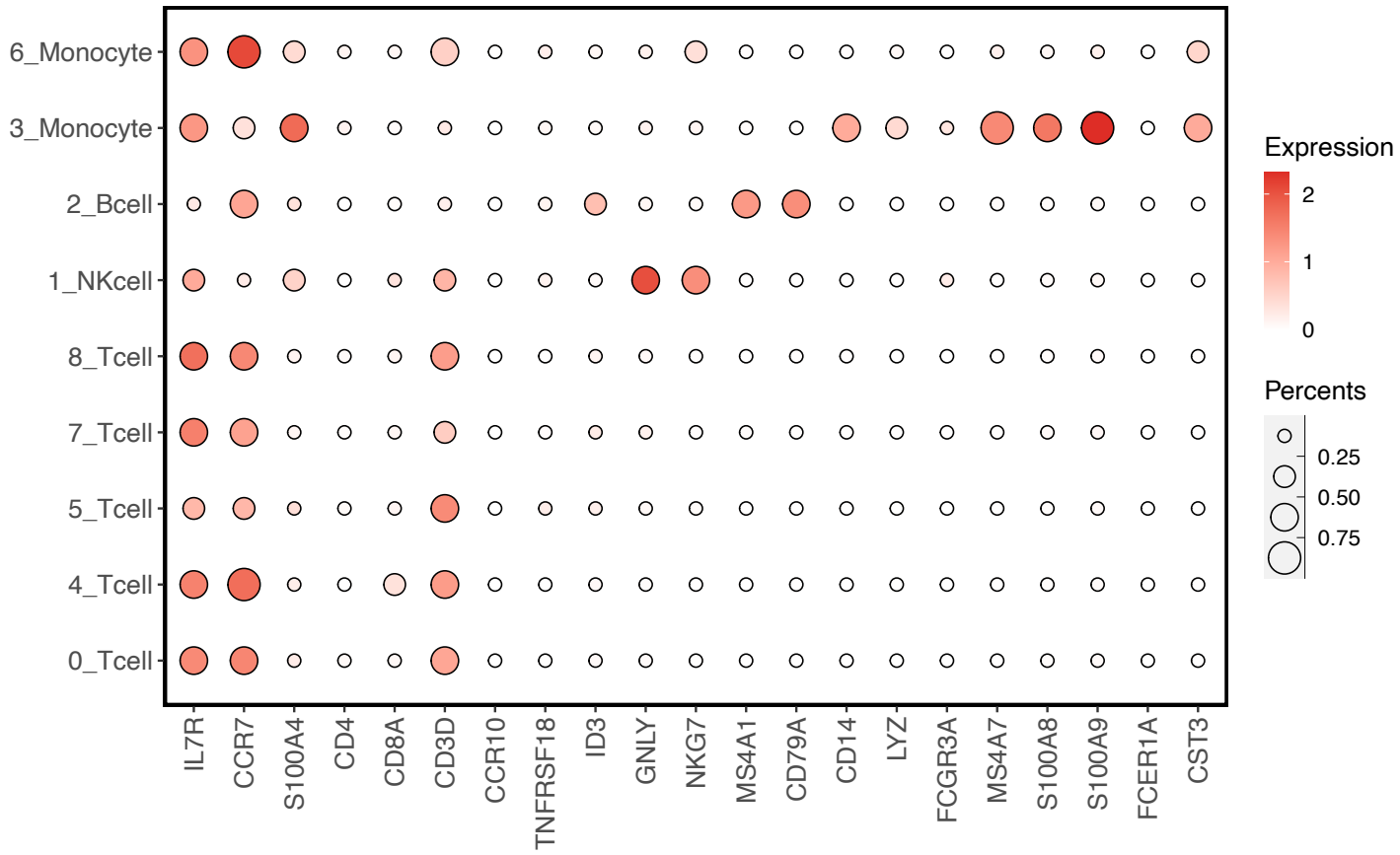

Figure S55: **Dot plots of cell type marker genes expressed in the Seurat clusters**. Red color represents high average expression values across cells in the cluster while the size of dots representing the proportion of cells expressed the marker gene in the cluster

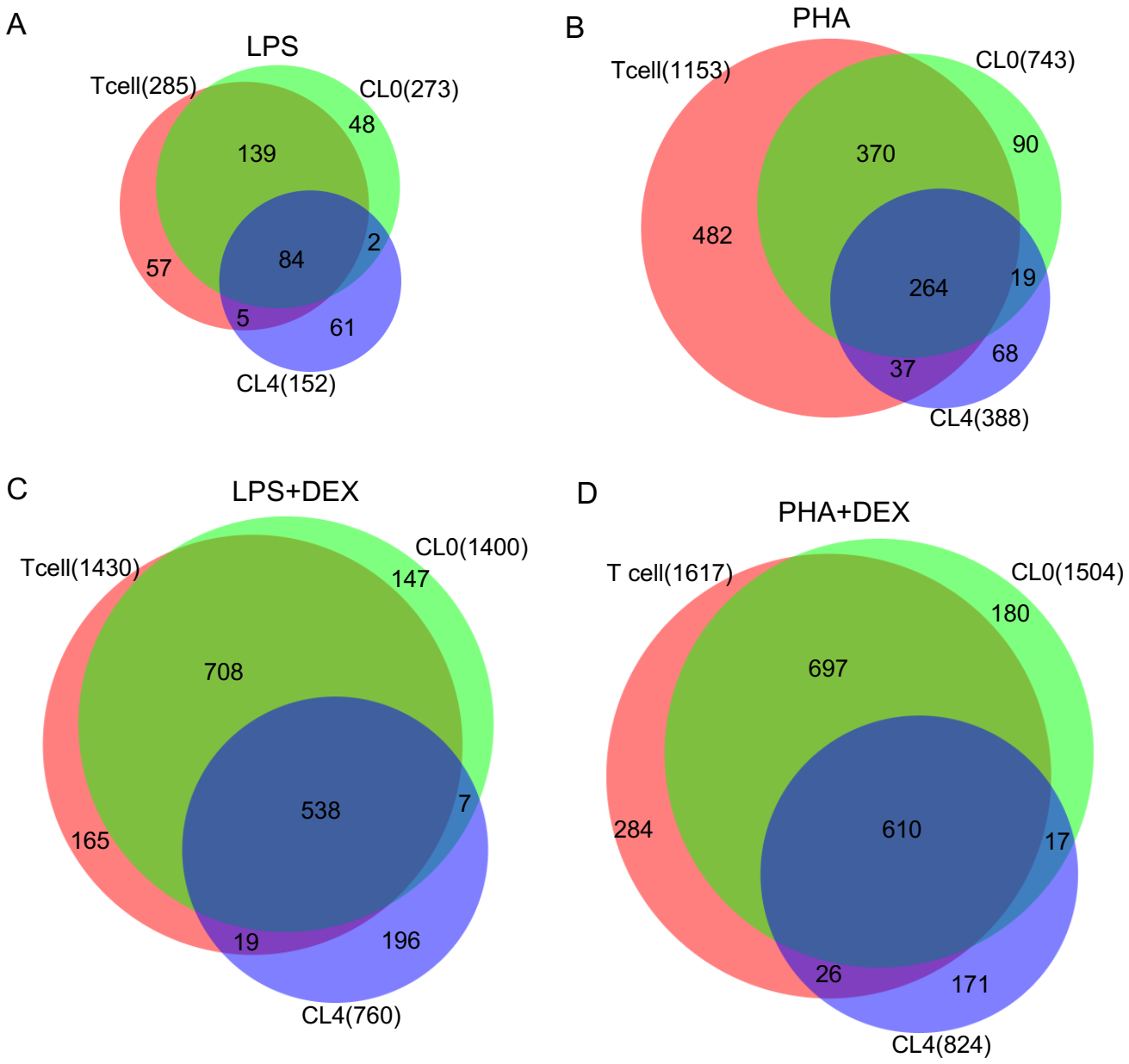

Figure S56: **Venn diagrams of overlapping DEGs in response to treatments between the overall T cells, and two major T cell sub-clusters (Cluster 0 and 4) :** A-D representing LPS, PHA, LPS+DEX and PHA+DEX respectively

Supplementary Tables

Table S1: **Summary statistics of single-cell data for each treatment**. Column 2, number of individuals for each treatment; Column 3, median values of number of cells per individual across individuals in each treatment; Column 4, median values of average UMIs per cell from the same individual across individuals in each treatment, Column 5, median values of average detection genes per cell from the same individual across individuals in each treatment

	#Individuals	# Cells per individual (median)	#UMIs per cell (median)	#Genes per cell (median)
CTRL	96	586	2,588	859
LPS	96	658	2,451	818
LPS+DEX	64	821	2,672	852
PHA	64	714	2,981	944
PHA+DEX	64	858	2,618	852

Table S2: **Summary cell type composition of individuals for each treatment**. Column 2-5, number of cells from B-cells, Monocyte, NK-cell and T cells of the individual for each treatment (median value). The full table detailing the number of cells in each cell type/treatment/individual combination can be found in Table S24.

	#B-cell per individual (median)	#Monocyte per individual (median)	#NK-cell per individual (median)	#T cell per individual (median)
CTRL	52	86	116	356
LPS-EtOH	65	67.5	114	396
LPS-DEX	69	108	128	514
PHA-EtOH	82.5	56	114	442
PHA-DEX	80	106	140	492

Table S3: eQTL mapping results. Number of significant eQTLs and eGenes based on FastQTL results (FDR<0.1, columns 2 and 3), and multivariate adaptive shrinkage results (LFSR<0.1), columns 4 and 5.

	FastQTL FDR<0.1		mash LFSR<0.1	
	eQTLs	eGenes	eQTLs	eGenes
Bcell CTRL	5378	291	110276	2649
Bcell LPS+DEX	4465	262	109921	2656
Bcell LPS	8135	396	109869	2650
Bcell PHA+DEX	3671	217	113168	2652
Bcell PHA	4347	268	109853	2678
Monocyte CTRL	4186	253	106399	2603
Monocyte LPS+DEX	4720	300	103217	2559
Monocyte LPS	5518	340	101642	2586
Monocyte PHA+DEX	4019	271	104661	2547
Monocyte PHA	2407	167	101235	2590
NKcell CTRL	5986	364	113162	2624
NKcell LPS+DEX	1566	122	103316	2592
NKcell LPS	5379	366	110434	2462
NKcell PHA+DEX	1427	97	104507	2602
NKcell PHA	1621	135	110859	2477
Tcell CTRL	20187	1297	109130	2605
Tcell LPS+DEX	15636	1052	114176	2642
Tcell LPS	22603	1386	112189	2684
Tcell PHA+DEX	14568	967	115410	2666
Tcell PHA	13279	884	112915	2712
Total Unique	62694	5190	129539	2984
Total Tested	4163269	13876	2,095,831	9556

Table S4: Overlap of eGenes with differentially expressed genes (DEGs, FDR<0.1) and differentially variable genes (DVGs, FDR<0.1). Columns represent: 1 – condition, 2 – number of eGenes which are also DEGs for the condition against its paired control, 3 – odds ratio of the overlap in column 2, 4 – p-value of the Fisher's exact test for enrichment of eGenes in DEGs, 5 - number of eGenes which are also DVGs for the condition against its paired control, 6 – odds ratio of the overlap in column 5, 7 – p-value of the Fisher's exact test for enrichment of eGenes in DVGs.

Condition	eGenes that are DEGs			eGenes that are DVGs		
	Overlap	OR	p-value	overlap	OR	p-value
Bcell LPS	111	2.19	5.1E-09	8	1.25	8.0E-01
Bcell LPS+DEX	297	1.61	1.5E-09	33	1.90	3.2E-02
Bcell PHA	406	1.46	1.8E-08	52	3.27	3.2E-06
Bcell PHA+DEX	355	1.58	2.2E-10	41	1.98	6.3E-03
Monocyte LPS	382	1.15	3.7E-02	199	2.33	2.1E-13
Monocyte LPS+DEX	368	1.19	1.2E-02	131	2.63	3.2E-11
Monocyte PHA	660	1.20	6.4E-04	292	2.78	3.5E-25
Monocyte PHA+DEX	400	1.27	2.9E-04	178	2.00	3.4E-09
NKcell LPS	104	1.99	3.0E-07	27	1.73	9.4E-02
NKcell LPS+DEX	410	1.61	1.2E-12	54	2.02	4.0E-03
NKcell PHA	376	1.54	7.4E-10	49	3.33	8.1E-06
NKcell PHA+DEX	493	1.60	4.2E-14	36	2.24	5.5E-03
Tcell LPS	79	1.98	9.1E-06	57	3.22	4.4E-08
Tcell LPS+DEX	347	1.43	5.5E-07	66	2.58	7.9E-07
Tcell PHA	282	1.48	7.9E-07	89	3.88	2.2E-14
Tcell PHA+DEX	408	1.50	1.7E-09	100	2.31	3.8E-08

Table S5: Overlap of reGenes with differentially expressed genes (DEGs, FDR<0.1) and differentially variable genes (DVGs, FDR<0.1). Columns represent: 1 – condition, 2 – number of reGenes which are also DEGs for the condition against its paired control, 3 – odds ratio of the overlap in column 2, 4 – p-value of the Fisher's exact test for enrichment of reGenes in DEGs, 5 - number of reGenes which are also DVGs for the condition against its paired control, 6 – odds ratio of the overlap in column 5, 7 – p-value of the Fisher's exact test for enrichment of reGenes in DVGs.

Condition	reGenes that are DEGs			reGenes that are DVGs		
	Overlap	OR	p-value	overlap	OR	p-value
Bcell LPS	2	1.95	2.8E-01	1	14.80	7.3E-02
Bcell LPS+DEX	11	3.12	2.4E-03	3	7.44	1.1E-02
Bcell PHA+DEX	10	1.76	1.3E-01	2	3.33	1.3E-01
Bcell PHA	3	0.72	7.9E-01	1	3.51	2.6E-01
Monocyte LPS	14	1.28	4.2E-01	8	2.21	5.8E-02
Monocyte LPS+DEX	5	0.57	2.7E-01	2	1.10	7.1E-01
Monocyte PHA+DEX	11	1.56	1.7E-01	7	3.08	1.4E-02
Monocyte PHA	16	1.01	1.0E+00	6	1.39	4.5E-01
NKcell LPS	3	3.56	6.1E-02	0	NA	NA
NKcell LPS+DEX	13	1.84	5.6E-02	1	0.97	1.0E+00
NKcell PHA	3	1.09	7.5E-01	0	NA	NA
NKcell PHA+DEX	12	1.44	2.7E-01	4	6.14	6.2E-03
Tcell LPS	0	NA	NA	1	2.07	3.9E-01
Tcell LPS+DEX	7	1.21	6.6E-01	0	NA	NA
Tcell PHA+DEX	6	1.09	8.2E-01	1	0.94	1.0E+00
Tcell PHA	3	0.61	6.3E-01	3	3.32	7.0E-02

Table S6: Overlap with previously known dexamethasone reGenes. Table lists dexamethasone reGenes significant in this study and in a previous study conducted in immortalized B cells Maranville *et al.* (2011).

condition	reGenes shared with Maranville, 2011
Bcell_LPS-DEX	BIRC3, RETREG1
Bcell_PHA-DEX	BIRC3
Monocyte_LPS-DEX	RETREG1
NKcell_LPS-DEX	MS4A7
Tcell_LPS-DEX	RETREG1, MS4A7
Tcell_PHA-DEX	BIRC3

Table S7: vQTL mapping results. Number of significant vQTLs and vGenes based on FastQTL results (FDR<0.1, columns 2 and 3), and multivariate adaptive shrinkage results (LFSR<0.1), columns 4 and 5.

	FastQTL FDR<0.1		mash LFSR<0.1	
	vQTLs	vGenes	vQTLs	vGenes
Bcell CTRL	37	6	3086	96
Bcell LPS+DEX	9	4	3042	98
Bcell LPS	0	0	2638	104
Bcell PHA+DEX	2	1	2728	100
Bcell PHA	0	0	2866	99
Monocyte CTRL	2	2	2816	101
Monocyte LPS+DEX	86	12	2827	96
Monocyte LPS	67	12	2573	100
Monocyte PHA+DEX	20	7	2937	100
Monocyte PHA	50	9	2856	103
NKcell CTRL	0	0	3211	99
NKcell LPS+DEX	0	0	2632	91
NKcell LPS	16	7	3010	82
NKcell PHA+DEX	0	0	2941	87
NKcell PHA	19	3	2819	90
Tcell CTRL	188	24	3052	106
Tcell LPS+DEX	23	4	3230	98
Tcell LPS	154	22	2989	107
Tcell PHA+DEX	17	3	3151	106
Tcell PHA	0	0	3089	101
Total unique	545	102	3563	123
Total tested	1549665	7055	242,494	1086

Table S8: Mean-eQTL mapping results. Number of significant mean-eQTLs and mean-eGenes based on FastQTL results (FDR<0.1, columns 2 and 3), and multivariate adaptive shrinkage results (LFSR<0.1), columns 4 and 5.

	FastQTL FDR<0.1		mash LFSR<0.1	
	mean-eQTLs	mean-eGenes	mean-eQTLs	mean-eGenes
Bcell CTRL	604	50	9420	222
Bcell LPS+DEX	1068	73	10252	238
Bcell LPS	4075	225	10882	232
Bcell PHA+DEX	812	54	11098	228
Bcell PHA	2018	125	10313	249
Monocyte CTRL	56	12	8616	203
Monocyte LPS+DEX	1	1	7995	187
Monocyte LPS	401	39	7925	187
Monocyte PHA+DEX	410	59	8294	200
Monocyte PHA	15	1	8239	186
NKcell CTRL	783	71	10929	245
NKcell LPS+DEX	104	14	11250	214
NKcell LPS	1089	94	8635	254
NKcell PHA+DEX	617	64	11446	202
NKcell PHA	702	56	7891	256
Tcell CTRL	11912	792	12404	285
Tcell LPS+DEX	9226	653	12463	286
Tcell LPS	11744	781	12465	302
Tcell PHA+DEX	7515	562	12156	288
Tcell PHA	6477	506	12441	287
Total unique	30493	2430	13164	366
Total tested	1549634	7055	241568	1084

Table S9: Overlap of vGenes with differentially expressed genes (DEGs, FDR<0.1) and differentially variable genes (DVGs, FDR<0.1). Columns represent: 1 – condition, 2 – number of vGenes which are also DEGs for the condition against its paired control, 3 – odds ratio of the overlap in column 2, 4 – p-value of the Fisher's exact test for enrichment of vGenes in DEGs, 5 - number of vGenes which are also DVGs for the condition against its paired control, 6 – odds ratio of the overlap in column 5, 7 – p-value of the Fisher's exact test for enrichment of vGenes in DVGs.

Condition	vGenes that are DEGs			vGenes that are DVGs		
	Overlap	OR	p-value	overlap	OR	p-value
Bcell LPS	7	6.81	5.5E-04	4	6.94	8.6E-03
Bcell LPS+DEX	10	2.27	3.1E-02	3	1.59	4.4E-01
Bcell PHA	18	2.70	1.1E-03	15	6.49	8.9E-07
Bcell PHA+DEX	12	1.81	7.5E-02	6	2.48	5.5E-02
Monocyte LPS	5	0.45	1.1E-01	7	0.89	1.0E+00
Monocyte LPS+DEX	3	0.45	2.7E-01	7	1.32	4.9E-01
Monocyte PHA	14	0.75	4.1E-01	16	1.28	4.4E-01
Monocyte PHA+DEX	9	1.25	5.5E-01	16	2.55	3.0E-03
NKcell LPS	5	2.35	8.8E-02	7	5.08	1.9E-03
NKcell LPS+DEX	9	1.11	7.0E-01	11	5.38	6.9E-05
NKcell PHA	8	1.21	5.4E-01	6	2.17	1.2E-01
NKcell PHA+DEX	13	1.21	5.1E-01	2	1.17	6.9E-01
Tcell LPS	6	4.53	6.3E-03	11	3.65	1.1E-03
Tcell LPS+DEX	13	1.69	1.3E-01	6	1.88	1.6E-01
Tcell PHA	16	3.04	6.2E-04	20	4.51	1.8E-06
Tcell PHA+DEX	18	2.13	1.3E-02	7	0.97	1.0E+00

Table S10: Summary of DLDA dynamic eQTL mapping and overlap with eGenes, and and immune diseases-associated genes identified from PTWAS

Cell type DLDA treatment	eQTLs(FDR<0.1)	eGenes	PTWAS Genes
Bcell LPS	139	32	2
Bcel LPS+DEX	0	0	0
Bcell PHA	114	40	7
Bcell PHA+DEX	27	2	0
Monocyte LPS	35	3	0
Monocyte LPS+DEX	37	3	1
Monocyte PHA	0	0	0
Monocyte PHA+DEX	0	0	0
NKcell LPS	4	3	0
NKcell LPS+DEX	2	2	0
NKcell PHA	6	4	1
NKcell PHA+DEX	3	2	0
Tcell LPS	2073	244	45
Tcell LPS+DEX	269	18	5
Tcell PHA	1329	225	39
Tcel PHA+DEX	1298	54	9
Total unique	3899	588	101

Table S11: **Results of differential expressed genes (DEGs) using DESeq2 pseudo bulk aggregated data**. Columns 1-7 are: 1) Cell type; 2) Treatment; 3) Ensembl gene ID; 4) $\log_2$ fold change of gene expression; 5) Standard error; 6) P-value; 7) FDR

`https://zenodo.org/record/7851053/files/Supplemental_Table_S11.txt.gz`

Table S12: **Results of differential gene expression variability (DGV)**. Columns 1-7 are: 1) Cell type; 2) Treatment; 3) Ensembl gene ID; 4) $\log_2$ fold change of gene variability; 5) Standard error; 6) P-value; 7) FDR

`https://zenodo.org/record/7851053/files/Supplemental_Table_S12.txt.gz`

Table S13: **FastQTL eQTL mapping results**. Results of eQTL mapping across the 20 conditions. Columns are: 1 - ENSEMBL gene name; 2 - genetic variant coordinates (GRCh37); major and minor alleles and dbSNP ID; 3 - genetic variant distance from the TSS of the gene; 4 - p-value of the effect of the genetic variant on expression of the gene; 5 - effect size of the genetic variant on expression of the gene; 6 - condition.

`https://zenodo.org/record/7851053/files/Supplemental_Table_S13.txt.gz`

Table S14: **mash eQTL effect estimates**. Multivariate adaptive shrinkage estimates of genetic effects on gene expression. Columns 1-20 are the conditions; rows are the tested gene-SNP pairs.

`https://zenodo.org/record/7851053/files/Supplemental_Table_S14.txt.gz`

Table S15: **mash eQTL significance**. Multivariate adaptive shrinkage significance (LFSR) of genetic effects on gene expression. Columns 1-20 are the conditions; rows are the tested gene-SNP pairs.

https://zenodo.org/record/7851053/files/Supplemental_Table_S15.txt.gz

Table S16: **61 reGenes overlapping with immune disease genes**. Columns are: 1-ENSEMBL gene name; 2-SYMBOL gene name

https://zenodo.org/record/7851053/files/Supplemental_Table_S16.txt.gz

Table S17: **FastQTL vQTL mapping results**. Results of vQTL mapping across the 20 conditions. Columns are: 1 - ENSEMBL gene name; 2 - genetic variant coordinates (GRCh37), major and minor alleles and dbSNP ID; 3 - genetic variant distance from the TSS of the gene; 4 - p-value of the effect of the genetic variant on gene expression variability of the gene; 5 - effect size of the genetic variant on gene expression variability of the gene; 6 - condition.

https://zenodo.org/record/7851053/files/Supplemental_Table_S17.txt.gz

Table S18: **mash vQTL effect estimates**. Multivariate adaptive shrinkage estimates of genetic effects on gene expression variability. Columns 1-20 are the conditions, rows are the tested gene-SNP pairs.

https://zenodo.org/record/7851053/files/Supplemental_Table_S18.txt.gz

Table S19: **mash vQTL significance**. Multivariate adaptive shrinkage significance of genetic effects on gene expression variability. Columns 1-20 are the conditions; rows are the tested gene-SNP pairs.

https://zenodo.org/record/7851053/files/Supplemental_Table_S19.txt.gz

Table S20: **FastQTL mean-eQTL mapping results**. Results of mean-eQTL mapping across the 20 conditions. Columns are: 1 - ENSEMBL gene name; 2 - genetic variant coordinates (GRCh37), major and minor alleles and dbSNP ID; 3 - genetic variant distance from the TSS of the gene; 4 - p-value of the effect of the genetic variant on mean expression of the gene; 5 - effect size of the genetic variant on mean expression of the gene; 6 - condition.

https://zenodo.org/record/7851053/files/Supplemental_Table_S20.txt.gz

Table S21: **mash mean-eQTL effect estimates**. Multivariate adaptive shrinkage estimates of genetic effects on gene expression mean. Columns 1-20 are the conditions, rows are the tested gene-SNP pairs.

https://zenodo.org/record/7851053/files/Supplemental_Table_S21.txt.gz

Table S22: **mash mean-eQTL significance**. Multivariate adaptive shrinkage significance of genetic effects on gene expression mean. Columns 1-20 are the conditions, rows are the tested gene-SNP pairs.

https://zenodo.org/record/7851053/files/Supplemental_Table_S22.txt.gz

Table S23: **Dynamic eQTL mapping results**. Results of dynamic eQTL mapping across 16 conditions, each file representing the results of dynamic eQTL mapping in one of the four cell types (B cells, Monocytes, NK cells and T cells) treated with LPS, LPS+DEX, PHA or PHA+DEX interacting with treatment response pseudotime. Columns 1-6 are: 1) Ensembl gene ID; 2) genetic variant coordinates (GRCh37); major and minor alleles and dbSNP ID; 3) genetic effect on gene expression interacting with response pseudotime; 4). Standard error of the interaction term; 5) P-value for the interaction term; 6) The stratified FDR q-value

`https://zenodo.org/record/7851053/files/Supplemental_Table_S23.txt.gz`

Table S24: **table of number of cells per combination (cell type+treatment+individual** across 1,536 combinations. Columns 1-5 are: 1) combination ID; 2) number of cells per combination; 3) cell type; 4) treatments; 5) individual ID

`https://zenodo.org/record/7851053/files/Supplemental_Table_S24.txt.gz`